TABLE OF CONTENTS

Page

LIST OF TABLES

Page

LIST OF FIGURES

LIST OF ABREVIATIONS

A: Austenitizing

AF: Acicular Ferrite

ANOVA: ANalysis Of Variance

ATF: AlloTriomorphic Ferrite

B: Bainite

BCT: Body Centered Tetragonal

BSE: Back Scattered Electron

C: Cryogenic treatment

CCT: Continuous Cooling Transformation

CHT: Conventionally Heat Treated

CP: Carbide Precipitation

CR: Cooling Rate

EDS: Energy Dispersive Spectroscopy

HRC: Hardness Rockwell C

Ht_C: Holding time at cryogenic temperature

HU: Heating Up

HV: Hardness Vickers

LSC: Large Secondary Carbide

M: Martensite

M_f: Martensite finish temperature

M_s: Martensite start temperature

OM: Optical Microscope

PC: Primary Carbide

PIPS: Precision Ion Polishing System

Q: Quenching

SAD: Selected Area Diffraction

SEM: Scanning Electron Microscopy

SSC: Small Secondary Carbide

T: Tempering

T_A: Austenitizing temperature

t_A: Holding time at austenitic temperature

T_C: Cryogenic Temperature

TEM: Transmission Electron microscope

T_T: Tempering temperature

UTS: Ultimate Tensile Strength

WF: Widmanstätten Ferrite

XRD: X-Ray Diffraction

LIST OF SYMBOLS AND UNITS OF MEASUREMENTS

$\bar{\vartheta}$: The average volume of the newly formed martensite plates

$\Delta G^{\gamma\rightarrow\alpha}$: The chemical driving force of austenite to martensite (ferrite) transformation

ΔG: The volume free energy change accompanying transformation

b: A material constant varying with chemical composition

d: The shrinkage due to expansion coefficient

dT: Temperature variation,

E (BCC-FCC): The strain energy of the transformation of FCC austenite to BCC martensite

E: The total dilatation at a i-th temperature

E_0: The dilatation at M_s

f_m: The volume fraction of martensite

i: i-th experimental point,

K: Kelvin

X^1_e and X^2_e: The boundaries for the miscibility gap

X^1_s and X^2_s: The limits of spinodal decomposition

x_c: Carbon content

ά: Martensite

α_m: The expansion coefficient of martensite

α_γ: The expansion coefficient of austenite

β: Rate parameter

γ: Austenite

ε: Strain

ε: Transition carbide

$\varepsilon_{\gamma\text{-}m}$: The strain due to lattice volume differences between austenite and martensite

η: Transition carbide

θ: Strain hardening coefficient

σ: Stress

σ_y: Yield strength of austenite

φ: A proportionality constant

χ: Cooling rate dependent strain energy

INTRODUCTION

Tool steels are known for their very high strength along with high wear resistance (Arai et al. 1991). These properties are due to their specific chemistry and a microstructure obtained through a heat treatment process comprised mainly of hardening (austenitizing and quenching) cycle, and one to three tempering cycles (Roberts et al. 1998). They generally contain 0.3 to 2 (wt%C), and alloying elements such as Mo, Cr, W, and V (Arai et al. 1991, Roberts et al. 1998). The final microstructure of these steels is composed of martensite as matrix, carbides and some undesired retained austenite (Roberts et al. 1998). Generally after quenching from austenitizing temperature, a fully martensitic microstructure is desired; however, compositional effects may push down the martensite transformation start (M_s) and finish (M_f) temperatures to very low values and stabilize the austenite phase at room temperature. The presence of non-transformed austenite after heat treatment is detrimental to the performance in service (Roberts et al. 1998). Cryogenic treatment, (holding at between 200K and 77K) as a supplemental step to the conventional heat treatment, has proved to be an efficient way for removing retained austenite (Singh et al. 2011). It has also shown very promising perspectives in achieving significant improvement in mechanical properties and wear resistance of tool steels (Singh et al. 2011).

However, there are controversies among the researchers about the possible root causes for the improved mechanical and wear properties obtained after cryogenic treatment. For example, on the time length for cryogenic treatment suggestions exist from few seconds to several days (Singh et al. 2011). Controversies are due to insufficient understanding on the fundamental mechanisms governing the phase transformation at cryogenic temperatures. A lack of systematic investigations about the operating mechanisms at cryogenic temperature and the influence of cryogenic process parameters on microstructure evolution and properties is evident. The objective of the present PhD research project is to address the above questions and develop a better understanding of the fundamental micromechanisms operating during cryogenic treatment.

This thesis starts with an overview on the conventional cryogenic treatment and its effect on microstructure evolution and enhancement in wear and mechanical properties (Chapter 1). This chapter summarizes different point of views on the root causes for obtaining better mechanical and wear properties in tool steels after cryogenic treatment. Then, the state-of-the-art on cryogenic treatment is described and the challenges are identified.

The first article from this work, published in Journal of Materials Science and Engineering A (24 March 2014, volume: 598, pp.413-419) is presented in Chapter 2. This chapter describes the results of an experimental study on conventional cryogenic treatment and discusses the possible reasons for strength and ductility enhancement in AISI D2 tool steel. A methodology is proposed to relate the mechanical properties enhancements to the analysis of strain hardening behavior during mechanical testing and carbides coarsening behavior. The objective is to find possible answers for some of the questions raised in Chapter 1 regarding the possible improvement in strength and ductility after cryogenic treatment.

The second article from this work, published in Journal of Materials Science and Engineering A (14 May 2015, volume: 634, pp.32-36) is presented in Chapter 3. This chapter discusses on the influence of starting microstructure on the response of the cryogenic treatment. Using high resolution dilatometry and electron microscopy, it is shown that conventional cryogenic treatment fails to fully transform austenite to martensite. An alternative transformation path is proposed which produces multiphase microstructure with mostly bainite and a few allotriomorphic ferrite, Widmanstätten ferrite, and acicular ferrite instead of martensitic. The proposed approach allows optimizing the cryogenic process for concomitant enhancement in the wear and mechanical properties.

The third article was adopted from Chapter 4 and published in International Journal of Advanced Manufacturing Technology (27 October 2015, online version, pp. 1-10). In this chapter, using design of experiment a series of dilatometry tests are carried out on samples with a fully martensitic structure before cooling to cryogenic temperatures. The influence of cryogenic process parameters on the hardness variation is discussed. Specifically the

influence of (1) cooling rate, (2) cooling temperature, (3) holding time at cryogenic temperature, (4) heating rate, (5) tempering temperature as controllable variables, and (6) surface density of carbides with average diameter below 1 µm as non-controllable variable are investigated.

The fourth article from this work, published in Journal of Materials Science (29 May 2015, volume: 50, pp.5758-5768) is presented in Chapter 5. This chapter discusses the findings on the characteristic of martensite produced by cryogenic treatment. The kinetics of martensitic transformation is investigated to determine the variation in the volume fraction of martensite during cryogenic cooling. For kinetic study, the dilatation data are analyzed using numerical methods and a modified equation is proposed for the determination of transformation rate parameter and the total volume fraction of martensite after cryogenic treatment. Using high resolution transmission electron microscopy, microstructural features are observed and discussed.

The fifth scientific article proposed and submitted from this work is presented in Chapter 6. This chapter focuses on identifying the nucleation sites responsible for the formation of η-carbides after cryogenic treatment. The formation of η-carbides has been reported as the possible root cause for enhanced mechanical and wear properties after cryogenic treatment. A methodology is proposed to calculate the chemical deriving force of martensitic transformation at cryogenic temperatures with considering Zener-ordering contribution where carbon mobility is sufficient. The applicability of the thermodynamic formalism is evaluated for temperatures down to 0K and the possibility of a secondary ordering versus Zener-ordering is investigated. The transformation barriers are determined to be the strain energy required for the activation of martensitic transformation at martensite start temperature and most importantly the cooling rate-dependent strain energy stored in austenite. This chapter discusses also on the mechanism responsible for the formation of η-carbides induced by cryogenic treatment.

Finally a summary covering all the information from Chapters 2 to 6 is presented in Conclusions section to link the outcomes from each chapter and present the original contribution to knowledge toward the principal objective of the thesis.

CHAPTER 1

LITERATURE REVIEW

1.1 Martensite in steels

Martensite is a hard microconstituent found in quenched carbon steels. Transformation of austenite (γ) to martensite ($\acute{\alpha}$) starts at a specific temperature called martensite start temperature (M_s), and it finishes at martensite finish temperature (M_f). The γ to $\acute{\alpha}$ reaction cannot take place until the specimen is cooled to a specific temperature below T_0, the temperature at which the free energy difference ($\Delta G^{\gamma \text{ to } \acute{\alpha}}$) between fcc-austenite (G^{γ}) and bct-martensite ($G^{\acute{\alpha}}$) of the same composition is zero (Fig. 1-1(a)) (Nishiyama 1987). The greater is the degree of supercooling; the larger will be the difference between the two crystal structures, because it is more difficult for the change to occur when the structures are very different. In the case of steel, the difference between the two structures is rather large and the difference between T_0 and M_s may be as large as 200K (Nishiyama 1987).

In carbon steels, the carbon atoms remain at octahedral sites during martensitic transformation and generate elastic strains around them. The elastic strains lead to the formation of tetragonal (bct) structure instead of bcc structure (Krauss 1999 and Bhadeshia 2002). This tetragonality strengthens the matrix and increases the hardness of steel. It can be said that the formation of martensite is carbon steels is one of the strengthening mechanisms of the matrix (Krauss 1999). Martensite, depending on the carbon content, can have either lath or plate or mixed morphology. The formation of twinned martensite is also possible (Krauss 1999). The martensite start and finish temperatures decrease by adding more carbon to steel. Figure 1-1(b) summarizes the relation between carbon content, M_s temperature, and resulted morphology in Fe-C alloys (Krauss 1999).

Martensite is produced through a diffusionless process. The evidences supporting this character are: (a) possibility of formation at very low temperatures (b) very high growth rate close to 1100 ms^{-1}, which is much higher than the fastest recorded velocity for solidification

front, and (c) the chemical composition of ά is shown to be identical to that of the parent γ (Bhadeshia 2002).

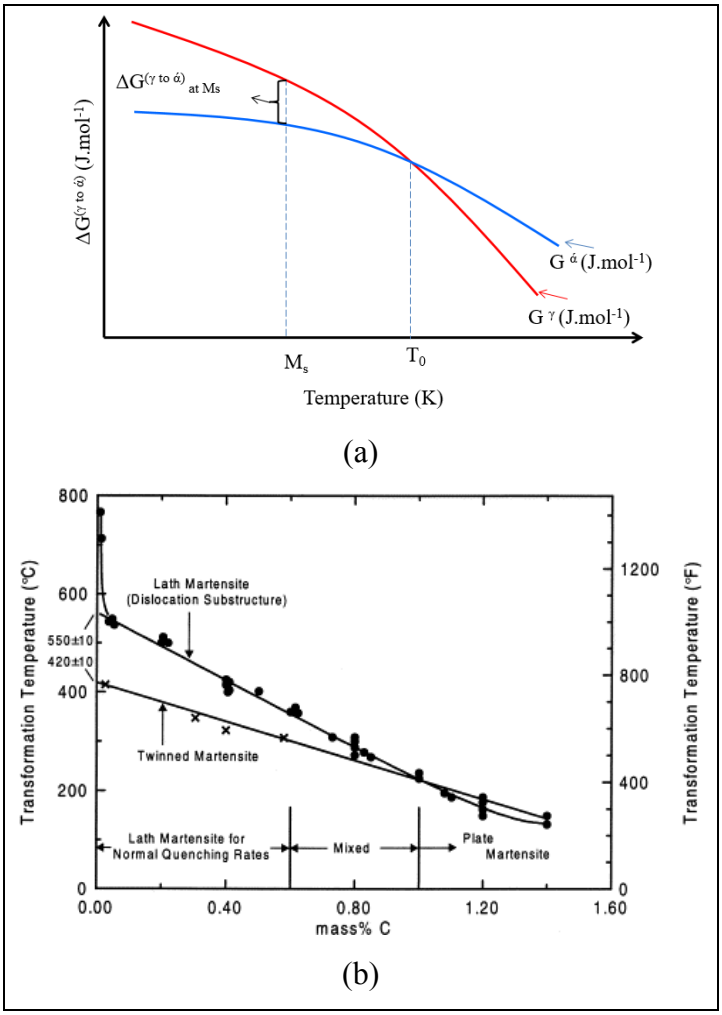

Figure 1-1(a) Free energy changes between γ and ά, (b) Martensite start (M_s) temperatures and martensite morphology as a function of carbon content in Fe-C alloys (Marder and Krauss 1967, Krauss 1991, Wilson 1994).

The tetragonality observed during martensitic transformation is not only the effect of diffusionless transformation and the interactions between Fe and C atoms may generate ordering in the martensite crystal structure (Zener 1946). The Zener ordering keeps the carbon atoms in this c-sublattice and prevents their migration to octahedral sites in other

sublattices only within the temperature range where carbon atoms are sufficiently mobile for such migration (Zener 1946). For steels such as AISI D2 with 0.52wt.% carbon in the martensite, the complete ordering is estimated to occur at temperatures close to 150K based on thermodynamic approach but the carbon mobility is also essential and should be taken into account. Therefore, the martensitic transformation doesn't complete by cooling to room temperature and it would be continued until cryogenic temperatures where carbon mobility is feasible (T>223K) (Tyshchenko et al. 2010). It has been reported that martensitic transformation has an athermal nature i.e. independent of time. Koistinen and Marburger (Bhadeshia 2002, Bhadeshia 2013) proposed an empirical equation (Equation 1-1) to study the kinetics of martensitic transformation and quantified the extent of transformation as a function of the degree of undercooling.

$$1-V_{\alpha'} = \exp[\beta(M_s - T)] \tag{1-1}$$

where β is - 0.011.

For example, in AISI D2 tool steel by considering M_s = 403K (Gavriljuk et al. 2013), quenching a sample to 173K and 123K gives 92 % and 95 % volume fraction of martensite, respectively. Hence, it can be said that at very low temperatures almost complete transformation of γ to ά is possible. Martensite and martensitic transformation are playing an important role in improving the mechanical properties of AISI D2 tool steel. Hence, a good understanding of martensite characteristics, the thermodynamics and kinetics of its transformation for investigated alloy will be very beneficial in order to optimize the strength, toughness, and wear characteristics of high strength steel where these properties are concomitantly required.

1.2 Introduction to tool steels

Tool steels are used for cutting, forming, or shaping a material into a part or component adjusted to a specified application (Arai et al. 1991). Cutting tool steels show high strength and wear resistance but they should have also good toughness to absorb high energies applied during service (Arai et al. 1991). In addition to cutting tools, many tool steels are also widely

used for machinery components and structural applications such as high-punches and dies, wear-resistant liners, etc (Arai et al. 1991). These alloys contain relatively large amounts of tungsten, molybdenum, vanadium, and chromium. These elements make it possible to meet increasingly rather high service demands and to provide greater dimensional control and freedom from cracking during heat treating. The chart in Table 1.1 contains some of the commonly used tool steels and their alloy content (wt. %) (Tarkany 2000).

Table 1.1 Commonly used tool steels (Tarkany 2000).

Steel type	C	Mn	Si	Cr	W	Mo	V
A2	1.0	0.9	0.3	5.25	0	1.15	0.3
D2	**1.5**	**0.5**	**0.3**	**12.0**	**0**	**0.9**	**0.9**
M2	0.85	0.3	0.3	4.15	6.4	5.0	1.9
M4	1.4	0.3	0.3	4.0	5.75	4.5	4.0
CPM 10V	2.45	0.5	0.9	5.25	0	1.3	9.75

Each grade of tool steel requires a specific heat treatment procedure in order to achieve the optimum properties for any given application (Weast 1981-1982, Arai et al. 1991, Tarkany 2000). The final microstructure of these steels is composed of martensite (matrix), carbides and some undesired retained austenite. In this project, the focus will be on the heat treatment cycle of AISI D2 tool steel.

1.3 General production cycle for a tool steel

The production cycle of a tool steel consists of ingot casting, thermomechanical (hot forging and/or rolling), machining, and thermal heat treatments (Arai et al. 1991, Roberts et al. 1998). The thermomechanical treatment starts after casting and it consists of hot forging or rolling in order to homogenize the cast microstructure and break down the large networks of eutectic carbides formed during casting (Arai et al. 1991, Roberts et al. 1998). After that, annealing stage is carried out to generate uniform microstructure. Most of the tool steels are formed or machined to produce the desired shape prior to hardening heat treatment (Arai et al. 1991, Roberts et al. 1998). Figure 1-2 (a) shows the typical initial thermomechanical

treatment and (b) conventional heat-treatment sequences including hardening (austenitization and quenching) and tempering as a function of time, temperature, and phase transformation (Arai et al. 1991, Roberts et al. 1998).

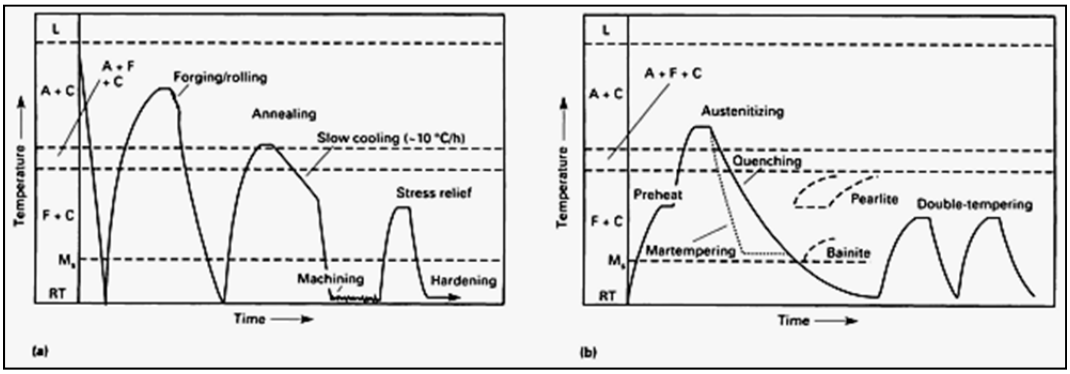

Figure 1-2 Plots of temperature versus time showing sequence of operations required to produce tool steels. (a) thermomechanical processing. (b) hardening heat treatment. L, liquid; A, austenite; C, cementite; F, ferrite; Ms temperature at which martensite starts to form on cooling; RT, room temperature (Arai et al. 1991).

During quenching, martensitic transformation progresses until temperature falls to M_f. The M_f temperature can be below room temperature, so austenite might only, to some extent, transform to martensite with the remaining structure being retained austenite and undissolved eutectic carbides. The carbon content and additive alloying elements affect both M_s and M_f temperatures (Fig.1-3). Some alloying elements increase M_s and M_f while others reduce them. In AISI D2 tool steel, carbon and chromium (main alloying elements) reduce both M_s and M_f temperatures (Fig.1-3). For AISI D2 tool steel M_s and M_f were measured as 403K and 173K, respectively (Gavriljuk et al. 2013). Martensitic microstructure after the hardening cycle (austenitizing and quenching) is hard and brittle (Speich and Leslie 1972). Tempering is the process of heating martensitic steels to temperatures close to 773K so that they become more ductile (Speich and Leslie 1972). Tempering involves the segregation of carbon to lattice defects, and the precipitation of carbides, and the decomposition of retained austenite. Based on the temperature range selection for tempering, different stages are proposed for microstructure evolution in tool steels (Speich and Leslie 1972).

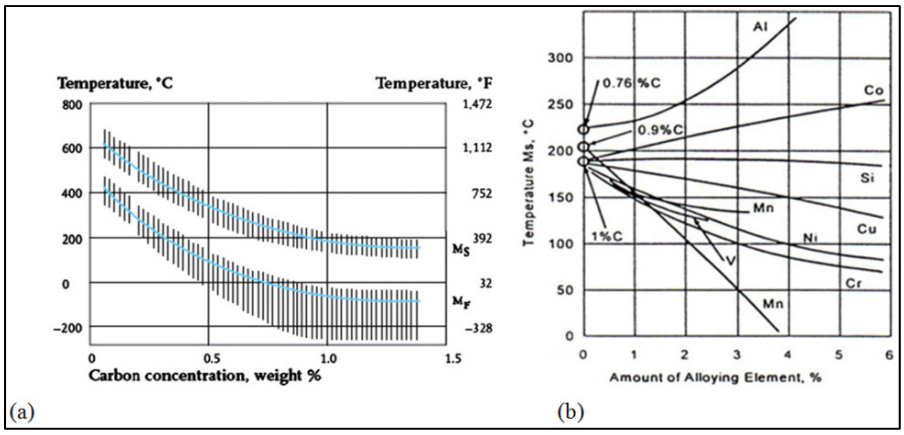

Figure 1-3(a) Effect of carbon content on M_s and M_f temperatures, (b) effect of alloy content on M_s temperature (Weast 1981-1982).

The first stage consists of heating to temperatures between 373K and 473K, which is the region for the formation of transitional carbides such as epsilon (ε) (hcp crystal structure) and eta-carbides (η) (orthorhombic crystal structure). The second stage is called decomposition of retained austenite and it occurs in the range of 473K to 573K. Cementite (Fe_3C, orthorhombic) forms when most steels are tempered between 523K and 973K. This step is called the third stage of tempering. If, carbide-forming alloying elements such as Ti, Mo, V, or W are added to the steel, a further and important strengthening reaction will occur between 773K and 873K. This stage will be the fourth stage of tempering and it is also called secondary hardening stage (Speich and Leslie 1972).

Studies on the evolution of mechanical properties of AISI D2 tool steel has shown good combination of high hardness and high wear resistance after conventional heat treatment (Roberts et al. 1998) but also researches have also reported poor ductility of the alloy after conventional heat treatment (Teymuri et al. 2011). The decomposition of austenite to ferrite, the formation of film like cementite, and the segregation of embrittling elements such as Cr at prior austenite grain boundaries during tempering are proposed as root causes for the observed poor ductility (Speich and Leslie 1972, Ghasemi-Nanesa and Jahazi 2014). In order to transform all the austenite to martensite before tempering, the M_f temperature should be reached during the quenching step.

1.4 Cryogenic treatment of tool steels

Cryogenic treatment was initially introduced as an additional step to the heat treatment cycle of tool steels to remove the retained austenite. It showed significant improvement in service wear life and hardness of tool steels (Miller 1980). Originally, it consisted of the following steps: (1) Austenitizing (A); (2) Quenching (Q); (3) Tempering (T); (4) Cryogenic treatment (C) (Tarkany 2000). Kelkar et al. (2007) have studied different combinations of the above steps:

(a) A+Q,

(b) A+Q+T,

(c) A+Q+T+C,

(d) A+Q+C, and

(e) A+Q+C+T.

They concluded that A+Q+C+T combination shows higher toughness in addition to the increase in hardness. A typical cryogenic treatment consists of cooling down from ambient temperature to the temperature of liquid nitrogen. When the material reaches approximately 77K, it is soaked for an appropriate time before being removed from liquid nitrogen and allowed to warm up to the ambient temperature (Fig.1-4) (Singh et al. 2011).

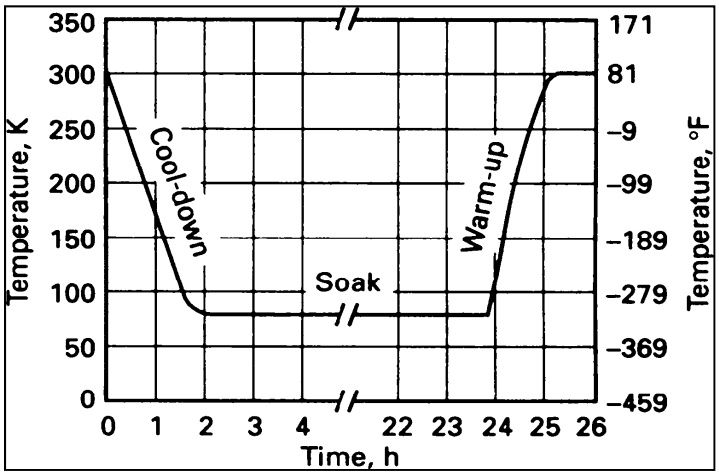

Figure 1-4 Plot of temperature versus time for the cryogenic treatment (Singh et al. 2011).

Two distinct approaches have been used for cooling and heating rates: 1) Cool or reheat the material as fast as possible to or from the cryogenic temperature, and 2) Apply a gradual (slow) cool down and reheating. In the latter case, several hours are required to complete this step (Reitz and Pendray 2001).

Direct immersion of components in liquid nitrogen bath and the resultant abrupt cooling to very low temperatures may lead to the development of excessive thermal stresses (and also structural stresses (Reed-Hill and Abbaschian 1992) which may induce cracking of the components. Kamody (1999) reported that cooling rate has little effect on the properties of final products and so it should be carried out as rapid as possible to minimize the treatment time. The same approach has been suggested by Kamody for the reheating rate from cryogenic temperature to room temperature. However, it is well recognized that cracking can occur by rapid cooling (Reitz and Pendray 2001). So, slow cooling and even slower heating rate is required in order to avoid crack initiation. Molinari et al. (2001) suggested that in order to avoid cracking of the component, cooling rate must not exceed 0.3 to 0.5 ($K.min^{-1}$). Commonly proposed cooling rates are 0.3 to 1.2 ($K.min^{-1}$). Lal et al. (1996, 2001) have used a cooling rate of 1.15 $K.min^{-1}$ and heating rate of 0.56$K.min^{-1}$ for AISI M2, D3 and T1 steels. However, some investigators have opted slow but identical rate for both cooling and heating, such as 1.0$K.min^{-1}$ for AISI M2 steel by Silva et al. (2006). For AISI D2 steel, Wang (2006) has reported that the faster the cooling rate is, the higher would be the level of improvement in hardness and wear resistance.

Another parameter in cryogenic treatment is the soaking time at cryogenic temperature. Kamody states that soaking time is unrelated to the final mechanical properties. According to his patent (Kamody 1993), the main objective is to transform retained austenite to martensite. This transformation is dependent only on the cryogenic temperature and not on the time held at that temperature. A soaking time of 10min is suggested to allow the material to achieve thermal equilibrium before it is removed and reheated. If the final properties of the material are independent of the time at cryogenic temperature, this time should be minimized to reduce the treatment cost. Reports have indicated that for H13 and D2 tool steels, there is

little or nothing gained by long soaking times (Barron 1983, Moore and Collins 1993, Reitz and Pendray 2001).

By contrast, Dobbins and Barron state that, the time the material is allowed to stay in the cryogenic condition impacts the final properties (Dobbins 1995, Collins 1996). This soaking time is required for the atoms in the material to diffuse to new locations; a time of the order of 20hrs is suggested (Barron 1983, Dobbins 1995). Moore and Collins (1993) reported the effect of soaking time on hardness of three different steel samples. They indicated that Vanadis 4 (a chromium-molybdenum-vanadium alloyed steel) and D2 tool steels were unaffected by the duration of cryogenic while H13 tool steel, showed a higher hardness after soaking for 400min. An optimum soaking time may therefore exist for each type of material as illustrated in Fig.1-5 for H13 steel (Reitz and Pendray 2001). Collins (1996, 1998) and Collins and Dormer (1997) showed that soaking time affects the hardness, wear resistance, and carbide density of a variety of steels. Additional time is important for any transformation/precipitation to be completed at such low temperatures because diffusion is very slow. On the contrary, work by Barron (1983) has shown that plain carbon steels and cast irons are not affected by soaking time during cryotreatment.

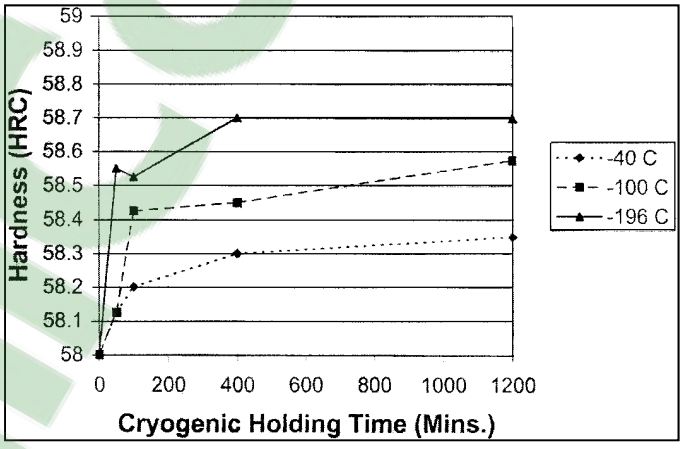

Figure 1-5 Changes in hardness of H13 tool steel with soaking time (Reitz and Pendray 2001)

From the processing point of view, the cooling and heating rates should be fast enough to achieve better performance of tool/die steel components by cryogenic treatment and to reduce the process cost; however, these rates should be slow enough to avoid development of

microcracks in the component. With the present state of knowledge, systematic studies are required to find the effect of cooling and heating rates and soaking time on microstructure evolution and mechanical properties.

1.5 Metallurgy of cryogenically treated tool steels

Available data in the literature relevant to the structure-property relations of tool steels subjected to cryogenic treatment are not coherent and the fundamental proposed reasons for achieving improved mechanical properties like wear resistance are not well documented. The proposed mechanism for the superior wear resistance of tool steels after cryogenic treatment can be generally classified in three categories:

1) Transformation of retained austenite to martensite (Barron 1983, Moore and Collins 1993, Dymchenko and Safronova 1993, Cohen and Kamody 1998, Blankinship 2001, Babu et al. 2005, Yang et al. 2006, Zhirafar et al. 2007),
2) Precipitation of refined carbide particles (Paulin 1993, Meng et al. 1994, Yugandhar et al. 2002, Zurecki 2005, Stratton 2007, Dhokey and Nirbhavne 2009), and
3) Combined effect from transformation of retained austenite to martensite and precipitation of fine carbide within martensite (Collins 1996, Collins and Dormer 1997, Yun et al. 1998, Mohan et al. 2001, Preciado 2006). Each of the above categories will be discussed in the following sections.

1.5.1 Transformation of retained austenite to martensite

As mentioned in section 1.3, austenite in tool steel transforms to martensite, undissolved eutectic carbides, and retained austenite. Thus, cooling to cryogenic temperatures ($T<M_f$) promotes the transformation of retained austenite to martensite and increases the hardness of steel. Gulyaev (1937) was the first who studied cryogenic treatment of tool steels and reported enhanced wear resistance. The transformation of retained austenite to martensite with a more stable structure was proposed as the root cause for the improvement brought by cryogenic treatment. The results obtained by Gulyaev were later confirmed by many other

researchers (Barron 1983, Moore and Collins 1993, Dymchenko and Safronova 1993, Cohen and Kamody 1998, Blankinship 2001, Babu et al. 2005, Yang et al. 2006, Zhirafar et al. 2007).

Barron (1983) used two different cryogenic temperatures, 198K and 77K, and concluded that treatment at 77K (deep process) was more productive in that more transformation of retained austenite to martensite took place. He also proposed that room temperature ageing of austenite should be avoided because it stabilizes the austenite and even the cryogenic treatment could not transform austenite to martensite. Finally, he proposed that in presence of retained austenite, wear behavior will not be improved. Zhirafar et al. (2007), using neutron diffraction technique, showed that the most important microstructural result of cryogenic treatment of AISI 4340 steel was a small reduction in the quantity of retained austenite, which was transformed to martensite (Fig.1-6). From the above discussion, it can be concluded that the conversion of retained austenite to martensite, and the related increase in hardness due to the higher amount of martensite, is considered by many researchers as the reason for enhanced wear resistance of tool steels. The analysis of published literature also indicates that in order to maximize the cryogenic effect, austenite stabilization must be avoided. To this end, the cryogenic treatment should be carried out immediately after quenching and γ-stabilizer alloying elements should be added more carefully to avoid austenite stabilization.

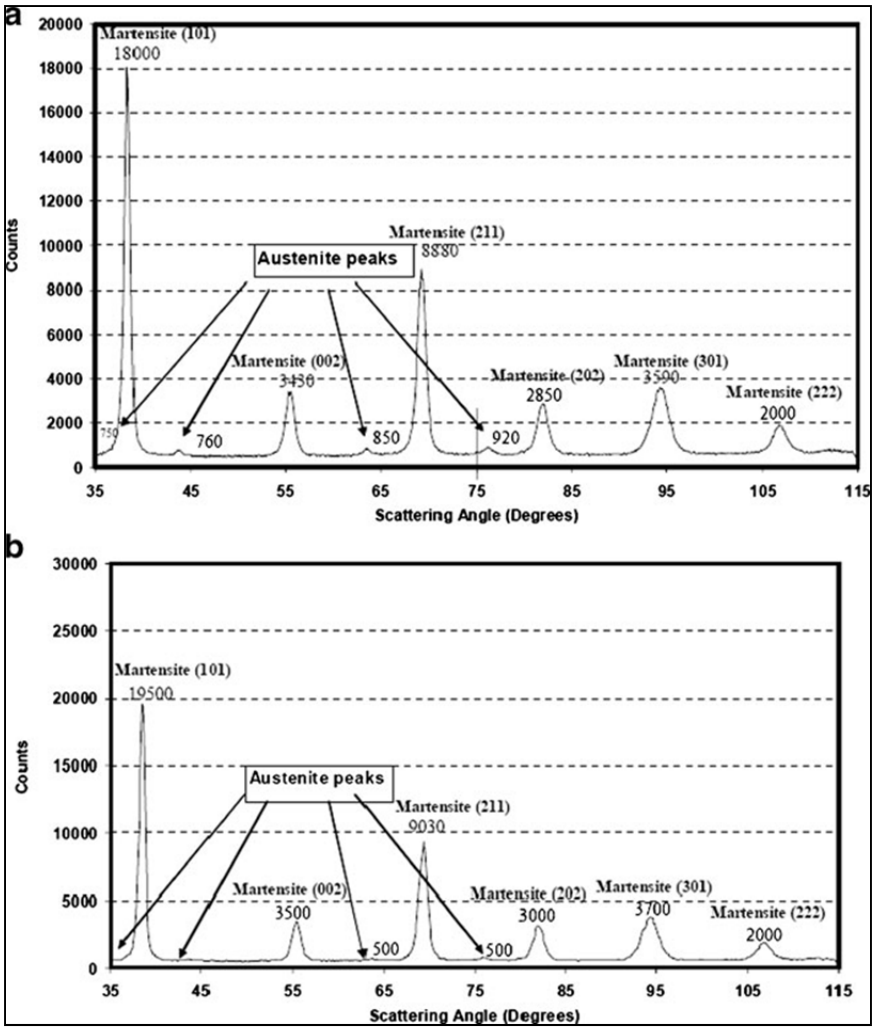

Figure 1-6 The neutron diffraction profile for (a) austenite at 1118K, oil-quenched, and (b) austenitized at 1118K, oil- quenched, and cryogenically treated (Zhirafar et al. 2007).

1.5.2 Precipitation of refined carbide particles

Another group of researchers have reported that cryogenic treatment, in addition to the transformation of retained austenite to martensite, brings metallurgical changes within the martensite which improves mechanical properties (Paulin 1993, Meng et al. 1994, Yugandhar et al. 2002, Zurecki 2005, Stratton 2007, Dhokey and Nirbhavne 2009). They attributed the improvement in the mechanical properties to inter-martensite alterations rather than to

austenite–martensite transformations (Paulin 1993, Meng et al. 1994, Yugandhar et al. 2002, Zurecki 2005, Stratton 2007, Dhokey and Nirbhavne 2009). Meng et al. (1994) studied the wear behavior of Fe-12wt%Cr-1 wt%Mo-1 wt%V-1.4 wt%C tool steel and related it to the formation of fine carbides (η-carbides) within martensite after cryogenic treatments and low temperature tempering cycle.

These carbides are different in size and shape from the primary carbides which are formed during the tempering process. These authors also reported changes in the lattice parameter of martensite after cryogenic treatment and indicated that these changes contribute more to enhance the strength and toughness of the material rather than the transformation of retained austenite to martensite (Meng et al. 1994). Yugandhar et al. (2002) found that precipitation of η-carbides occurs only during the tempering process after deep cryogenic treatment which is a different result from the ones reported by Meng (1994). Zurecki (2005) studied the effects of various quenching media including liquid nitrogen (77K) and liquid helium (4K) on microstructure and selected properties of A2 grade tool steel. The author reported the presence of a large number of finely dispersed dark carbides, with a typical size of 100-250nm in cryogenically treated samples as shown in Fig.1-7 (Zurecki, 2005). Stratton (2007) reported that time dependent decomposition of primary martensite at cryogenic temperature is related to nucleation of numerous coherent nano carbides (η-carbides) which bring wear resistance enhancement. This finding is in agreement with the work reported by Meng et al. (1994). In a recent study, Dhokey and Nirbhavne (2009) employed AISI D3 steel, with multiple tempering after cryogenic treatment, and showed that multiple tempering coarsens the carbides formed during cryogenic treatment resulting in reduced wear resistance of the final product.

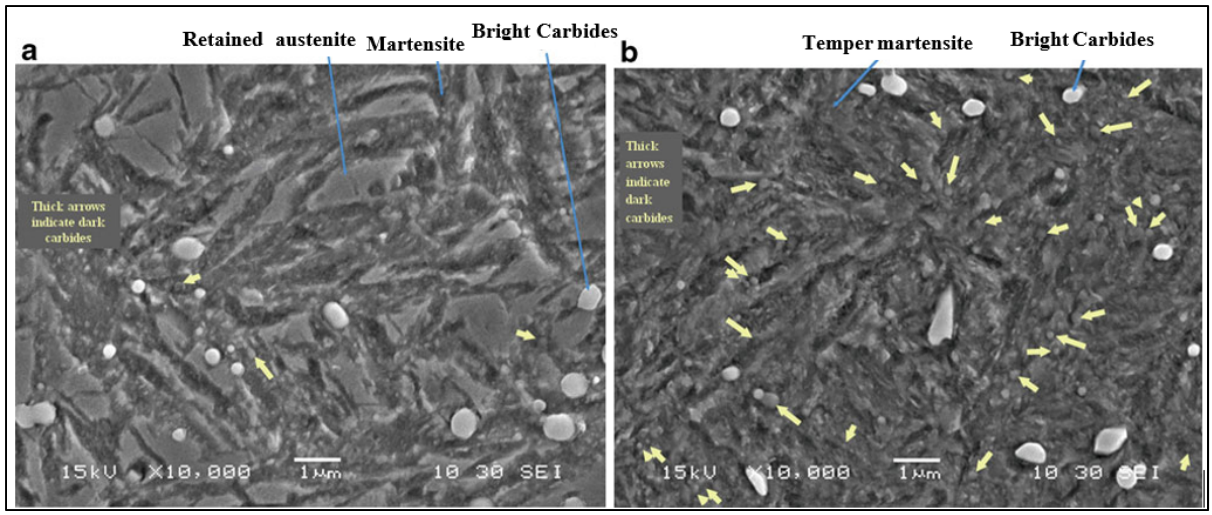

Figure 1-7 Scanning electron microscopy (SEM) image of A2 sample: (a) oil-quenched and tempered; (b) cryogenically treated in liquid nitrogen for 24 hrs (Dhokey and Nirbhavne 2009).

1.5.3 Combined effect from retained austenite transformation to martensite and fine carbide precipitation within martensite

The third group of researchers reported that the transformation of retained austenite into martensite and the modification of martensite and precipitation of a different type of carbides are playing important roles in wear resistance improvements of tool steels (Collins 1996, Collins and Dormer 1997, Yun et al. 1998, Mohan et al. 2001, Preciado 2006).

Collins (1996) studied the influence of cryogenic treatment on the enhancement of properties such as hardness, toughness, wear resistance, dimensional stability, corrosion resistance of cold work (D2) and high-speed (ASP 23) steels. He observed hardness enhancement, increase in dimensional stability, toughness reduction, and a small increase in wear resistance. These findings were related to the full transformation of austenite to martensite. He also found that holding at cryogenic temperature for sufficient time would produce a large number of fine carbides during subsequent tempering which will improve wear resistance and toughness. Collins and Dormer (1997) examined the effect of cryogenic treatment on hardness, toughness, wear resistance, and microstructure of D2 tool steel. Results showed the presence of retained austenite after cryogenic treatment and little variation in size and

distribution of carbides (Collins and Dormer 1997). The effect of cryogenic temperature on carbide count (carbides finer than 5nm) is shown in Fig.1-8 (Collins and Dormer 1997). It can be seen that by reducing temperature to cryogenic range for a constant austenitizing temperature, the number of counted carbides increases. However, by increasing austenitization temperature, the number of carbides was reduced (Collins and Dormer 1997).

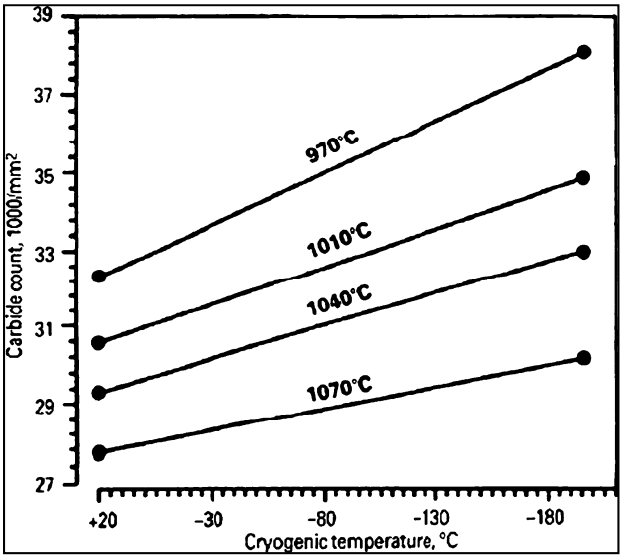

Figure 1-8 Effect of cryogenic temperature on carbide counts in D2 tool steel, after austenitizing at various temperatures (Collins and Dormer 1997).

The effect of holding time at cryogenic temperature on the count of carbides is shown in Fig.1-9. For a constant austenitizing temperature, longer soaking time at cryogenic temperature increases the number of carbides but their rate of formation is reduced. In addition, higher austenitizing temperature shows lower count for carbides because of their dissolutions at higher temperatures. Based on Collins and Dormer study (1997), the complete transformation of retained austenite to martensite does not happen after cryogenic treatment and instead new carbides are formed. However, in their work the governing mechanisms and the required driving force for the formation of the new type of carbides were not discussed.

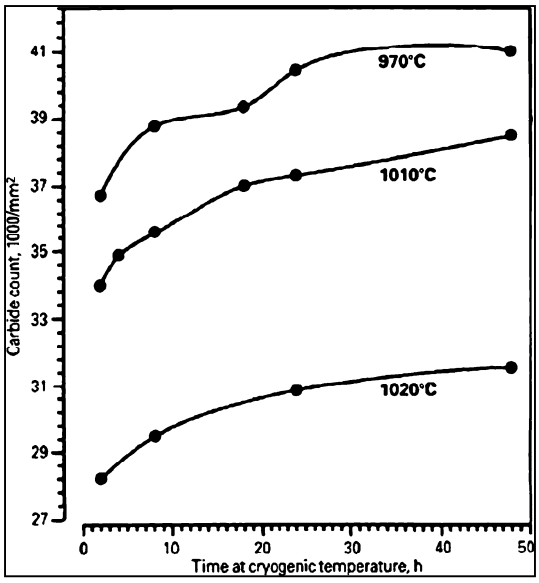

Figure 1-9 Effect of holding time at 77K on carbide counts in D2 tool steel, after austenitizing at various temperatures (Collins and Dormer 1997).

1.6 Cryogenic treatment: state-of-the-art today

The above literature review showed that the benefits of cryogenic treatment are well recognized by the scientific community and the question on the possible benefits of cryogenic treatment has changed to how this process works. In the present literature review, the ideas for these improvements proposed by different researchers have reviewed; but it is very difficult to draw a cohesive picture. One of the main reasons is the lack of systematic studies covering the entire cycle of the cryogenic process. Specifically, many researchers do not give the complete cycle of their procedure and processing routes. Also, heat treatment cycles, sample size, equipment type, etc are different from one paper to another, thereby making difficult any in-depth analysis. In this thesis, through a systematic design of experiments, the most critical cryogenic process parameters are analyzed and it is attempted to develop a better understanding of the fundamental mechanisms governing cryogenic treatment.

CHAPTER 2
ARTICLE 1: SIMULTANEOUS ENHANCEMENT OF STRENGTH AND DUCTILITY IN CRYOGENICALLY TREATED AISI D2 TOOL STEEL

Hadi Ghasemi-Nanesa, Mohammad Jahazi,

Department of Mechanical Engineering, École de Technologie Supérieure, 1100 rue Notre-Dame Ouest, Montréal (QC) H3C 1K3 Canada.

An article adopted from this chapter has been published in Journal of Materials Science and Engineering A, vol. 598 (2014), pp. 413-419. DOI: 10.1016/j.msea.2014.01.065

Abstract

In this research, the effect of cryogenic treatment on microstructural evolution and mechanical properties enhancement of AISI D2 tool steel was investigated. Cryogenic treatment down to liquid nitrogen temperature (77K) was added to the conventional heat treatment between hardening and tempering steps. Electron microscopy investigation showed higher volume fraction of fine carbides with average diameter below 1μm indicating effective retardation in carbide coarsening process as a results of cryogenic treatment. A modification in types of carbides was also observed after cryogenic treatment. X-ray diffraction diagrams revealed transformation of retained austenite to martensite at cryogenic temperature. Weakening or removal of carbides peak in the X-ray diagram was considered as evidence of carbides different behavior at cryogenic temperature. Mechanical testing results indicated higher ultimate tensile strength, better ductility, and higher elastic modulus after cryogenic treatment. Analysis of stress-strain diagrams revealed different strain hardening behavior for cryogenically treated alloy when compared to the conventionally heat treated one. Fractography results confirmed strain hardening behavior and showed cleavage fracture for conventionally treated alloy but mixed cleavage - ductile fracture mode for cryogenically treated alloy. The improved mechanical properties after cryogenic treatment are interpreted in terms of the influence of higher volume fraction and uniform distribution of fine carbides in reducing the average active dislocations length and enhancement of the flow stress at any given plastic strain.

2.1 Introduction

Tool steels are extensively used in modern industry for applications where high strength along with wear resistance and toughness are required [1]. These alloys are characterized by relatively large amounts of alloying elements such as tungsten, molybdenum, vanadium, and chromium and obtain their superior mechanical properties through heat treatment processes specific to each alloy [1-3]. The *conventional* heat treatment of tool steels consists of solutionizing in the austenitic region followed by quenching and simple or double tempering. The final microstructure of these steels is composed of martensite matrix, primary carbides, and secondary carbides (formed during the tempering step) and some undesired retained austenite [4, 5].

Cryogenic treatment is an additional process to the conventional heat treatment of tool steels originally intended to transform the residual austenite in the microstructure and therefore improve the wear resistance. The process involves cooling the materials down to liquid nitrogen temperature (77K), holding for specific time, and then heating up to room temperature (RT) followed by final tempering [4]. A number of cold work tool steels, high-speed tool steels, carburized steels, and stainless steels have been submitted to cryogenic treatments and the reports show considerable enhancement in wear resistance of these steels [6-10]. Despite the reported results on beneficial effects of cryogenic treatment, investigations about the fundamental mechanism governing cryogenic treatment and their effect on the microstructure of tool steels started only in late 1990's [6, 11-15].

Transformation of retained austenite to martensite, precipitation of fine η-carbides and relaxation of residual stresses reliefs have been suggested by researchers as possible mechanism responsible for the observed enhancement of wear resistance after cryogenic treatment [6]. However, these studies which mostly started in late 1990's are limited and have been carried out on different alloys and/or for different heat treatment conditions [6]. Moreover, in recent years in addition to superior wear resistance properties simultaneous high levels strength and ductility are also required, thereby further increasing the interest for

a better understanding of the fundamental mechanisms governing the evolution of the microstructure during cryogenic treatment and its influence on the mechanical properties of tool steels [16-19].

AISI D2 tool steel is cold work tool steel with high strength and good wear resistance after conventional heat treatment but it suffers from poor ductility and brittle fracture. However, in most applications of AISI D2, high strength and good ductility are simultaneously required [7-10]. Although some authors have reported wear resistance enhancement of D2 steels after cryogenic treatment [7-10], others have reported hardness improvement but toughness reduction after cryogenic treatment [20]. More work is therefore required to better understand the interrelationships between cryogenic process parameters, microstructure evolution, and mechanical properties. The present work inscribes in this context and aims to study such interactions after cryogenic treatment of AISI D2 cutting tool steel with the view to find optimum combination of the tensile properties and ductility. In this regard, microstructure evolution and mechanical properties of conventionally and cryogenically treated specimens have been studied using advanced characterization methods and the obtained results analyzed in the framework of existing theories on dislocation interaction with carbon atoms and precipitates.

2.2 Experimental procedure

AISI D2 sheets with following chemical composition of Fe-1.54wt%C-0.33wt%Si-0.32wt%Mn-11.88wt%Cr-0.76 wt%Mo-0.75 wt%V-0.008 wt%P-0.008wt%S were employed in this research. Samples were taken in random selection from a large industrial heat treatment batch. The heat treatment process was carried out in an industrial vacuum furnace, consisting of the following: 1) two preheating steps at 950K and 1150K, respectively; followed by temperature rise to 1300K, 2) austenitization at 1300K for 20 minutes followed by Argon quenching with a pressure of 2 bars at about 323K to avoid quench - cracking. For conventional heat treated alloy, three tempering cycles were conducted at 790K-2hrs for each cycle. For cryogenic treatment, the plates were cooled down to 77K with a processing time of

4hrs between quenching and tempering. After cryogenic treatment, two tempering cycles were applied at 790K and 780K, each with duration of 2hrs. The schematics of heat treatment cycles for conventionally (a) and cryogenically (b) treated samples are shown in Fig.2-1.

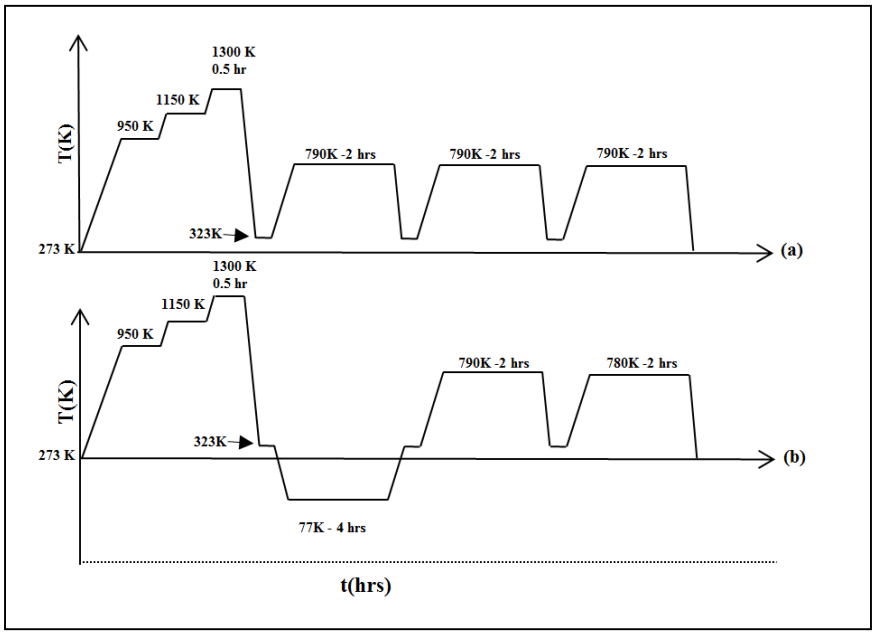

Figure 2-1 Schematic representing typical time-temperature profile of the applied heat treatment cycles: (a) conventional heat treatment: austenitizing, quenching, and triple tempering (b) cryotreatment: austenitization, quenching, cryogenic cycle, and double tempering.

For macrohardness measurement, Rockwell(C) hardness tester with major load of 150kg was used. Sub-size samples for tensile tests were prepared according to ASTM-E8 standard. Uniaxial tensile tests were carried out using MTS793 machine with a crosshead speed of $1mm.min^{-1}$ using extensometer in order to precisely measure mechanical properties including the ultimate tensile strength (UTS), the ultimate tensile strain, and the elastic modulus. To accurately examine the presence of phases, X-ray diffraction (XRD) analyses were conducted on as-quenched, conventionally treated, and cryogenically treated samples. Angular ranges of 35-105° 2θ with Cu-Kα radiation at 45kV and 40mA and a step scanning at 0.02°2θ with count time of 1second per point were used for the XRD experiments. 3%Nital solution was utilized for etching. Fractographical and microstructural investigations of both

conventionally and cryogenically treated samples were conducted using S3600N (Hitachi) conventional scanning electron microscope (SEM) and field emission SEM- SU70 (Hitachi). The volume fraction of carbides and other second phase particles were calculated using the MIP® image analysis software (Nahamin Pardazan Asia, www.metsofts.com).

2.3 Results

2.3.1 Microstructure characteristics

The initial microstructure before hardening treatment is usually the annealed condition (as-received alloy). In the annealed condition, the matrix is composed of ferrite and globular carbides as shown in Fig.2-2. The larger carbides are mostly primary M_7C_3 carbides formed on the austenite grain boundaries and then dispersed as a result of hot working [21]. The other carbides such as M_2C and $M_{23}C_6$ are the result of secondary precipitation in the spherodiziation of carbides produced by the transformation of austenite on cooling after normalizing heat treatments. The formation of MC, M_2C (same chemical composition to M_7C_3 carbides), and $M_{23}C_6$ carbides are possible based on thermodynamic calculations [21].

Figure 2-3 shows SEM images from the microstructure of both conventionally and cryogenically treated specimens. The microstructure is composed of tempered martensite, primary carbides (PCs), large secondary carbides (LSCs), and small secondary carbides (SSCs). Comparison between microstructures obtained after cryogenic treatment and conventional treatment indicates that a higher volume fraction of SSCs is present in the microstructure after cryogenic treatment.

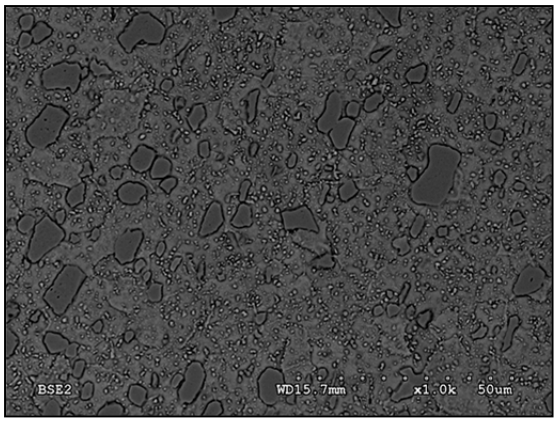

Figure 2-2 SEM micrograph of the starting microstructure of the AISI D2 tool steel (annealed condition). Matrix is composed of ferrite and globular carbides. Larger carbides are mostly primary M_7C_3 carbides. Small carbides are either M_2C or $M_{23}C_6$.

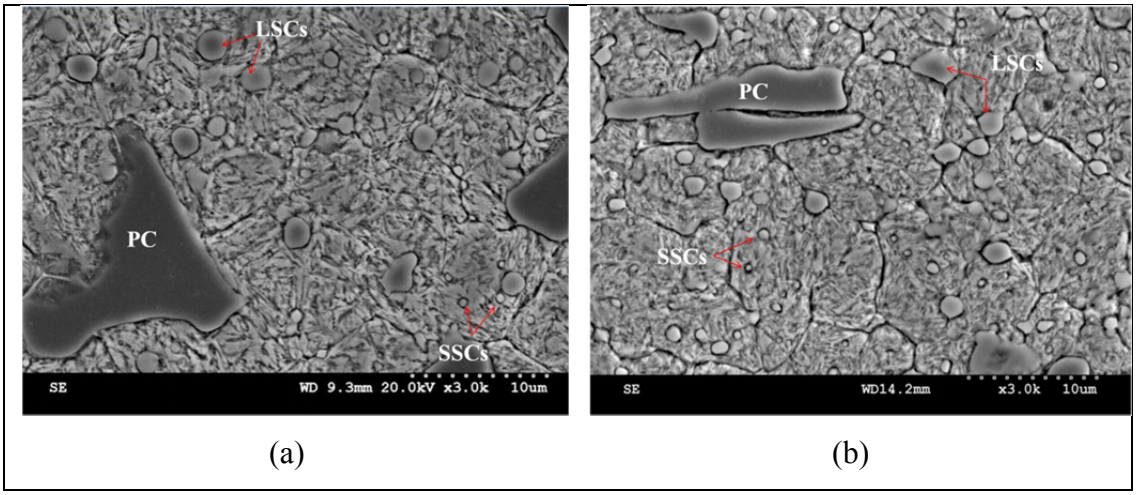

Figure 2-3 Effect of two applied heat treatment cycles on the presence of carbides with average diameter below 1µm, in the microstructure of: (a) conventionally heat treated specimen and (b): cryotreated specimen. The microstructures revealed by etching with 3%Nital solution exhibit tempered martensite, primary carbide (PC), large secondary carbide (LSC), and small secondary carbide (SSC). Higher population of SCCs is clearly visible after (b).

Further information about the size and volume fraction of secondary carbides was obtained from image analysis of the unetched microstructure. In fact, etching could cause higher

volume fraction measurement due to the bigger perceptible area for carbides and lower amount for small carbides (as they may be washed out during the etching process). Figure 2-4 shows the image analyses results about the size and volume fraction of carbides for (a) as-quenched condition, (b) conventionally treated, and (c) cryogenically treated samples. In the present work, the carbides were divided in three ranges of sizes: (1) smaller than or equal to 1µm (SSCs); (2) between 1µm and 5µm (LSCs); (3) larger than or equal to 5µm (PCs). Das et al. [14] have considered a forth range between 0.1µm and 1µm. However, Farina et al. [22] reported that image analysis around 0.1µm does not show any differences between conventionally and cryogenically treated samples because of background noise effect. As shown in Fig. 2-4b and c, after cryogenic treatment, the volume fraction of carbides with average diameter below 1µm is higher than conventionally treated one and for carbides larger than or equal to 5µm it is lower for the cryogenically treated sample. Hence, it can be assumed that cryogenic treatment in addition to delaying carbides coarsening, results in the formation of more fine carbides.

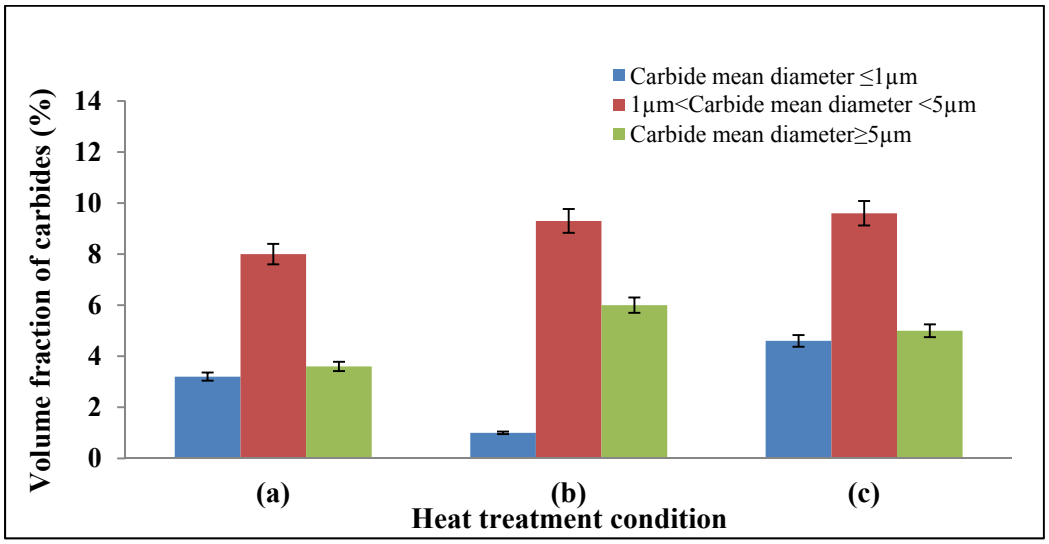

Figure 2-4 Influence of cryotreatment process on the size distribution and volume fraction of carbides in comparison with conventional heat treatment using image analysis results from the microstructures of: (a) as-quenched, (b) conventionally heat treated, and (c) cryogenically treated samples. Higher volume fraction of carbides with average diameter below 1µm was obtained after (c) in comparison with (b).

2.3.2 Crystallographic studies by XRD

XRD experiments were conducted on (a) as-quenched, (b) conventionally treated, and (c) cryogenically treated samples with the view to investigate the presence of various phases after each heat treatment, to study carbides behavior, and to measure carbon content of martensite using the (110) and (200) reflections with a method mentioned in Ref.23. Four peaks for martensite (M), one small peak for austenite- $\gamma(222)$ just in as-quenched sample (Fig.2-5a), and carbides peaks for each heat treatment condition were identified by X'Pert HighScore software as well as by searching in the published literature [10,14] as illustrated in Fig.2-5. For 2θ angles between 35°- 55°, four peaks were detected corresponding to M_7C_3, Cr_7C_3, M_7C_3 and $M_{23}C_6$ carbides, and martensite. The analysis of the results indicate that, M_7C_3 (420), Cr_7C_3 (150) carbides peaks show superposition close to 39° and M_7C_3 (202), Cr_7C_3 (112) peaks show superposition close to 42°. Small amounts of retained austenite, which were observed during the metallography examination process of the as-quenched condition has no trace in the XRD diagrams after both heat treatments. For the conventionally heat treated sample, two superposed peaks of M_7C_3, Cr_7C_3 in 39° and 42° show intensity enhancement, which could be related to increase in the volume fraction of carbides.

It should be mentioned that as the peak intensity of M_7C_3 (402) around 52.5° is almost identical for the three microstructural conditions therefore the observed augmentation in the peak intensity is related to Cr_7C_3 carbides. In contrast, for cryogenically treated specimens there is a reduction and even peak removal for Cr_7C_3 carbides in 39° and 42°. It is probable that the enhancement in the volume fraction of Cr_7C_3 carbides which takes place after conventional heat treatment has been significantly slowed down or even stopped by cryogenic treatment.

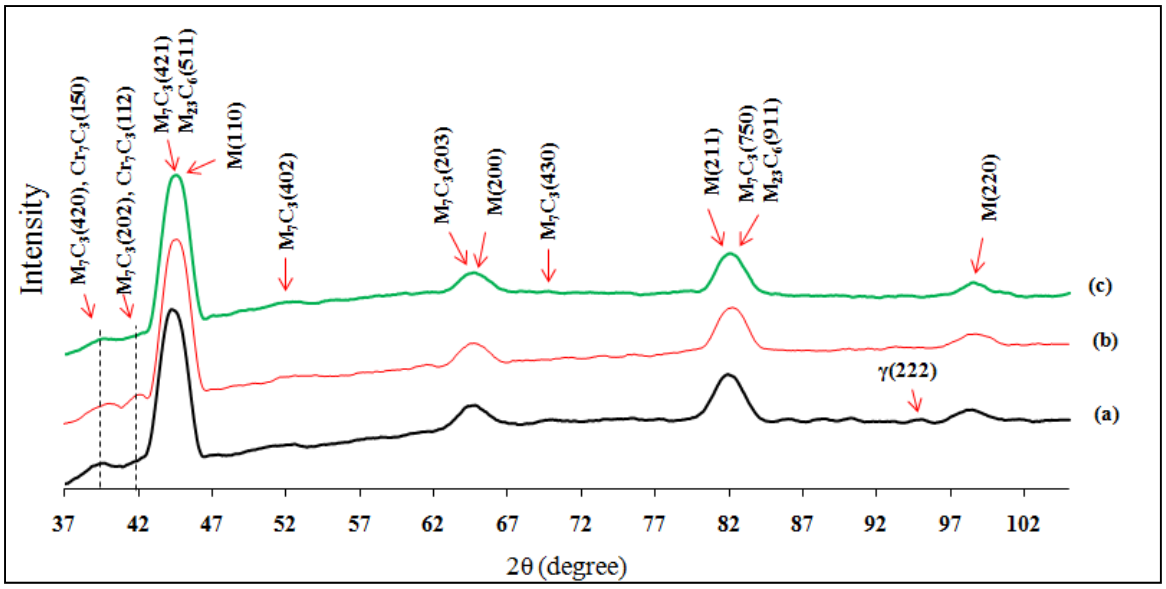

Figure 2-5 X-ray diffraction line profiles of (a) quenched, (b) conventionally heat treated, and (c) cryogenically treated specimens showing different evolution in carbides types after each treatment. Each profile represents the set of (hkl) indicating different diffraction planes of martensite, M_7C_3, $M_{23}C_6$, Cr_7C_3 carbides (existence of small (222) peak of retained austenite in the quenched sample). Retained austenite peak was eliminated after (b) and (c) treatments in different ways. Enhancement in the volume fraction of Cr_7C_3 carbides observed after conventional heat treatment (b) was slowed down or even stopped by (c) cryogenic treatment.

The carbon content of martensite shows the clear dependency of the matrix to the level of tetragonality in the crystal lattice. This factor was measured to be about 0.62wt% for the as-quenched sample, and 0.60wt% for the conventionally treated alloy. But this value was found to be 0.51wt% for cryogenically treated alloy indicating lower carbon content after cryogenic treatment. Lower carbon content was reported by Li et al. [24] on a cryogenically treated tool steel as well.

2.3.3 Mechanical properties

The influence of cryogenic treatment on mechanical properties was studied by conducting uniaxial tensile tests in both conventionally and cryogenically treated alloys as shown in Fig. 2-6(a-b). True stress (σ)-strain (ε) diagrams of cryogenically treated alloy showed 60%

ductility enhancement with 6% enhanced strength. Ductility enhancement after cryogenic treatment is analyzed in terms of its impact on the strain hardening coefficient θ (dσ/dε) and justified based on the theory proposed by Koneva and Kozlov [25].

The θ-ε diagram in Fig.2-6(a-b) shows different stages in strain hardening behavior. The stage 1 shows strain independent positive and constant coefficient, θ, for both treated alloys. In stage 2, the parabolic behavior in which, θ decreases with more straining (ε) was observed. Stage 2 is finished with constant and nearly equal to zero value for θ. In stage3, θ is negative indicating that the neck develops. For the conventionally treated alloy, immediate fracture is observed in stage 3. By contrast, for cryogenically treated alloy, after stage 3, a fourth stage with negative and almost constant θ was observed. This post-uniform plastic strain, which is a major component of the total elongation and area-reduction, started after UTS.

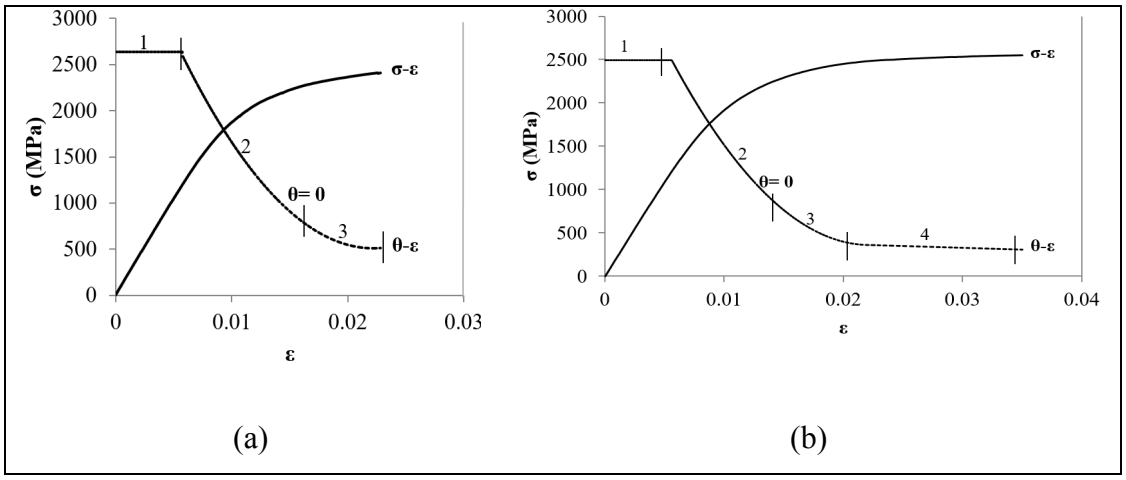

Figure 2-6 Simultaneous enhancement in strength and ductility from (a) conventionally heat treated sample to (b) cryogenically treated samples using true stress-strain(σ-ε) diagrams and related strain hardening behavior (θ-ε diagrams). θ is defined in the figure. In the case of the cryogenically treated samples (b) a fourth stage was revealed in the θ-ε diagram showing negative and almost constant θ (i.e. post-uniform plastic strain) indicating that cryogenic treatment results in concomitant increase of strength and ductility.

SEM micrographs from the fracture surface of both conventionally and cryogenically treated samples are shown in Fig.2-7(a-c). The main characteristics of fracture surface are cleavage

facets on PCs, cracking of PCs, and cracking at the interface between the PCs and the matrix (all shown in the area with dashed line) for both treated alloys. LSC and SSC particles are readily observable in fracture surfaces (shown by numbers 1 to 3). Unlike PCs, no cracking of SC particles could be identified on the fracture surfaces in both conventionally and cryogenically treated alloys. Generally, fracture starts with the cracking of primary carbides, cracking of primary carbides-matrix interfaces and nucleation of microvoids by decohesion of secondary carbides followed by cleavage fracture. However in the fracture surface of cryogenically treated sample, areas showing post uniform plastic deformation were observed (Fig.2-7(c)).

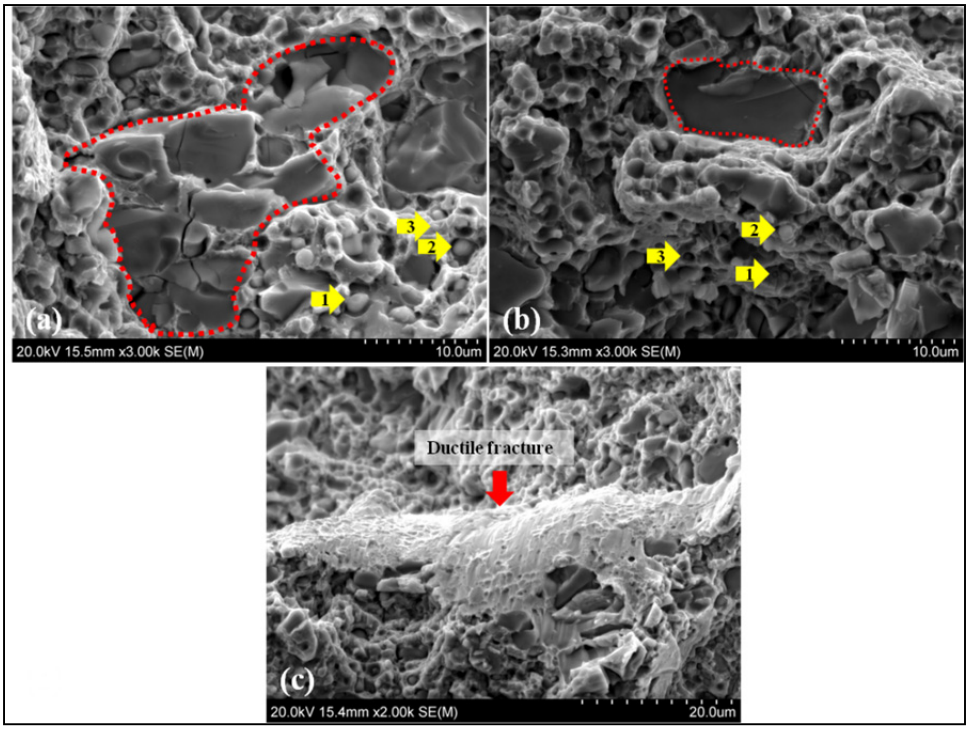

Figure 2-7 SEM micrographs from the fracture surface of (a) conventionally heat treated and (b) cryogenically treated samples after uniaxial tensile tests. Cleavage facets in primary carbides, cracking of primary carbides, indicated by red dashed lines, and dimples on secondary carbides, numbered from 1 to 3, are present for the two conditions. In (c) an area from sample (b) showing ductile fracture is illustrated.

The main characteristics of fracture surface are cleavage facets on PCs, cracking of PCs, and cracking at the interface between the PCs and the matrix (all shown in the area with dashed line) for both treated alloys. LSC and SSC particles are readily observable in fracture surfaces (shown by numbers 1 to 3). Unlike PCs, no cracking of SC particles could be identified on the fracture surfaces in both conventionally and cryogenically treated alloys. Generally, fracture starts with the cracking of primary carbides, cracking of primary carbides–matrix interfaces and nucleation of microvoids by decohesion of secondary carbides followed by cleavage fracture. However in the fracture surface of cryogenically treated sample, areas showing post uniform plastic deformation were observed (Fig.2-7(c)). The presence of such features is indicative of partly ductile fracture of the material and confirms the occurrence of post-uniform plastic strain during tensile testing in cryogenically treated material. Table 2.1 shows the results for tensile tests of (a) conventionally treated, and (b) cryogenically treated samples and macrohardness measurements as well. Interestingly, simultaneous 60 % enhancement of ductility and 6 % enhanced UTS were observed after cryogenic treatment. Also, the slope of σ-ε curves for both treated alloys showed slight enhancement of the elastic modulus after cryogenic treatment which is in agreement with results reproduced by Baldissera et al. [17, 18]. Li et al. [26] also have reported elastic modulus enhancement after cryogenic treatment with internal friction studies for a newly developed cold work die steel. The hardness measurement showed +1HRC enhancement for cryogenically treated sample which may be related to the transformation of retained austenite to martensite at cryogenic temperature. The Macrohardness enhancements in the range of +0.5 HRC to +4 HRD have been reported in the literature and related to retained austenite transformation to martensite during cryogenic treatment [6, 24].

Table 2.1 Tensile test results for (a) conventionally heat treated, (b) cryogenically treated samples.

	UTS (MPa)	Ultimate tensile strain (ε)	Elastic Modulus (GPa)	Hardness (R_C)
a	2410	0.022	209	57
b	2550	0.035	214	58

2.4 Discussion

2.4.1 Variation in characteristics of small secondary carbides

Comparison of the XRD diagrams in Fig.2-5(a to c) reveals that the higher intensity of the two superposed peaks observed around 39° and 42° in Fig. 2-5(b) (i.e. after conventional heat treatment) can be associated with the rapid growth of Cr_7C_3 carbides. Das et al. [14] have reported that the presence of some Cr_7C_3 carbide along with alloyed carbides is inevitable in AISI D2 tool steel. Also Speich and Leslie [27] reported that in conventional tempering temperature range of 773K-873K, Cr addition delays the softening, but little or no secondary hardening take place because Cr_7C_3 coarsens very rapidly at this tempering range. However, the XRD results for cryogenically treated specimens (Fig.2-5(c)) indicate that there is a reduction and even peak removal for Cr_7C_3 carbides around 39° and 42° after final tempering. As shown in Fig.2-4, the higher volume fraction of SSCs (<1μm diameter) after cryogenic treatment can be related to both retardation in the volume fraction enhancement of Cr_7C_3 carbides and dissolution of some Cr_7C_3 carbides (Fig.2-5(c)) as suggested by Tyshchenko et al. [28].

The proposed mechanism is based on the provision of more carbon atoms through the dissolution of primary carbides and the increased interactions of these carbon atoms with dislocations at cryogenic temperature. The interactions between carbon atoms, in saturated state, in the octahedral sites of martensite crystal lattice and dislocations form potential sites for SSCs nucleation at cryogenic temperature followed by precipitation during subsequent tempering [6, 28-31]. Also, studies on the effect of Cr on the dissolution of cementite in cold worked pearlitic steels indicated that Cr can increase the enthalpy of binding between carbon atoms and dislocations, but it doesn't show strong effect on the strengthening of interatomic bonds in the carbide's lattice [30-32]. On the basis of the above analysis, it can be reasonably assumed that the dissolution of some Cr_3C_7 carbides is occurring during cryogenic treatment which leads to XRD peak weakening or removal around 39° and 42° as well as higher volume fraction of SSCs (i.e. size <1μm diameter) after tempering.

2.4.2 On the enhancement of ductility

Fracture surface of conventionally treated sample indicates the brittle nature of the fracture (Fig.2-7(a)). Several origins have been reported for the observed brittle fracture including high tetragonality of martensite or high carbon content of martensite, fragmentation in large carbides interfaces with matrix, temper embrittlement by segregation of embrittling elements such as Mn and Cr to prior austenite grain boundaries in the ~640K to ~840K temperature range, and austenite decomposition at tempering temperature leading to film-like cementite formation at the interface of austenite with martensite [27, 30, 32].

The results obtained in the present research indicate that a combination of the above factors has contributed to the observed brittleness of the alloy after conventional heat treatment. Specifically, the carbon content of martensite in the conventionally treated alloy is higher than that of the cryogenically treated one (0.61wt% instead of 0.51wt%). Although measurement of the level of martensite tetragonality before and after cryogenic treatment was out of the scope of the present work; however, such data has already been reported in the literature consistently [26, 33]. The enhanced intensity of Cr_7C_3 carbides peaks was observed (Fig.2-5(b)), the tempering temperature is in the range of temper embrittlement, and small amount of austenite has disappeared during conventional tempering (Fig.2-5(b)).

In contrast, for cryogenically treated sample, post-uniform plastic strain was observed (Fig.2-6(b)). The peak intensities of Cr_7C_3 carbides were weakened or removed after cryogenic treatment (Fig.2-5(c)). As the reduction in the peak intensity has direct relation with reduction in the volume fraction of each phase, it can therefore be said that the volume fraction of Cr_7C_3 has reduced after cryogenic treatment. The dissolution of some of Cr_7C_3 carbides in the microstructure aided to form nucleation sites for SSCs (higher volume fraction of SSCs from Fig.2-4(c)). It can be concluded that the ductility enhancement for tempered martensite after cryogenic treatment (Fig.2-7(c) and Table 2.1) is related to a combined effect of lower carbon content of martensite and reduction in the volume fraction of Cr_7C_3 carbides (Fig.2-4(c)).

2.4.3 On the enhancement of strength

Figure 2-8 shows the stitched images taken from 3 different sections employed for the measurement of volume fraction of carbides with average diameter below 1μm for conventionally (a) and cryogenically (b) heat treated specimens, respectively. More uniform distribution of carbides was measured for cryogenically treated specimens. Precipitated carbides during tempering especially SSCs with average diameter ≤ 1μm (Fig.2-4(c)) provide strength enhancement (Table 2.1). Indeed dislocations cannot pass through incoherent precipitates such as SSCs, but they bow around and pass by the Orowan mechanism [34]. As the Orowan stress is inversely proportional to the distance between the precipitates, higher amounts of fine carbides with more uniform distribution reduces the average active dislocation link length and enhances the flow stress at any given plastic strain [32, 34].

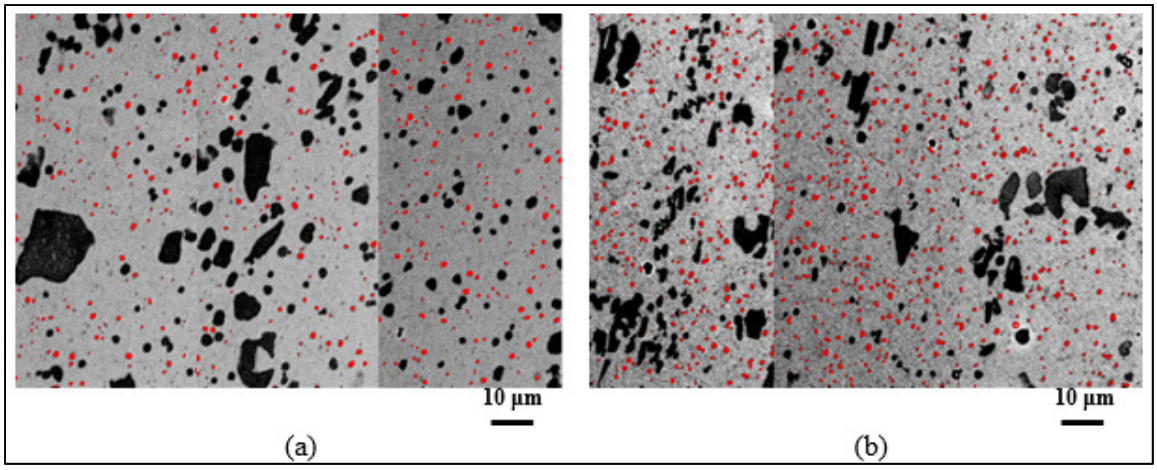

Figure 2-8 The carbides with average diameters below 1μm are highlighted by red spots in the image using image analyzing software to compare their volume fraction and distribution in (a) conventionally treated sample and (b) cryogenically treated one. Higher volume fractions with more uniform distribution of carbides is shown in (b) which results in higher UTS as indicated in mechanical testing results (Fig.2-6).

The concomitant improvement of strength and ductility after cryogenic treatment can be related to three distinct microstructural changes: 1) higher volume fraction and more uniform distribution of carbides with average diameter below 1μm (improvement of strength), 2) removing retained austenite by transformation to martensite (improvement of hardness) and

3) lower carbon content of martensite and reduction in the peak intensity of Cr_7C_3 carbides illustrated in XRD diagram of cryogenically treated alloy (improvement of ductility).

2.5 Conclusions

The influences of cryogenic treatment on microstructure evolution and mechanical properties of AISI D2 tool steel was studied and compared with conventional heat treatment. Simultaneous enhancement of ductility and strength with higher elastic modulus was obtained for cryogenically treated alloy. Lower carbon content of martensite and higher volume fraction with more uniform distribution of carbides with average diameter below 1μm made major contributions to mechanical properties improvement in the cryogenically treated alloy. Also the transformation of retained austenite present after quenching to martensite at cryogenic temperature resulted in higher strength and hardness. The application of cryogenic treatment appears to have delayed the coarsening of precipitates; therefore no loss in tensile-strength properties was observed. Post-uniform plastic strain was observed for cryogenically treated alloy. The higher ductility level for cryogenically treated samples was further confirmed by fractography studies.

Acknowledgements

The authors would like to thank the National Sciences and Engineering Research Council of Canada (NSERC) for their support and financial contribution through the ENGAGE program. The authors also appreciate the collaboration of DK SPEC Inc. in providing materials and experiments. Special thanks are due to Mr. Gil Trigo, Consultarc Inc. for valuable discussions throughout the project.

References

[1] A. P. Gulyaev, Improved methods of heat treating high speed steels to improve the cutting properties, Metallurgy 12 (1937) 65-70.

[2] F. Meng, K. Tagashira, R. Azuma, H. Sohma, Role of eta-carbide precipitations in the wear resistance improvements of Fe-12Cr-Mo-V-1.4C tool steel by cryogenic treatment, ISIJ International 34 (1994) 205-210.

[3] D. N. Collins, Deep cryogenic treatment of tool steels: A review, Heat Treatment of Metals 23-2 (1996) 40-42.

[4] ASM Handbook, Vol. 4: Heat treating, ASM International (1991).

[5] K. E. Thelning, Steels and its heat treatment, Butterworth & Co Publishers Ltd, London (1975).

[6] S. G. Singh, J. Singh, R. Singh, H. Singh, Metallurgical principles of cryogenically treated tool steels - A review on the current state of science, International Journal of Advanced Manufacturing Technology 54 (2011) 59-82.

[7] D. N. Collins, J. Dormer, Deep cryogenic treatment of a D2 cold-work tool steel, Heat Treatment of Metals 24-3 (1997) 71-74.

[8] R. F. Barron, Cryogenic treatment of metals to improve wear resistance, Cryogenics 22 (1982) 409-413.

[9] D. Das, A.K. Dutta, K.K. Ray, Inconsistent wear behaviour of cryotreated tool steels: Role of mode and mechanism, Materials Science and Technology 25 (2009) 1249-1257.

[10] D. Das, A.K. Dutta, K.K. Ray, On the enhancement of wear resistance of tool steels by cryogenic treatment, Philosophical Magazine letters 88 (2008) 801-811.

[11] D. Yun, L. Xiaoping, X. Honoshen, Deep cryogenic treatment of high-speed steel and its mechanism, Heat Treatment of Metals 3 (1998) 55-59.

[12] A. Bensely, A. Phadhakaran, L. Mohan, G. Nagarajan, Enhancing the wear resistance of case carburized steel (En 353) by cryogenic treatment, Cryogenics 45 (2005) 747-754.

[13] P. F. Stratton, Optimising nano-carbide precipitation in tool steels, Materials Science and Engineering A 449-451 (2007) 809-812.

[14] D. Das, A. K. Dutta, K. K. Ray, Sub-zero treatments of AISI D2 steel: Part I. Microstructure and hardness, Materials Science and Engineering A 527-9 (2010) 2182-2193.

[15] V. G. Gavriljuk, W. Theisen , V. V. Sirosh, E. V. Polshin, A. Kortmann, G. S. Mogilny, Y. N. Petrov, Y. V. Tarusin , Low-temperature martensitic transformation in tool steels in relation to their deep cryogenic treatment, Acta Materialia 61 (2013) 1705-1715.

[16] S. Zhirafar, A. Rezaeian, M. Pugh, Effect of cryogenic treatment on the mechanical properties of 4340 steel, Journal of Materials Processing Technology 186-1-3 (2007) 298-303.

[17] P. Baldissera, Fatigue scatter reduction through deep cryogenic treatment on the 18NiCrMo5 carburized steel, Materials and Design 30 (2009) 3636-3642.

[18] P. Baldissera, C. Delprete, Effects of deep cryogenic treatment on static mechanical properties of 18NiCrMo5 carburized steel, Materials and Design 30 (2009) 1435-1440.

[19] S. Harish, A. Bensely, D. Mohan Lal, A. Rajadurai, Gyöngyvér B. Lenkey, Microstructural study of cryogenically treated En 31 bearing steel, Journal of Materials Processing Technology 209 (2009) 3351-3357.

[20] I. Wierszyllowski, The influence of post-quenching deep cryogenic treatment on tempering processes and properties of D2 tool steel. studies of structure, XRD, dilatometry, hardness and fracture toughness, Defect and Diffusion Forum 258-260 (2006) 415-420.

[21] D. Bombac, M. Fazarinc, A. Saha Podder, G. Kugler, Study of carbide evolution during thermo-mechanical processing of AISI D2 tool steel, Journal of Materials Engineering and Performance 22-3 (2013) 742-747.

[22] P. F. da Silva Farina, C. A. Barbosa, H. Goldenstein, Microstructural characterization of an AISI D2 tool steel submitted to cryogenic treatment, ASTM special technical publication 1532 (2012) 57-70.

[23] G. V. Kurdjumov, Martensite crystal lattice, mechanism of austenite-martensite transformation and behavior of carbon atoms in martensite, Metallurgical Transactions A 7 (1976) 999-1011.

[24] S. Li, Y. Xie, X. Wu, Hardness and toughness investigations of deep cryogenic treated cold work die steel, Cryogenics 50 (2010) 89-92.

[25] N. A. Koneva, É. V. Kozlov, Physical nature of stages in plastic deformation, Soviet Physics Journal 33-2 (1990) 165-179.

[26] S. Li, L. Deng, X. Wu, The mechanism investigation of deep cryogenic treatment on high alloy martensitic steel by low frequency internal friction, Cryogenics 50-8 (2010) 433-438.

[27] G. R. Speich, W. C. Leslie, Tempering of steels, Metallurgical Transactions 3-5 (1972) 1043-1054.

[28] A.I. Tyshchenko, W. Theisen, A. Oppenkowski, S. Siebert, O.N. Razumov, A.P. Skoblik, V.A. Sirosh, Yu.N. Petrov, V.G. Gavriljuk, Low-temperature martensitic transformation and deep cryogenic treatment of a tool steel, Materials Science and Engineering A 527 (2010) 7027-7039.

[29] L. Cheng, C.M. Brakman, B.M. Korevaar, E.J. Mittemeijer, The tempering of iron-carbon martensite; dilatometric and calorimetric analysis, Metallurgical Transactions A 19 (1988) 2415-2426.

[30] K.A. Taylor, G.B. Olson, M. Cohen, J.B. Vander Sande, Carbide precipitation during stage I tempering of Fe-Ni-C martensites, Metallurgical Transactions A 20 (1989) 2749-2765.

[31] L. Cheng, N.M. van der Pers, A. Böttger, Th.H. de Keijser, E.J. Mittemeijer, Lattice changes of iron-carbon martensite on aging at room temperature, Metallurgical Transactions A 22 (1991) 1957-1967.

[32] G. Krauss, Martensite in steel: Strength and structure, Materials Science and Engineering A 273-275 (1999) 40-57.

[33] R. Kelkar, P. Nash, Y. Zhu, Understanding the effects of cryogenic treatment on M2 tool steel properties, Heat Treating Progress 7 (2007) 57-60.

[34] D. Hull, D. J. Bacon, Introduction to Dislocations, Fifth ed., Butterworth- Heinemann, Burlington (2011).

CHAPTER 3

ARTICLE 2: ALTERNATIVE PHASE TRANSFORMATION PATH IN CRYOGENICALLY TREATED AISI D2 TOOL STEEL

Hadi Ghasemi-Nanesa, Mohammad Jahazi,
Department of Mechanical Engineering, École de Technologie Supérieure, 1100 rue Notre-Dame Ouest, Montréal (QC) H3C 1K3 Canada.

An article adopted from this chapter has been published in Journal of Materials Science and Engineering A, vol. 634 (2015), pp. 32-36. DOI: doi:10.1016/j.msea.2015.03.028

Abstract

This study based on dilatometry test and microstructural observations showed a different phase transformation path during conventional heat treatment of AISI D2 tool steel instead of the traditionally expected fully martensitic transformation. Transformation started with carbide precipitation and continued with allotriomorphic ferrite, Widmanstätten ferrite, acicular ferrite, and finally bainite formation. This microstructure showed microhardness value of 730HV, which is very high for conventionally cooled samples. They are not expected to have gone under martensitic transformation. The results indicated that bainitic transformation take place even at temperatures near 173K and to obtain fully martensitic microstructure, cooling rates in the range of 50K.s^{-1} must be utilized.

3.1 Introduction

AISI D2 tool steel is widely used in mold making industry and as high speed cutting tools, where ultra-high strength with high wear resistance and good toughness is required [1-3]. Conventional heat treatment consisting of austenitizing + cooling to room temperature + tempering is the principal process used for this alloy. The microstructure of conventionally heat treated alloy (CHT) is composed of laths of martensite, a variety of carbides, and some retained austenite [1-3]. After CHT, AISI D2 tool steel shows ultrahigh strength and

excellent wear resistance; however it suffers from low toughness in service [4]. The decomposition of retained austenite to ferrite and cementite during tempering process (≈ 773K has been related to the loss of toughness of this alloy [4]. It is also generally accepted that martensite start and finish temperatures for AISI D2 steel are at sub-zero temperatures [5, 6] and in order to reduce the amount of retained austenite, an additional step, cryogenic cooling, has been used to insure attaining martensite finish temperature and therefore to obtain the maximum volume fraction of martensite [4].

Most of the research studies on AISI D2 tool steel have been conducted on the microstructure after tempering and little attention has been paid to the microstructure of the as-hardened alloy [4-7]. Moreover, in all the above studies the microstructure before tempering is considered as fully martensitic with very little or no metallographic supports. In the present study, dilatometry tests combined with detailed microstructure observations was carried out and revealed that the microstructure of as hardened (i.e. prior to tempering) AISI D2 steel is composed of mainly bainite (B) with partial carbide precipitation (CP), allotriomorphic ferrite (ATF), Widmanstätten ferrite (WF), and acicular ferrite (AF) formation. This finding can open a new chapter in hardening process of this alloy and bring many possibilities for microstructure engineering. BÄHR DIL 805 A/D dilatometer with a 50nm resolution at high speed cooling rates was used to carry out the hardening treatment. $0.5K.s^{-1}$ and $50K.s^{-1}$were specifically used in this study. The first cooling rate was selected in order to simulate cooling rates employed in conventional hardening heat treatment and the second one was selected fast enough to insure the occurrence of martensitic transformation. The critical cooling rate to get full martensitic microstructure without carbide precipitation during cooling has been reported to be about $10K.s^{-1}$ [8]. In order to pass both martensite start and finish temperatures and also to follow transformations at sub-zero temperatures, the final cooling temperature was selected to be 173K.

3.2 Material and methods

The as-received AISI D2 sheet's chemical composition was Fe-1.54wt%C-0.33wt%Si-0.32wt%Mn-11.88wt%Cr-0.76wt%Mo-0.75wt%V-0.008wt%P-0.008wt%S. Samples were cut into 10mm height and 4mm diameter cylinders. They were then heated to 1303K and maintained for 1200 seconds (20 minutes) following by continuous cooling to 173K with the two above mentioned rates. Finally, they were reheated to room temperature at heating rate of $10K.s^{-1}$.

In order to avoid any oxidation and decarburization, the heat treatment was conducted in vacuum environment. Microstructural studies were conducted using NADE NMM-800TRF optical microscope (OM) and Hitachi-TM3030 scanning electron microscope (SEM), and an FEI Tecnai G2 F20 transmission electron microscope (TEM) operated at 200kV. An etchant with the following composition 40g NaOH+60g H_2O+15g $NaNO_3$ initially proposed by Gouné et al. [9] was modified and successfully used to differentiate bainite (bright) from non-tempered martensite (dark) and to reveal prior austenite grain boundaries (PAGBs). Dilatometry results with their first derivative diagrams were analyzed to study the different phase transformations taking place during cooling. Hardness of the matrix was estimated using Vickers method using an applied load of 200gf for 15s. Special care was taken during hardness measurements to avoid large carbides. The volume fraction of carbides were calculated using S3600N (Hitachi) conventional SEM and the MIP® image analysis software [10].

3.3 Results and discussion

Figure 3-1(a-d) shows the microstructure of the sample cooled at $0.5K.s^{-1}$. In this figure, part (a) displays OM image of the microstructure with the bright area representing bainite and the dark area PAGBs. WF (indicated by the arrow Figure 3-1(b)) was found at PAGBs or developed from any ATF present in the microstructure (indicated by the arrow in Figure 3-1(c) [11]. On the other hand, as shown in Figure 3-1(d); AF grows directly from the interface

of carbides with austenite. Figure 3-1(e) and 3-1(f) show OM and SEM images of the fully martensitic microstructure obtained after a cooling rate of 50K.s^{-1}. No evidence of ATF, WF, AF, and B and no elemental concentration gradient at grain boundaries were found in this sample, indicating similar chemical composition with the parent austenite.

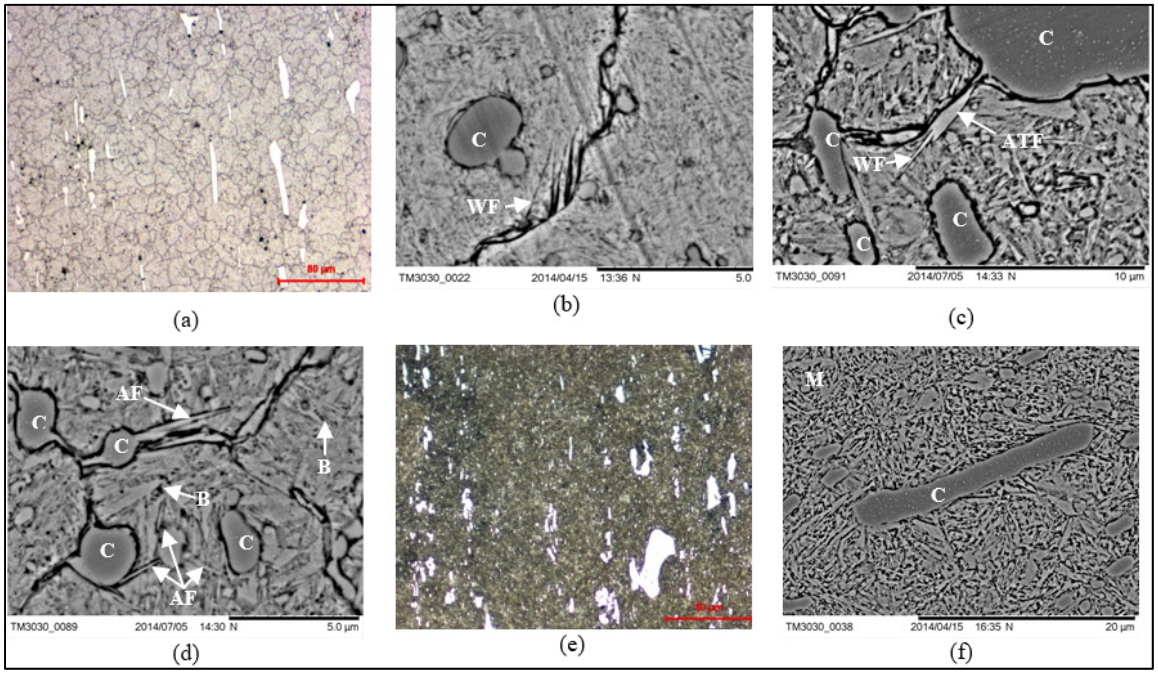

Figure 3-1 Influence of cooling rate on the resulted microstructure (a: optical image) and (b to d: SEM micrographs): cooling rate 0.5K.s^{-1} (e to f): cooling rate 50K.s^{-1} , observation of carbides (C), AlloTriomorphic ferrite (ATF), Widmanstätten ferrite (WF), Acicular ferrite (AF), and Bainite (B) during low cooling rate (a-d) and observation of C and martensite (M) for high cooling rate conditions (e: optical image, f: SEM micrograph).

Figures 3-2(a-b) show TEM micrographs representing bainitic plates including smaller sub-units while Figures 3-2(c-d) depict mixed morphology of laths and plates for martensite. Phase transformations and their related slope changes with associated first derivative curve for the two investigated cooling rates are shown in Figures 3-3 and 3-4. At 0.5K.s^{-1} cooling rate (Fig.3-3(a)), four distinct regions were determined depending on the transformation temperatures and slope changes on dilatometry diagrams. Region (1) is associated with carbide precipitation (CP). Region (2) is related to the temperature interval for ATF and WF formation [12]. Region (3) is associated with AF formation range and region (4) corresponds

to bainitic transformation. The small drop observed around 300K is due to the introduction of liquid nitrogen in the system in order to cool the sample down to 173K. Detailed examination of the first derivative curve of the dilatometry data for region (3) (Fig.3-3(b)) showed slight deviation from linear behavior between 580K and 510K and is ascribed to AF start and finish temperatures. Using first derivative curve, the bainite start temperature (B_s(T)) was measured to be 480K. At 50K.s^{-1} cooling rate, no trace of regions 1, 2, 3 and 4 was discerned.

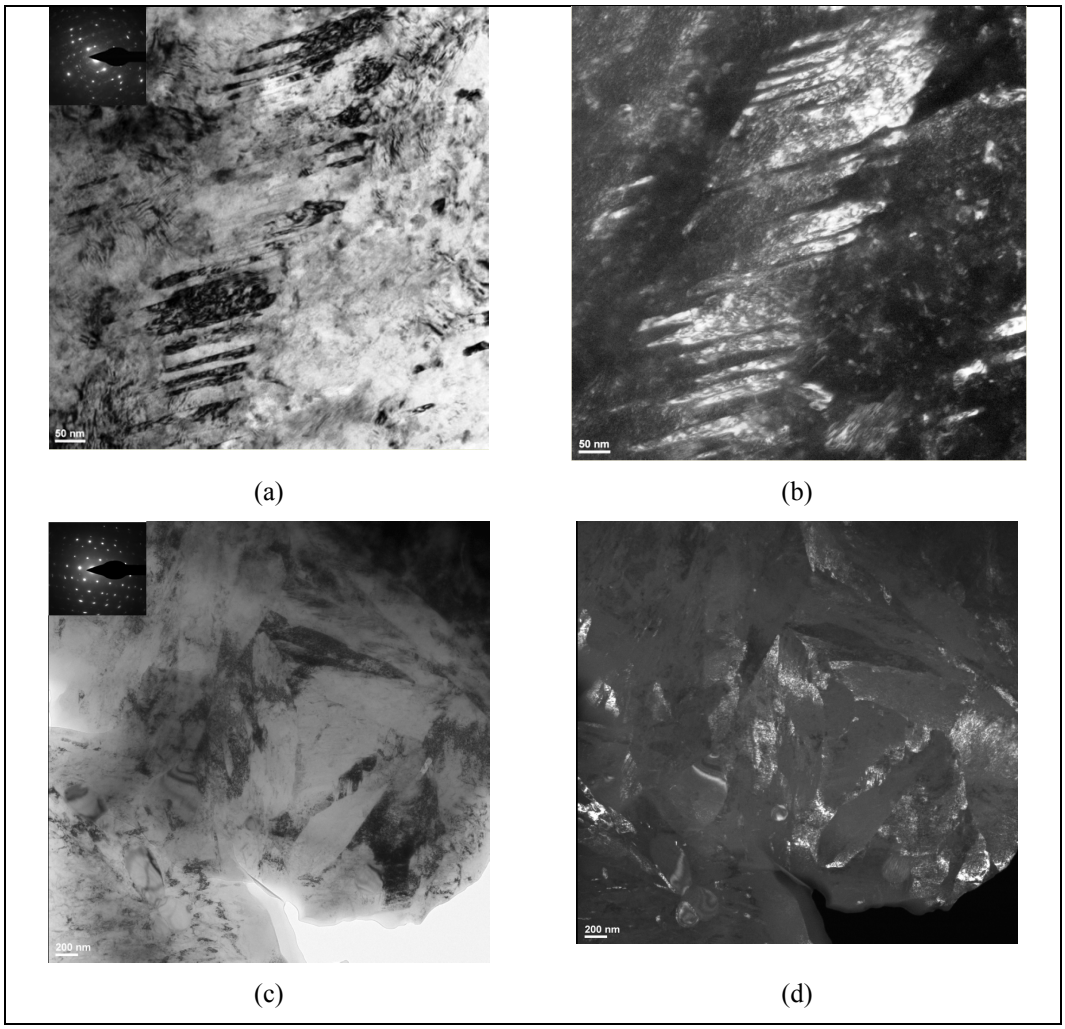

Figure 3-2 (a) and (b) Bright and dark field TEM micrograph showing bainite plate consisted of much smaller subunits after cooling at a rate of 0.5K.s^{-1}, (c) and (d): Bright and dark field TEM micrographs from martensitic microstructure showing mixed laths and plates of martensite after cooling at a rate of 50K.s^{-1}.

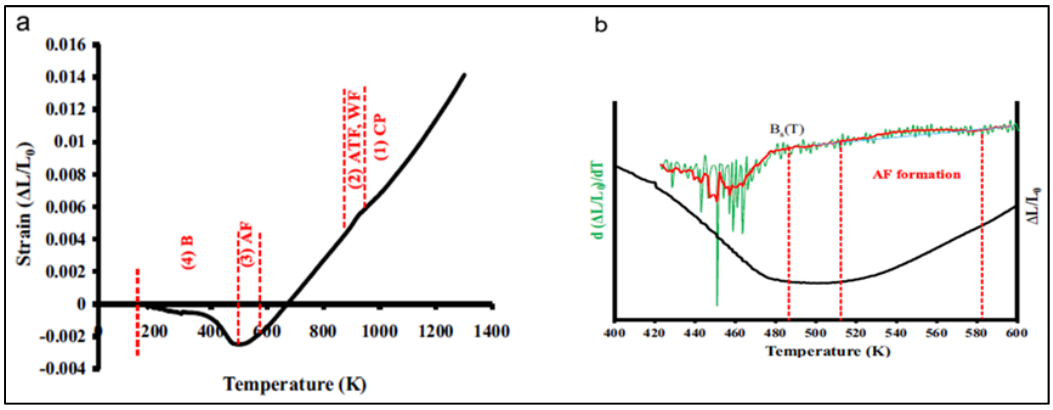

Figure 3-3 Dilatometric curve of alloy during cooling at rate of 0.5K.s^{-1} with determination of different phase transformation ranges (b) Changes in dilatational strain (black curve) between 400K and 600K from part (a) and its temperature derivative (d ($\Delta L/L_0$)/dT (green curve) revealing AF formation region before start of bainitic transformation. (Symbol description: (CP): Carbides precipitation, (ATF): AlloTriomorphic ferrite, (WF): Widmanstätten ferrite, (AF): Acicular ferrite, and (B): Bainite.

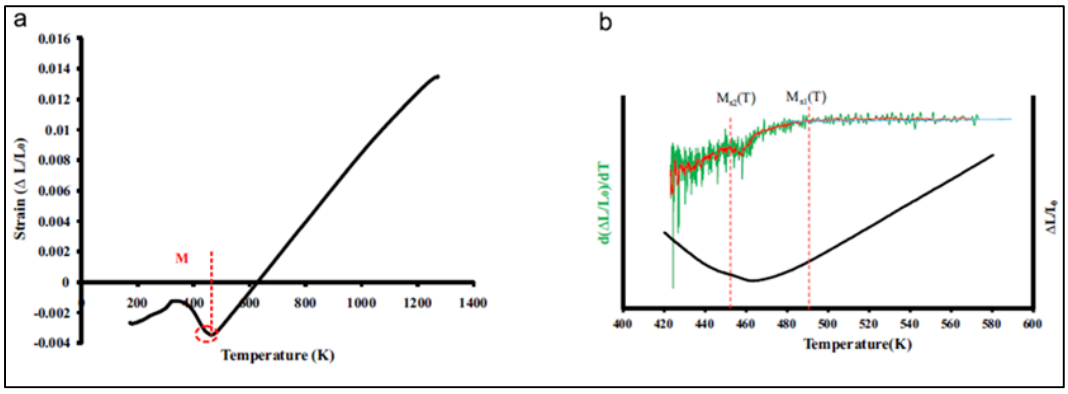

Figure 3-4 (a) Dilatometric curve of alloy during cooling at rate of 50K.s^{-1} depicting the start of martensitic transformation, (b) Changes in dilatational strain (black curve) between 420K and 580K from part (a) and its temperature derivative (d ($\Delta L/L_0$)/dT (green curve) to determine M_{s1} (T) and M_{s2} (T). (Symbol M denotes martensite)

However, splitting phenomenon [13] for martensitic transformation was detected as shown by dashed circle in Figures 3-4(a-b). Here again, for higher accuracy purposes, martensite start temperatures ($M_{s1,2}$(T)) were measured using first derivative curve. The value of M_{s1} (T) was determined to be around 490K while for M_{s2} (T) it was found to be around 450K. The sudden change in cooling rate drop observed around 300K is also due to the introduction of

liquid nitrogen in the system. Hardness measurements of the sample quenched at 0.5K.s^{-1} was indicated a value of 730±15HV while this value was 910±55HV for the fully martensitic microstructure. It is interesting to note 730HV is very high for conventionally cooled samples without any martensitic transformation. To better understand this behavior, more in depth microstructural examination was carried out. Initially, the size and volume fraction of carbides were obtained from image analysis of the unetched microstructure with a method used in reference 14. In fact, etching could cause higher volume fraction measurement due to the bigger perceptible area for carbides and lower amount for smaller carbides (as they may be washed out during the etching process). Figures 3-5 (a) and (b) show the image analysis results related to the size and volume fraction of carbides after (a) 0.5K.s^{-1} and (b) 50K.s^{-1} cooling rates, respectively.

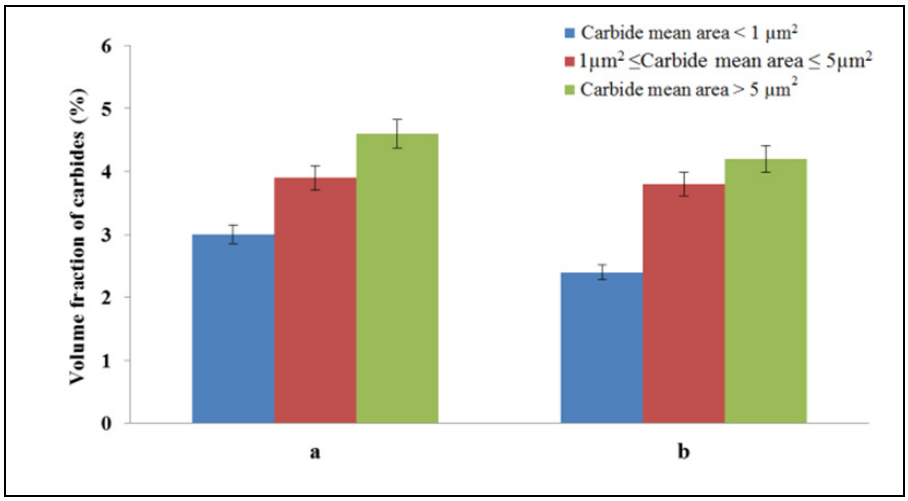

Figure 3-5 Effect of two applied cooling rates on the volume fraction of carbides with average area below 1 µm^2 in the microstructure after (a): cooling rate 0.5K.s^{-1} and (b): cooling rate 50K.s^{-1}.

As illustrated, higher volume fraction of carbides with surface area below 1µm^2 is obtained for the sample cooled with conventional rate but no major differences were found for larger carbides. The above findings confirm that the observed change in dilatometry curve for this sample (region 1 in Fig.3-3(a)) correspond to carbide precipitation. The absence of such change in the dilatometry curve of the samples cooled at 50K.s^{-1} probably prevents

redistribution of carbon atoms during cooling and does not allow for their clustering and eventually formation of carbides. As a result, no change is observed in the slope of the dilatometry curve (Fig.3-4(a-b)). For conventionally cooled sample, the first phase transformation, when cooling from the austenitizing temperature of 1300K down to around 960K, corresponds to the precipitation of M_7C_3 carbides. Thermocalc studies by Bombac et al. [15] have shown that this range corresponds to carbides formation only. Further cooling to eutectoid temperature initiates the formation of a small amount of ATF at grain boundaries as a result of austenite decomposition by diffusion controlled processes [16-18]. It has been reported that the interface between the newly formed ATF and austenite can be inert or active and that WF and B can form only at the interface when the latter is active [19]. Therefore, the presence of WF and B at the interface of the ATF and austenite boundary found in the present investigation confirms that the boundary is active [18]. It must be noted that, WF forms at higher temperatures compared to B [12]. The analysis of the AF characteristics revealed that this phase nucleates mostly on M_7C_3 and $M_{23}C_6$ carbides. These two carbides are the most ones present in AISI D2 steel (Fig.3-1(d)) [20, 21].

Finally, after partial formation of acicular ferrite, the remained austenite undergoes bainitic transformation. No sign of double deviation from linear behavior [13] that would show the activation of martensitic transformation after bainitic transformation was found in dilatometry diagram of conventionally cooled sample. Therefore the transformation path for AISI D2 steel is more of bainitic type with carbide precipitation instead of a fully martensitic structure. It must be noted that AF has more importance than B as it directly contributes to the toughness and strength of the alloy. As a result, the formation of AF on carbides must be taken into consideration during heat treating of AISI D2 steel. As indicated by dilatometry results (Fig.3-3(a)), decreasing the temperature down to 173K showed that the bainitic transformation still goes on. Thus cooling until room temperature is not enough to obtain martensitic or fully bainitic microstructures and retained austenite will be present in the microstructure after cooling. This austenite can decompose to ferrite and cementite during subsequent high temperature tempering and cause embrittleness.

3.4 Conclusions

Dilatometry results coupled with microstructural investigations showed an alternative phase transformation path during conventional heat treatment of AISI D2 tool steel. Instead of traditionally believed martensitic transformation, the obtained microstructure was composed of higher volume fraction of carbides with area below 1μm^2, allotriomorphic ferrite, Widmanstätten ferrite, acicular ferrite, and mostly bainite. Also, it was found that for the investigated D2 steel cooling to room temperature is not enough to obtain fully martensitic or bainitic microstructures and retained austenite will be present in the microstructure after cooling.

Acknowledgements

The authors would like to thank the National Sciences and Engineering Research Council of Canada (NSERC) for their support and financial contribution through the ENGAGE and ENGAGE plus programs. The authors also appreciate the collaboration of DK SPEC Inc. for providing experimental materials, support from CanmetMATERIALS in the framework of RIEM program for dilatometry experiments, Hitachi Canada for privileged access to advanced microscopy facilities.

References

[1] A. P. Gulyaev, Improved methods of heat treating high speed steels to improve the cutting properties, Metallurgy 12 (1937) 65-70.

[2] K. E. Thelning, Steels and its Heat Treatment, Butterworth & Co Publishers Ltd, London (1975).

[3] T. Arai et al. ASM Handbook, Heat Treating, ASM International, USA (1991).

[4] S. G. Singh, J. Singh, R. Singh, H. Singh, Metallurgical principles of cryogenically treated tool steels - A review on the current state of science, International Journal of Advanced Manufacturing Technology 54 (2011) 59-82.

[5] V. G. Gavriljuk, W. Theisen, V. V. Sirosh, E. V. Polshin, A. Kortmann, G. S. Mogilny, N. Petrov , Y. V. Tarusin, Low-temperature martensitic transformation in tool steels in relation to their deep cryogenic treatment Acta Materialia 61 (2013) 1705-1715.

[6] E. A. Huallpa, J. C. Sánchez, L. R. Padovese, H. Goldenstein, Determining Ms temperature on a AISI D2 cold work tool steel using magnetic Barkhausen noise, Journal of Alloys and Compound 577 (2013) S726-S730.

[7] D. Das, A. K. Dutta, K. K. Ray, Sub-zero treatments of AISI D2 steel: Part I. Microstructure and hardness, Materials Science and Engineering A 527 (2010) 2182-2193.

[8] http://www.metalravne.com/selector/steels/OCR12VM.html

[9] M. Gouné, O. Bouaziz, S. Allain, K. Zhu, M. Takahashi, Kinetics of bainite transformation in heterogeneous microstructures, Materials Letters 67-1 (2012) 187-189.

[10] Nahamin Pardazan Asia, http://en.metsofts.ir/, Iran (2014).

[11] D. E. Laughlin, K. Hono, Physical Metallurgy, 5th ed., Elsevier, Amsterdam (2014).

[12] H. K. D. H. Bhadeshia, Phase transformations contributing to the properties of modern steels, Bulletin of the polish academy of sciences: Technical sciences 58 (2010) 255-265.

[13] C. García de Andrés, F. G. Caballero, C. Capdevila, L. F. Alvarez, Application of dilatometric analysis to the study of solid-solid phase transformations in steels, Materials Characterization 48 (2002) 101-111.

[14] H. Ghasemi-Nanesa, M. Jahazi, Simultaneous enhancement of strength and ductility in cryogenically treated AISI D2 tool steel, Materials Science and Engineering A 598 (2014) 413-419.

[15] D. Bombac, M. Fazarinc, A. Saha Podder, G. Kugler, Study of Carbide Evolution During Thermo-Mechanical Processing of AISI D2 Tool Steel, Journal of Materials Engineering and Performance 22 (2013) 742-747.

[16] J. W. Christian, Theory of phase transformation in metals and alloys, 2nd ed,. Pergamon Press, Oxford (1975).

[17] H. K. D. H. Bhadeshia, Diffusional formation of ferrite in iron and its alloys, Progress in Materials Science 29 (1985) 321-386.

[18] J. D. Watson, P. G. McDougall, The crystallography of Widmanstätten ferrite, Acta Metallurgica 21 (1973) 961-973.

[19] S. S. Babu, H. K. D. H. Bhadeshia, Stress and the acicular ferrite transformation, Materials Science and Engineering A 156 (1992) 1-9.

[20] S. S. Babu, H. K. D. H. Bhadeshia, Mechanism of the transition from bainite to acicular ferrite, Materials Transactions 32 JIM (1991) 679-688.

[21] I. Madariaga, I. Gutiérrez, C. García-de Andrés, C. Capdevila, Acicular ferrite formation in a medium carbon steel with a two stage continuous cooling, Scripta Materialia 41 (1999) 229-235.

CHAPTER 4

ARTICLE 3: INFLUENCE OF CRYOGENIC PROCESS PARAMETERS ON MICROSTRUCTURE AND HARDNESS EVOLUTION OF AISI D2 TOOL STEEL

Hadi Ghasemi-Nanesa, Heithem Touazine, Mohammad Jahazi

Department of Mechanical Engineering, École de Technologie Supérieure, 1100 rue Notre-Dame Ouest, Montréal (QC) H3C 1K3 Canada.

An article adopted from this chapter has been published online in International Journal of Advanced Manufacturing Technology. DOI: 10.1007/s00170-015-7980-7

Abstract:

Microstructure evolution and hardness variation in AISI D2 steel were investigated after cryogenic treatment at 173K or 123K. Statistical analysis using STATGRAPHICS and analysis of variance (ANOVA) were carried out in order to identify the most important process parameters on the variation of hardness. In addition to process parameters such as heating rate, cooling rate, holding time and tempering temperature, the influence of surface density of carbides as microstructural variable is also included in the statistical analysis. The obtained results indicated equal impacts on the hardness for the as-cooled condition while for the as-tempered samples, the most significant factor was found to be the tempering temperature. A regression equation taking into account all the critical variables is proposed and very good approximation to the experimental hardness values was obtained. Precipitation of transition carbides and their influence on the extent of martensite recovery are considered as possible mechanisms responsible for hardness evolution after cryogenic treatment.

4.1 Introduction

AISI D2 tool steel is a key alloy in mold making and cutting tools industries as it provides an excellent combination of high strength and high wear resistance [1-3]. The hardening heat

treatment of this steel consists of: (a) solutionizing in the dual phase region (austenite + carbides), (b) cooling to ambient temperature in air or by compressed gas, and (c) double tempering in the temperature range of 473K-773K [3]. The high carbon content of this alloy does not allow complete martensitic transformation by conventional heat treatment and the microstructure contains some retained austenite upon quenching. This phase decomposes into ferrite and cementite during subsequent tempering and reduces mechanical properties [4]. Cryogenic treatment is generally added to the above heat treatment cycle in order to remove the retained austenite [4]. In cryogenic treatment, after conventional quenching to room temperature, the material is then cooled to temperatures between 77K and 200K, hold from a few minutes to several hours; then they are heated up to room temperature before tempering as shown schematically in Fig.4-1 [4-9].

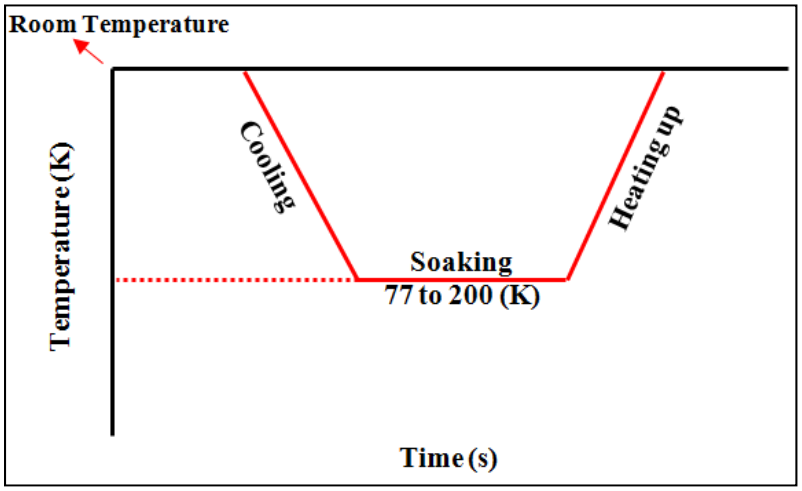

Figure 4-1Typical cryogenic treatment of tool steels.

The improvement in both hardness and wear resistance after cryogenic treatment of AISI D2 tool steel have been reported by Collins and Dormer [5], Barron [6], Das eta al. [7,8], and Ghasemi-Nanesa and Jahazi [10]. In this regard, cryogenic process parameters and their influences on final mechanical and wear properties have been the subject of extensive researches [6-8, 11-17]. Austenitization temperature, cooling rate, cryogenic temperature, holding time at cryogenic temperature, heating rate to tempering temperature, tempering temperature, and holding at tempering temperature can each contribute to the effectiveness of

the cryogenic treatment. However, to date, among the above parameters, the most studied one has been the holding time at cryogenic temperature. Specifically for AISI D2 steel, a wide range of holding times have been suggested, from a few minutes proposed by Kamody [11, 12], to 3 hrs by Wojcieszynski [13], 16 hrs by Wierszyllowski [14], 20 hrs by Rhyim [15], 24 hrs by Barrons [6], 35 hrs d by Pellizzari and Molinari [16], and 36 hrs by Das et al. [7,8]. In the above mentioned researches on AISI D2 tool steel, the influence of cooling rate from austenitization temperature to room temperature and then to the cryogenic temperature in the activation of martensitic transformation has not been considered. In general, the microstructure at the start of cryogenic treatment is assumed to be martensite with some retained austenite and this even under very slow cooling rates. [18]. However, recent studies by the present authors [19] have shown that cooling rate to cryogenic temperature has a clear influence on the microstructure obtained at the start of the cryogenic holding. Specifically, it was found that cooling at a rate of $0.5K.s^{-1}$ to 173K resulted in the formation of a multiphase microstructure composed mostly of bainite instead of martensitic while when the cooling rate is increased to $50K.s^{-1}$, a fully martensitic structure is obtained. It can be therefore said that, at least part of the controversies about the influence of holding time at cryogenic temperature may originate from the starting microstructure at cryogenic temperature.

A similar analysis can be provided for other cryogenic process parameters, demonstrating that few systematic studies have been carried out on the influence of different cryogenic process parameters on microstructure and mechanical properties evolution of AISI D2 steel. The main objective of the present work is therefore to address the above questions and focuses on identifying the most critical cryogenic process parameters and quantify their influences on microstructure and hardness evolution of AISI D2 steel.

A combination of statistical analysis and microstructural examinations are used in the present investigation. For the statistical analysis, a regression equation, comprising individual significant factors and their interactions including the surface density of fine carbides as microstructural feature is proposed for predicting hardness evolution. The reliability of the proposed equation is then examined by comparing the regression prediction with

experimental results. For microstructural analysis, a portion of the dilatometry diagrams showing the activation of different carbide precipitations during heating from cryogenic to tempering temperature are discussed and related to hardness evolution.

4.2 Experimental work

AISI D2 12 mm thick plates with the nominal chemical composition of Fe-1.54wt%C-0.33wt%Si-0.32wt%Mn-11.88wt%Cr-0.76 wt%Mo-0.75wt%V-0.008wt%P-0.008wt%S were utilized in this research. The as-received materials were cut into 10mm height and 4mm diameter cylinders. BÄHR DIL 805 A/D dilatometer with a 50nm resolution and high speed cooling rates were used to carry out the cryogenic cooling and tempering treatments. Samples were heated to 1303K and maintained for 1200 seconds followed by continuous cooling to 173K or 123K using two different cooling rates, $10K.s^{-1}$ or $50K.s^{-1}$. Both cooling rates were selected based on continuous cooling transformation (CCT) diagram of AISI D2 tool steel reported in (http://www.metalravne.com/steelselector/steels/OCR12VM.html) (see Fig.4-2). According to Fig.4-2, a fully martensitic structure could be obtained any cooling rates above $3K.s^{-1}$.

Three holding times at cryogenic temperature, 10s, 300s, and 3600s were selected. Two different heating rates, $0.5K.s^{-1}$ and $5K.s^{-1}$, were used to heat up the samples from cryogenic to the tempering temperature. Two tempering temperatures, one in the range of transition carbide formation (473K) and the other in the range of main carbide formation (773K) were selected [20]. Finally, a constant holding time of 600s at tempering temperature was considered for all conditions. Figure 4-3 summarizes the experimental procedure used in the present investigation and Table 4.1 identifies the selected parameters and their levels for the statistical analysis. The two values for cryogenic temperatures were selected based on industrial applicability. In order to insure comparable starting microstructure before cryogenic cooling, a single austenitization treatment (1303K, 1200s) was applied to all samples. The following five factors: 1) cooling rate, 2) cryogenic temperature, 3) holding time, 4) heating rate, and 5) tempering temperature can be considered as “controllable

factors". In the present work a "noncontrollable" factor representing the surface density of secondary carbides with diameters below 1 μm was also added to the statistical analysis.

For microstructural examination, an etchant with the following composition 40g NaOH+60g H_2O+15g $NaNO_3$ initially proposed by Gouné et al. [22] was modified and successfully used for revealing martensite. Hitachi-TM3030 scanning electron microscope (SEM) and image analysis software-MIP [23] were used for measuring the surface density of fine carbides. In this regard, three images were taken by random area selection and the number of carbides with diameters below 1μm were counted, and then divided by the total area. An illustrative example is shown in Fig.4-4 where a phase contrast image from a specific testing condition shows carbides as dark spots and the corresponding measured surface density.

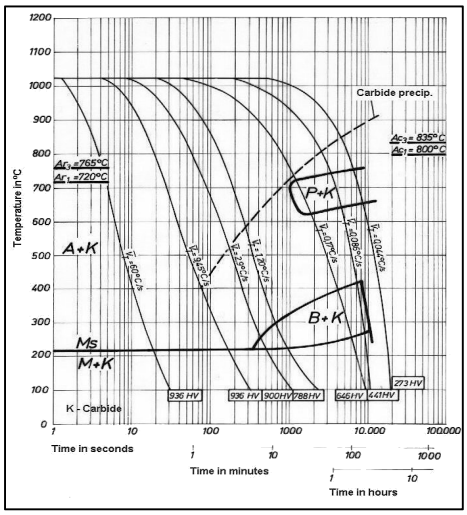

Figure 4-2 CCT diagram for AISI D2 tool steel, cooled from 1300K (http://www.metalravne.com/ steelselector /steels/OCR12VM.html).

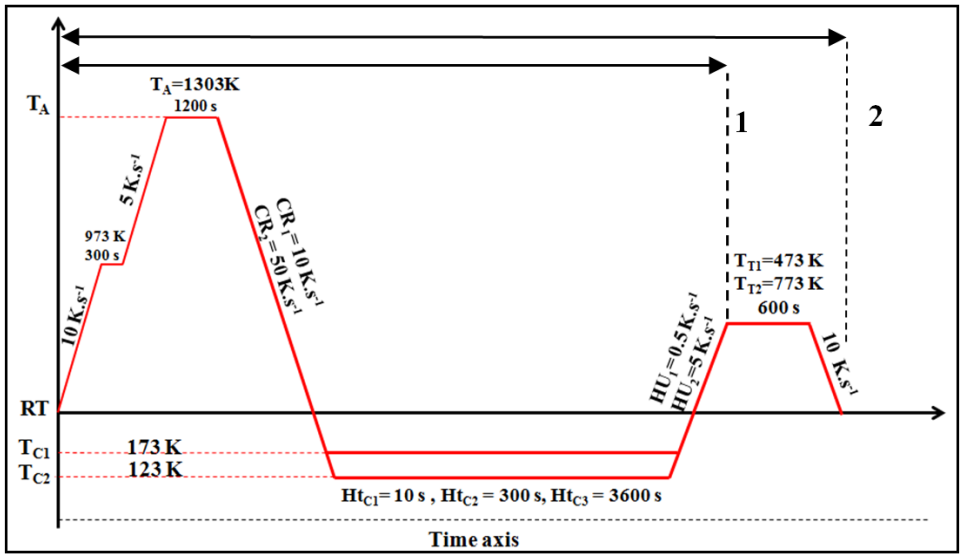

Figure 4-3 Different test paths used for cryogenic treatment and tempering: Austenitizing temperature (T_A), holding time at austenitic temperature (t_A), cooling rate (CR), cryogenic temperature (T_C), holding time at cryogenic temperature (Ht_C), heating up rate (HU), and tempering temperature (T_T), No.1 and No.2 show the two different sets of experiments used in this investigation.

Table 4.1 Factors and level descriptions for statistical analysis.

Factor	Value	Level
A: Cooling rate (CR)	CR_1=10K.s^{-1} CR_2=50K.s^{-1}	2
B: Cryogenic temperature (T_C)	T_{C1}=173K T_{C2}=123K	2
C: Holding time at cryogenic temperature (Ht_C)	HT_{C1}=10s, HT_{C2}=300s, HT_{C3}=3600s	3
D: Heating up rate (HU) – from T_C to T_T	HU_1=0.5K.s^{-1} HU_2=5K.s^{-1}	2
E: Tempering temperature (T_T) Holding time: 600 s	T_{T1}=473K T_{T2}=773K	2

The hardness of the matrix was calculated using Vickers method with 200gf applied load and a dwell time of 15s. Special care was taken during hardness measurements to avoid the proximity effect of large primary carbides. The statistical analysis using a full factorial design was carried out with STATGRAPHICS software and analysis of variance (ANOVA)

[24]. Details regarding the terms and expressions used in the ANOVA table are provided in Appendix A1.

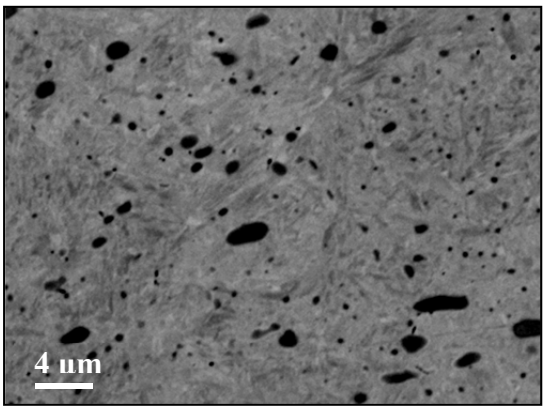

Figure 4-4 Example used for measuring the surface density of carbides with diameter ≤ 1μm, testing condition: A: 10K.s^{-1}, B: 173K, C: 10s, as cooled without tempering.

4.3 Results and discussion

4.3.1 Determination of significant process parameters by statistical analysis

Figure 4-5 depicts the measured hardness values of as-cooled and as non-tempered samples (Set No.1 as shown in Fig.4-3). STATGRAPHICS software and the statistical analysis were carried out. Table 4.2 summarizes the ANOVA table obtained from the software. The last column showing values for P is a key parameter to evaluate the significance (i.e. reliability) of the model. P values less than 0.05 indicate that the model terms are significant. As indicated in Table 4.2, all P values obtained from the ANOVA analysis are well above the 0.05 threshold, indicating that none of the model terms are significant. On this basis, experiments with 3600s holding time at cryogenic temperature were discarded from the experimental plan. For tempered samples, a full factorial testing batch comprised of 32 runs was carried out and then the hardness levels were measured. Details of the test conditions and measured hardness values are provided in Appendix A2 (Table A2). In this table, the surface density of carbides, as a microstructural feature affecting the final hardness, is also added.

The data in Table A2 was then inserted as inputs in the STATGRAPHICS software to carry out the statistical analysis and determine the influence of different processing factors and their mutual contributions. The ANOVA table summarizing the statistical terms for the 32 investigated samples is illustrated in Fig.4-6(a-c). In the Pareto graph (Fig.4-6(a)) and the response graph (Fig.4-6(b)), variation in the hardness value indicates the significance of that factor.

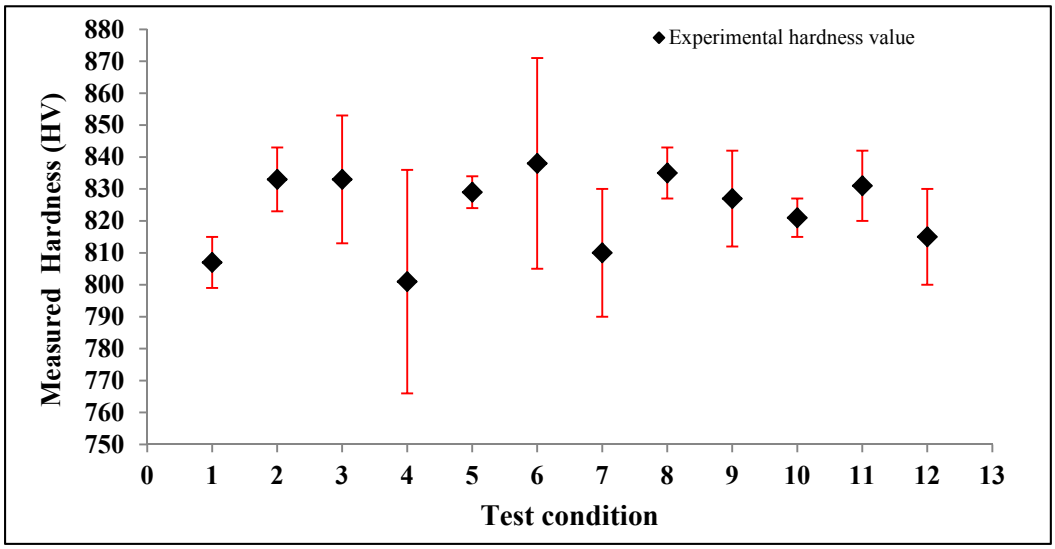

Figure 4-5 Hardness measurements of samples after batch No.1 of experiments as shown in Fig.4-3.

Table 4.2 ANOVA results for the main factors and the interactions

Source	Sum of Squares	Degree of Freedom	Mean Square	F-Ratio	P-Value
Model	1516.17	9	168.46	2.33	0.3361
A	0.33	1	0.33	0.0046	0.9520
B	8.33	1	8.33	0.12	0.7665
C	1135.17	2	567.58	7.86	0.1129
AB	0.000	1	0	0	1.0000
AC	346.17	2	173.08	2.4	0.2945
BC	26.17	2	13.08	0.18	0.8467
Residual	144.5	2	72.25		
Total	1660.67	11			

For instance, it is evident that the most significant individual factor appears to be the tempering temperature. While, other factors are not significant individually, but in

combination, they have an important impact. The only exception is heating rate which is neither significant individually nor in interaction with other factors (Fig.4-6(b)). In statistical analysis, if a parameter is not significant alone but becomes important when combined with other factors, then it can be taken into account, and added to the regression equation [24].

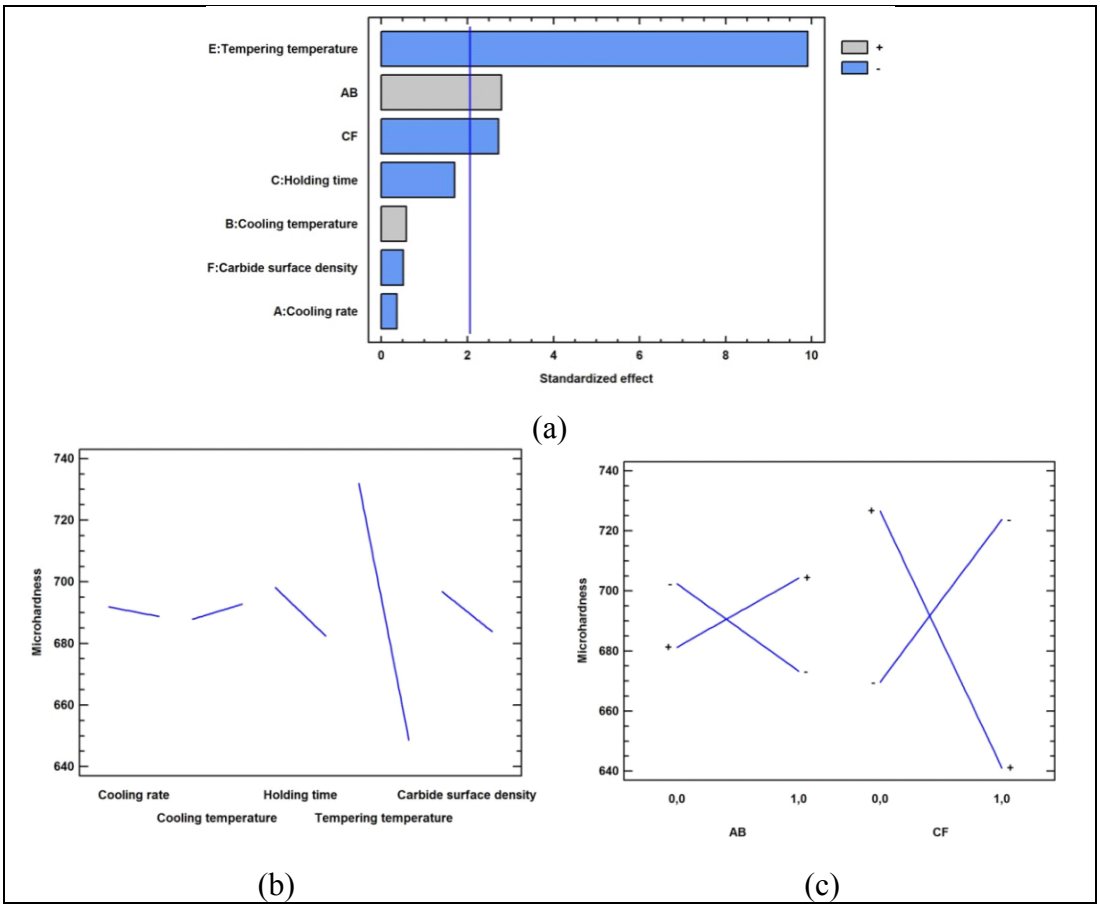

Figure 4-6 (a) Pareto graph for standardized hardness (vertical line showing the value limit of significance), (b) response graph of factors affecting hardness, and (c) response graph showing the influence of interactions on hardness evolution(coded variable was used for data analysis).

The influence of significant interactions on the hardness value is illustrated in Fig.4-6(c). It can be seen that cooling rate in interaction with cooling temperature, and holding time in interaction with carbide surface density, have significant influences on hardness evolution. Also in Table 4-3 ANOVA results obtained from STATGRAPHICS are illustrated. It can be

seen that the P values for parameter E, interactions AB and CF are below 0.05, indicating the significance of these terms. Using data in Table 4-3 and Fig.4-6, the following regression equation was determined from statistical analysis by adjusting the coefficients for all significant factors and their interactions:

Table 4.3 ANOVA results for the main factors and the significant interactions

Source	Sum of Squares	Degree of freedom	Mean square	F-Ratio	P-value
A	71.0427	1	71.0427	0.13	0.7236
B	188.268	1	188.268	0.34	0.5657
C	1606.55	1	1606.55	2.90	0.1018
E	54534.4	1	54534.4	**98.28**	**0.0000**
F	146.361	1	146.361	0.26	0.6122
AB	4329.49	1	4329.49	**7.80**	**0.0101**
CF	4101.98	1	554.91	**7.39**	**0.0120**
Residual	13317.8	24			
Total	78034	31			

$$Hardness(HV) = 723,4 - 29.1\times(A) - 21.2(B) + 54.2\times(C) - 83.3\times(E) - 139.7\times(C)\times(F) + 52.2\times(A)\times(B) + 56.9\times(F) \quad (4.1)$$

Constant values were rounded to one digit after point for simplification purposes and it was verified that this did not affect the predicted values by the model. R square and Durbin-Watson statistic for this regression equation were 83% and 2.5457 (no autocorrelation), respectively. The 83% value for R-squared indicates that the obtained values by the statistical model show very good agreement with the measured values. Using Eq.1 the hardness values for 32 runs were calculated and are compared to the measured ones as shown in Fig.4-7. As it can be seen, the predicted values, with a maximum error of 7.7%, are in good agreement with the measured ones demonstrating a good reliability for the statistical model.

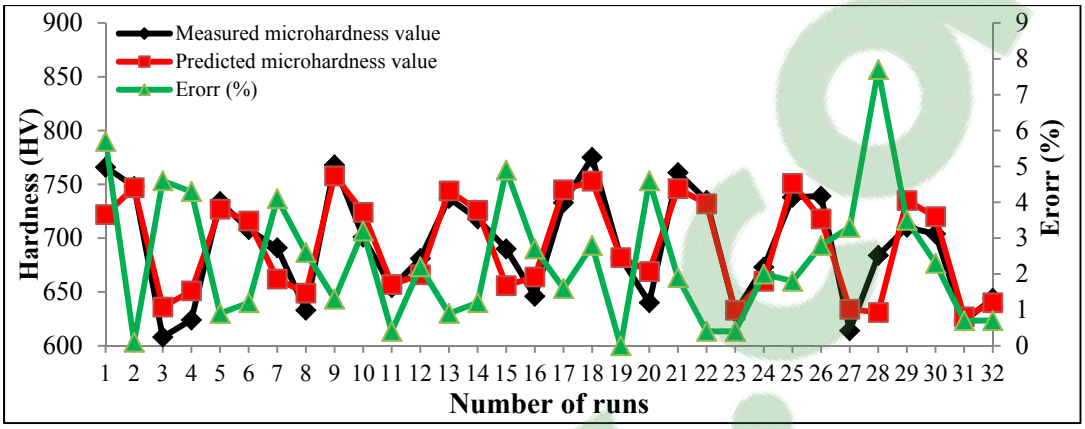

Figure 4-7 A comparison between measured hardness values and predicted ones using Eq.4.1.

The optimum processing conditions leading to maximum hardness for the AISI D2 steel can therefore be extracted from Eq.4.1 as follow: 1) cooling the material from 1303K to 173K at the rate of 50K.s^{-1}, 2) 10 s holding at this temperature, and 3) heating it up to 473K at the rate of 5K.s^{-1} and then tempering for 600s at this temperature.

The validation of the statistical model is usually carried out with a confirmation test. First, a distinct factor level mixture is predicted on the basis of the analysis [19, 24]. Then an experiment with the same level is carried out and the results of the calculated and actual experiments are compared which should show an overlap within the confidence interval of the model [19, 24]. To this end, a sample was heat treated according to the above optimum conditions predicted by the statistical model and reached a hardness of 773HV while the predicted hardness value according to the regression equation was 754HV. The very small difference (less than 3%) between the predicted and experimental values confirms the validity of the regression equation and a reliable confidence limit.

Moreover, ANOVA analysis without considering carbide surface density was carried out and the results were presented in Appendix A3. In Appendix A3, carbide surface density is eliminated from factors and also interactions from insignificant factors even if they show significance in interaction were not considered in regression equation. Results showed that the only individual significant factor is again the tempering temperature however 2 or 3

tempering tests in the suggested interval for tempering temperature should be conducted to confirm ANOVA analysis.

4.3.2 Role of tempering temperature on the hardness evolution of cryotreated alloy

Since tempering temperature was found to be the most significant factor, it is necessary to study the evolution of microstructure during heating from cryogenic temperature to the tempering temperature and relate it to hardness reduction after tempering. Dilatometry is an efficient in-situ method for studying solid state phase transformations such as martensitic transformation or carbide precipitation [25]. High resolution dilatometers such as the one used in this investigation (BÄHR DIL 805 A/D) allow for very accurate temperature control and recording of nanometric volume changes. Such precise controls are necessary for revealing the early stages of phase transformations and differentiation of overlapped processes, which can't be revealed with conventional dilatometers. In the present study, using the above equipment, dilatometry experiments, simulating the cryogenic treatment indicated in Fig.4-1, were carried out and the portion of dilatation diagrams corresponding to the heating stage (i.e. cryogenic temperature to tempering temperature) were examined and related to hardness values after tempering at 473K and 773K.

Figure 4-8(a-b) exhibits dilatation results for the investigated conditions where two distinct behaviors can be observed: 1) for the material with a holding time of 10s at the cryogenic temperature, the heating portion (Fig.4-8(a)) shows a non-linear expansion before 200K and returns to a linear behavior afterwards until the appearance of the first transformation. By contrast, when a holding time of 300s was used, the dilatation curve was a nearly linear over the entire heating cycle until 200K (Fig.4-8(b)).

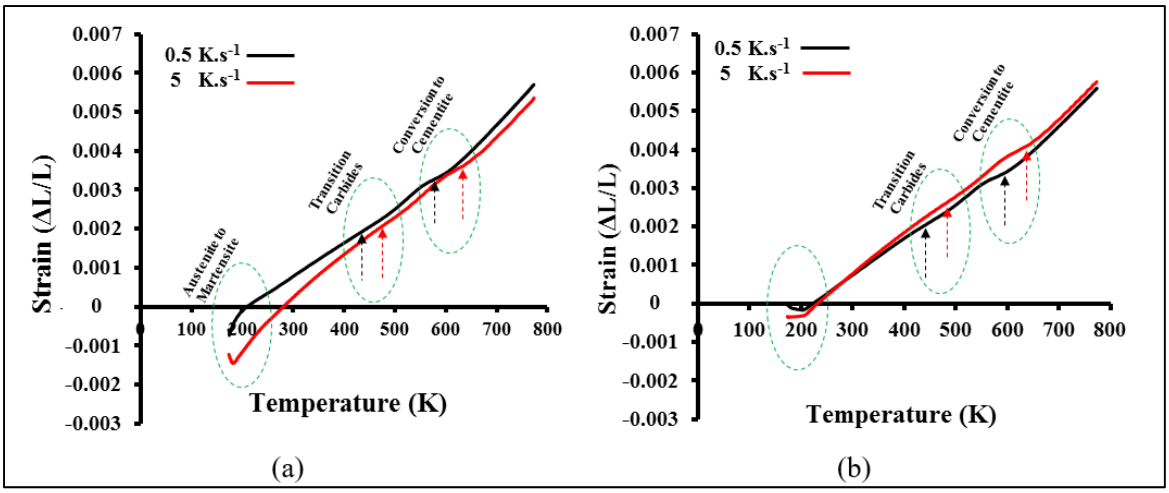

Figure 4-8 Dilatometry diagrams, heating portion from cryogenic temperature to tempering temperature : (a) CR: 50K.s^{-1}, T_C: 173K, HT_C: 10s, HU: 0.5 and 5 (K.s^{-1}), T_T: 500K, (b) CR: 50K.s^{-1}, T_C:173K, HT_C: 300s, HU: 0.5 and 5 (K.s^{-1}), T_T: 500K, symbols denoting: (CR: Cooling rate, T_C: Cryogenic temperature, HT_C: Holding time at cryogenic temperature, HU: heating up rate, T_T: tempering temperature).

Microstructure evolution during tempering of carbon steels or alloyed steels has been the subject of extensive research works mainly because the final mechanical properties are significantly influenced by precipitation of different types of carbides [20, 26-28]. A typical tempering process is composed of five transformation stages: Carbon enrichment of the matrix occurs in stage 1 while stage 2 is associated with the periodic arrangement of the enriched area below 353K [20, 26-28]. In stage 3, transition carbides precipitate between 353K and 453K [20, 26-28]. In stage 4, the retained austenite transforms to ferrite and cementite between 473K and 623K [20, 26-28]. The fifth stage, involves the conversion of transition carbides into cementite and matrix recovery at temperatures between 523K and 773K [20, 26-28]. The temperature intervals mentioned above are not fixed and can vary with the chemical composition of the steel [20, 26-28]. In this study, as shown in Fig.4-8 (a-b), a broad peak, related to the formation of transition carbides with an inflection point at 432K at heating rate of 0.5K.s^{-1}, was observed. As indicated in Fig.4-8(a), this temperature is increased by 45K when a higher heating rate, 5K.s^{-1}, is used. No trace of transformation of retained austenite to ferrite and cementite was found in any of the examined samples indicating that full martensitic transformation has taken place during cryogenic treatment. A second peak with an inflection point at 580K was also observed (Fig.4-8(a) and (b)). This

temperature is in the range corresponding to the conversion of transition carbides to cementite. This temperature also increases by about 50K when the $5K.s^{-1}$ heating rate is used.

In addition, for the samples soaked for 10s at cryogenic temperature, an expansion peak between cryogenic temperature and 200K was found. Mittemeijer [20] has also observed this peak in his investigations and related it to continued transformation of retained austenite to martensite. The results obtained in the present investigations concords with the above findings and confirm that tempering temperature is the major factor influencing microstructure evolution. Specifically, increasing the tempering temperature from 473K to 773K results in the formation of two distinct types of carbides (transition carbides (η) and cementite) thereby lowering the hardness of the material. Hardness measurements of the two samples heated at the rate of $0.5K.s^{-1}$ (Fig.4-8) showed a reduction of 40HV because of the formation of transition carbides during tempering at 473K for 600s. This reduction was about 200HV after tempering at 773K under the same conditions because of the conversion of transition carbides to cementite and the recovery of the microstructure in comparison with the as-cooled and non-tempered condition [20, 26-28]. A similar behavior was obtained when the higher heating rate of $5K.s^{-1}$ was used.

4.4 Conclusions

In this study, the effect of cryogenic process parameters on hardness variation in a commercial AISI D2 tool steel is studied. Using a comprehensive statistical analysis, tempering temperature was determined as the most significant factor influencing the hardness. A regression equation taking into account all the critical variables is proposed and very good approximation to the experimental hardness values was obtained with a maximum error of 7.7%. The analysis of dilatation data for the reheating part from cryogenic temperature to tempering temperature revealed the activation of two different phase transformations. By tempering at 473K, transition carbides formed and resulted in 40HV drop in hardness while by tempering at 773K, the conversion of transition carbides to cementite and martensite recovery occurred and led to a 200HV reduction in hardness.

Acknowledgements

The authors would like to thank MITACS Canada and the National Sciences and Engineering Research Council of Canada (NSERC) for their support and financial contribution. The authors also appreciate the collaboration of DK SPEC Inc. for providing experimental materials, support from CanmetMATERIALS in the framework of RIEM program for dilatometry experiments, Hitachi Canada for privileged access to advanced microscopy facilities.

References

[1] T. Arai et al. ASM Handbook, Heat Treating, ASM International, USA (1991).

[2] A. P. Gulyaev, Improved methods of heat treating high speed steels to improve the cutting properties, Metallurgy 12 (1937) 65-70.

[3] K. E. Thelning, Steels and its Heat Treatment, Butterworth & Co Publishers Ltd, London (1975).

[4] S. G. Singh, J. Singh, R. Singh, H. Singh, Metallurgical principles of cryogenically treated tool steels - A review on the current state of science, International Journal of Advanced Manufacturing Technology 54 (2011) 59-82.

[5] D. N. Collins, J. Dormer, Deep cryogenic treatment of a D2 cold-work tool steel, Heat Treatment of Metals 24-3 (1997) 71-74.

[6] R. F. Barron, Cryogenic treatment of metals to improve wear resistance, Cryogenics 22 (1982) 409-413.

[7] D. Das, A.K. Dutta, K.K. Ray, Inconsistent wear behaviour of cryotreated tool steels: Role of mode and mechanism, Materials Science and Technology 25 (2009) 1249-1257.

[8] D. Das, A.K. Dutta, K.K. Ray, On the enhancement of wear resistance of tool steels by cryogenic treatment, Philosophical Magazine letters 88 (2008) 801-811.

[9] D. N. Collins, G. O'Rourke, The response of tool steels to deep cryogenic treatment effect of alloying elements. Heat treating: Proceedings of the 18th Conference (1998) 229-247.

[10] H. Ghasemi-Nanesa, M. Jahazi, Simultaneous enhancement of strength and ductility in cryogenically treated AISI D2 tool steel, Materials Science and Engineering A 598 (2014) 413-419.

[11] D. Kamody, Cryogenics process update. Advanced Materials Processing 155-6 (1999) H67-H69.

[12] P. Cohen, D. Kamody, Cryogenics goes deeper. Cutting Tool Engineering 150-7 (1998) 46-50.

[13] A. L. Wojcieszynski, Cryogenic treatment a mystery or misery of heat treatment. ASM Proceedings: Heat Treating (1999) 237-243.

[14] I. Wierszyllowski, The influence of post-quenching deep cryogenic treatment on tempering processes and properties of D2 tool steel: studies of structure, XRD, dilatometry, hardness and fracture toughness, Defect and Diffusion Forum 258-260 (2006) 415-420.

[15] Y. M. Rhyim, S. H. Han, Y. S. Na, J. H. Lee, Effect of deep cryogenic treatment on carbide precipitation and mechanical properties of tool steel. Solid State Phenomena 118 (2006) 9-14.

[16] M Pellizzari, A. Molinari, Deep cryogenic treatment of cold work tool steel. In: The use of steels: experience and research. Proceedings of the 6th International Tooling Conference, Karlstad University (2002) 657-669.

[17] A. Oppenkowski, S. Weber, W. Theisen, Evaluation of factors influencing deep cryogenic treatment that affect the properties of tool steels. Journal of Materials Processing Technology 210-14 (2010) 1949-1955.

[18] V. G. Gavriljuk, W. Theisen , V. V. Sirosh, E. V. Polshin, A. Kortmann, G. S. Mogilny, Y. N. Petrov, Y. V. Tarusin , Low-temperature martensitic transformation in tool steels in relation to their deep cryogenic treatment , Acta Materialia 61 (2013) 1705-1715.

[19] H. Ghasemi Nanesa, M. Jahazi, Alternative phase transformation path in cryogenically treated AISI D2 tool steel, Materials Science and Engineering A 634 (2014) 32-36.

[20] E. J. Mittemeijer, Analysis of the kinetics of phase transformations, Journal of Materials Science 27 (1992) 3977-3987.

[21] J. Wei, O. Kessler, M. Hunkel, F. Hoffmann, P. Mayr, Anisotropic phase transformation strain in forged D2 tool steel, Materials Science and Technology 20 (2004) 909-914.

[22] M. Gouné, O. Bouaziz, S. Allain, K. Zhu, M. Takahashi, Kinetics of bainite transformation in heterogeneous microstructures, Materials Letters 67-1 (2012) 187-189.

[23] Nahamin Pardazan Asia, http://en.metsofts.ir/, Iran (2014).

[24] M. J. Kiemele, S. R. Schmidt, R. J. Berdine, Basic statistics: tools for continuous improvement, forth edition, AIR ACADEMY PRESS, Colorado, USA (1997).

[25] C. García de Andrés, F. G. Caballero, C. Capdevila, L. F. Alvarez, Application of dilatometric analysis to the study of solid-solid phase transformations in steels, Materials Characterization 48 (2002) 101-111.

[26] J. A. V. Leiva, E. V. Morales, E. Villar-Cociña, C. A. Donis, I. de S. Bott, Kinetic parameters during the tempering of low-alloy steel through the non-isothermal dilatometry, Journal of Materials Science 45-2 (2010) 418-428.

[27] M. Preciado, M. Pellizzari, Influence of deep cryogenic treatment on the thermal decomposition of Fe-C martensite, Journal of Materials Science 49-23 (2014) 8183-8191.

[28] G. R. Speich, W. C. Leslie, Tempering of steel, Metallurgical Transactions 3-5 (1972) 1043-1054.

Appendix A1

Terms and expressions used for statistical analysis throughout the article are described as follow [25]:

1) Sum of squares: difference between group means and grand means,

2) Degree of freedom: the number of values in the final calculation of a statistic that are free to vary,

3) Mean Square: sum of squares / degree of freedom,

4) F- Ratio: Mean Square model/ Residual,

5) P-value: It is the number that the test statistic must exceed to reject the test. This value is 0.05. Any value <0.05 shows that the factor is significant and it should be included in the model. For P-value > 0.1, it means factor is not significant and it should not be included in the model. For $0.05 \leq$ P-value ≤ 0.1, test is in gray zone and most experimenters will place the factor in the model,

6) Durbin-Watson statistic: If there is any autocorrelation in the residual from a statistical analysis, the Durbin-Watson statistic shows it. This value is always between 0 and 4 (A value of 2 means that there is no autocorrelation in the sample).

Appendix A2

The hardness values of the 32 test runs used for statistical analysis are shown in Table A1, as follow:

Table 4A.1. Hardness measurements for all 32 tested conditions

Run Number	CR ($K.s^{-1}$)	T_C (K)	HT_C (s)	HU ($K.s^{-1}$)	T_T (K)	Carbide surface density (μm^{-2})	Hardness (HV)	Hardness (HV) Model	Error (%)
1	10	173	10	0.5	473	0.20	766	722	5.7
2	10	173	10	5	473	0.27	748	747	0.1
3	10	173	10	0.5	773	0.19	608	636	4.6
4	10	173	10	5	773	0.23	624	651	4.3
5	10	173	300	0.5	473	0.20	734	727	0.9
6	10	173	300	5	473	0.22	708	716	1.2
7	10	173	300	0.5	773	0.17	691	662	4.1
8	10	173	300	5	773	0.19	633	649	2.6
9	10	123	10	0.5	473	0.24	768	758	1.3
10	10	123	10	5	473	0.15	701	724	3.2
11	10	123	10	0.5	773	0.19	654	657	0.4
12	10	123	10	5	773	0.22	681	666	2.2
13	10	123	300	0.5	473	0.21	737	744	0.9
14	10	123	300	5	473	0.24	718	726	1.2
15	10	123	300	0.5	773	0.22	690	656	4.9
16	10	123	300	5	773	0.20	646	664	2.7
17	50	173	10	0.5	473	0.20	733	745	1.6
18	50	173	10	5	473	0.25	775	753	2.8
19	50	173	10	0.5	773	0.25	682	682	0
20	50	173	10	5	773	0.22	640	669	4.6
21	50	173	300	0.5	473	0.21	761	746	1.9
22	50	173	300	5	473	0.23	735	732	0.4
23	50	173	300	0.5	773	0.26	631	633	0.4
24	50	173	300	5	773	0.21	673	660	2
25	50	123	10	0.5	473	0.30	738	751	1.8
26	50	123	10	5	473	0.21	739	718	2.8
27	50	123	10	0.5	773	0.21	614	634	3.3
28	50	123	10	5	773	0.20	684	631	7.7
29	50	123	300	0.5	473	0.17	710	735	3.5
30	50	123	300	5	473	0.20	704	720	2.3
31	50	123	300	0.5	773	0.22	623	627	0.7
32	50	123	300	5	773	0.19	644	640	0.7

Appendix A3

ANOVA analysis when carbide surface density is removed from individual factors and the interaction of only significant factors presented in regression equation if there was any.

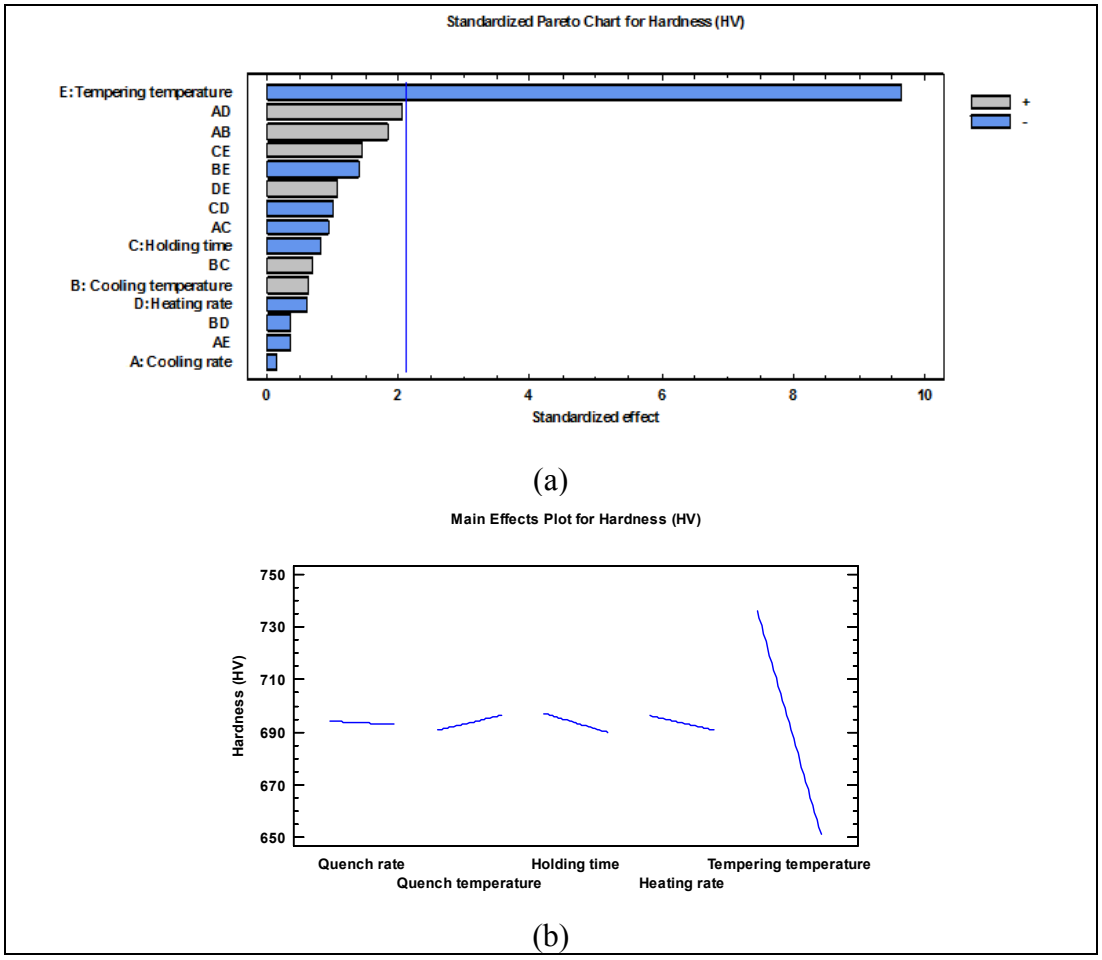

Figure 4-A3: ANOVA analysis for factors indicated in Table 4. 1 without considering carbide surface density as influential factor: (a) Pareto graph for standardized hardness (vertical line showing the value limit of significance), (b) response graph of factors affecting hardness.

The regression equation of above mentioned analysis is therefore written as follow:

$$Hardness(HV) = 735.938 - 84{,}8125 \times (\mathrm{E}) \qquad \text{(A3. 1)}$$

R square and Durbin-Watson statistic for this regression equation were 73% and 2.2938 (no autocorrelation), respectively.

CHAPTER 5

ARTICLE 4: MARTENSITIC TRANSFORMATION IN AISI D2 TOOL STEEL DURING CONTINUOUS COOLING TO 173 K

Hadi Ghasemi Nanesa[a], Mohammad Jahazi[a], Reza Naraghi[b]

[a] Department of Mechanical Engineering, École de Technologie Supérieure, 1100 rue Notre-Dame Ouest, Montréal (QC) H3C 1K3 Canada.

[b] Department of Materials Science and Engineering, KTH Royal Institute of Technology, Brinellvägen 23, SE-10044 Stockholm, Sweden

An article adopted from this chapter has been published in Journal of Materials Science, vol. 50-17 (2015), pp. 5758-5768. DOI: 10.1007/s10853-015-9123-9

Abstract:

Martensitic transformation of AISI D2 tool steel continuously cooled from 1303K to the cryogenic temperature of 173K is investigated by dilatometry using $10K.s^{-1}$ or $50K.s^{-1}$ cooling rates. A 'typical' expansion takes place from the M_s temperature and reaches a maximum at 325K. However, an atypical behavior is observed below this temperature implying the activation of further martensitic transformation. A modification to existing equations is proposed, which allows for more accurate description of the kinetics of martensitic transformation. Scanning electron microscopic studies indicated the presence of plate and lath martensite for both cooling rates. Carbide precipitation takes place at the rate of $10K.s^{-1}$ before the start of martensitic transformation while it was not observed when the $50K.s^{-1}$ rate was used. Transmission electron microscopic studies revealed that the microstructure also contains a significant amount of nano twined martensite.

5.1 Introduction

AISI D2 tool steel is widely used in mold making industry as well as high speed cutting tools, where a combination of ultrahigh strength with high wear resistance and good toughness is required [1]. The conventional heat treatment of this steel consists of three main steps: 1) Solutionizing in the austenitic region (from 1273K to 1313K) [2]; 2) Air or gas cooling to room temperature (close to $1K.s^{-1}$ [2]); 3) Single or double tempering (from 423K to 823K) [3, 4]. The starting microstructure (i.e. the as-received condition) before hardening treatment is the annealed condition. In the annealed condition, the matrix is composed of ferrite and several types of carbides [2]. The larger or primary ones, M_7C_3, formed at the austenite grain boundaries and then dispersed as a result of hot working [2]. The other carbides, M_2C and $M_{23}C_6$, are the result of secondary precipitation during normalizing heat treatment [5-7]. It must be mentioned that some authors have proposed a sub-classification of secondary carbides as “large” and “small” secondary carbides in D2 steel [5]. The formation of MC and M_2C (similar chemical composition as M_7C_3), and $M_{23}C_6$ carbides are possible based on thermodynamic calculations [2].

As reported by several authors [4-7], after conventional quenching, the microstructure is composed of 1) fresh martensite, 2) a mixture of the M_2C and $M_{23}C_6$ carbides, and 3) retained austenite. The latter can decompose into ferrite and cementite during subsequent tempering between 573K and 773K thereby affecting the mechanical properties of the alloy [3]. Also, in a recent study [8] the present authors reported that conventional hardening treatment of this steel does not result in martensitic microstructure and instead a mostly bainitic microstructure was obtained. Therefore, higher cooling rates as well as very low cooling temperatures are required for complete martensitic transformation to take place in AISI D2 steel.

The effect of cryogenic treatment on microstructure evolution, wear, and mechanical properties of Fe-C steel, tool steels, and specifically AISI D2 tool steel has been previously reported by many researchers [10-21]. The temperature ranges studied by researchers varies from 223K to 77K and depending on the investigated temperature interval, the

denominations are different: ‘cold treatment’ for the interval 223K-193K; ‘shallow cryogenic treatment’ for the 193K-113K interval; and ‘deep cryogenic treatment’ for the 113K-77K interval. Preciado and Pellizzari [10], Olia et al. [12], and Das et al. [19, 21] have presented the most recent studies on the influence of cryogenic treatment and subsequent tempering on the sequence of precipitation of temper carbides and the evolution of mechanical and wear properties. However, in spite of the extensive amount of work, little information is available on martensite’s characteristics and the kinetics of martensitic transformation during direct cooling to 173K (shallow cryogenic temperature). In the present research, the above aspects are studied using a combination of high resolution dilatometer, scanning electron microscope (SEM), and transmission electron microscope (TEM). The obtained results are correlated with the existing models for martensitic transformation in steels and an equation is proposed which better describes the phase transformation for AISI D2 steel.

5.2 Mathematical analysis of dilatometry curves

Dilatometry is a powerful in-situ method to monitor solid state phase transformations characterized by changes in the lattice structure (e.g. austenite to martensite transformation) which are translated into variation of the specific volume of the specimen [22, 23]. However, it is not always possible to detect with precision the amount of volume change during the transformation as well as transformation start and finish points. High resolution dilatometry permits for precise temperature control and recording of nanometric volumes changes thereby allowing for the detection of the early stages of phase transformations as well as differentiation of superimposed processes which cannot be revealed with conventional dilatometry equipment. The transformation start and finish temperatures are often determined using tangent line method [24] and first derivative or off-set methods [25]. In order to estimate the volume changes during the martensitic transformation, mathematical equations are used to fit the experimental dilatation curves [26]. Yamamoto [26] proposed a model in which the total volume change during martensitic transformation is dependent on the sum of three variables: (1) shrinkage of the retained austenite, (2) shrinkage of newly formed

martensite, and (3) the expansion as a result of austenite-martensite transformation. This model is briefly described in equations 5.1 and 5.2 [26].

$$d_{i+1} = d_i - (f_m \alpha_m + f_\gamma \alpha_\gamma)\Delta T \tag{5.1}$$

$$E_{i+1} = d_{i+1} + \varepsilon_{\gamma-m} f_m \tag{5.2}$$

where i shows i-th experimental point, d the shrinkage due to expansion coefficient, E the total dilatation at a i-th temperature, α_m the expansion coefficient of martensite,α_γ the expansion coefficient of austenite, $\varepsilon_{\gamma\text{-}m}$ the strain due to lattice volume differences between austenite and martensite, and f_m the volume fraction of martensite stated with Koistinen and Marburger (K-M) equation [27] (Eq.5.3).

$$f_m = 1 - \exp[-b(M_s - T)] \tag{5.3}$$

In equation (5.3), M_s is martensite start temperature; b is a material constant varying with chemical composition and T is cooling start temperature [28]. Qui et al. [28] have reassessed Yamamoto's model and reported several inconsistencies including: no unique f_m for a given material, problems regarding the measurements of α_m, difficulty in finding unique b, M_s, $\varepsilon_{\gamma\text{-}m}$, and errors between calculated and experimental results [26]. Equations (5.1) and (5.2) were reformulated as shown in Eq.5.4 where it can be seen that five variables need to be determined in order to obtain an accurate fitting of the dilatation results [28].

$$E = E_0 + (\varepsilon_{\gamma-m} - \alpha_m M_s - (\alpha_\gamma - \alpha_m)/b) + \alpha_m T + ((\alpha_\gamma - \alpha_m)/b - \varepsilon_{\gamma-m}).\exp(-b(M_s - T)) \tag{5.4}$$

In the above equation E represents the total dilatation during transformation and E_0 corresponds to the dilatation at M_s temperature. In the present work the approach proposed by Qui et al. [28] was used to obtain the best fit for the dilatometry curves obtained during the experiments. On the basis of this analysis a more simplified equation is proposed (Eq.5.5) and it is also demonstrated that b is not a constant value but rather varies as a function of the cooling rate.

$$E = E_0 - 3.83 \times 10^{-6} + \alpha_m T - 4.235 \times 10^{-3} (\exp(-b(M_s - T))) \quad (5.5)$$

5.3 Materials and methods

The as-received AISI D2 material was Fe-1.54wt%C-0.33wt%Si-0.32wt%Mn-11.88wt%Cr-0.76wt%Mo-0.75wt%V-0.008wt%P-0.008wt%S in 15mm thick rolled sheet. Samples were cut into 10mm height and 4mm diameter cylinders with their height parallel to the rolling direction. High resolution BÄHR DIL 805 A/D dilatometer with a 50nm resolution at high speed cooling rates was used to carry out the experiments. Samples were heated to 1303K and maintained for 1200 seconds followed by continuous cooling to 173K at $10K.s^{-1}$ or $50K.s^{-1}$. The $50K.s^{-1}$ cooling rate was selected in order to avoid any carbide precipitation before the start of the martensitic transformation and also to insure an almost fully martensitic structure upon quenching. Finally, the samples were brought to room temperature with a heating rate of $10K.s^{-1}$. In order to examine the kinetics of austenite to martensite transformation a significantly lower cooling rate, $10K.s^{-1}$, was used. In order to avoid any oxidation and decarburization, the heat treatment cycle was conducted in vacuum environment. An etchant with the following composition 40g NaOH+60g H_2O+15g $NaNO_3$ initially proposed by Gouné et al. [29] was modified and successfully used for revealing martensite. Hitachi-TM3030 SEM and X-ray diffraction diagrams (XRD) were used for microstructural studies. The carbides count was calculated using the MIP® image analysis software [30]. For TEM studies, the sample cooled at rate of $50K.s^{-1}$ was prepared by precision ion polishing system (PIPS). Thin foils were then examined using an FEI Tecnai G^2 F20 TEM operated at 200kV.

5.4 Results

5.4.1 Dilatometry analysis

The dilatation curves versus undercooling are presented in Figs.5-1(a-d) and 5-2(a-d) for cooling rates of $10K.s^{-1}$ and $50K.s^{-1}$, respectively. The contraction curve showed parabolic

behavior for the 10K.s^{-1} cooling rate (Fig.5-1(a)) while almost linear behavior was observed for the 50K.s^{-1} cooling rate (Fig.5-2(a)) before the start of martensitic transformation. Splitting phenomena was observed around 480K for the slow cooling rate (Fig.5-1(a)) and 450K for the fast one (Fig.5-2(a)). De Andrés et al. [31] and Caballero et al. [32] have studied this effect in detail and related it to the presence of concentration gradients in the austenite, due to partial or total dissolution of carbides upon austenitization. Considering the similarities between the results obtained by the present investigation and those reported by the above authors, the observed splitting phenomena is also associated with the presence of chemical heterogeneities in the austenite which are revealed by the high resolution dilatometer. It is worth noting that the sudden change in dilatation observed around 300K in both conditions is due to the introduction of liquid nitrogen into the test chamber and is not related to any microstructural phenomenon.

Figs.5-1(b) and 5-2(b) show comparison between experimental results (black curve) and modeled data (red curve). The occurrence of martensitic transformation from M_s to 173K can be observed in both cases. Two distinct behaviors are distinguishable: 1) regular behavior consisting of expansion starting at M_s and reaching a maximum value around 325K; 2) an atypical behavior below 325K, where either another expansion is observed (Fig.5-1(b) - black curve) or the normal contraction expected at these low temperatures does not occur (Fig.5-2(b)-black curve). The second expansion in dilatation curve, as indicated in Fig.5-1(b), has been also observed by Wierszyllowski [33] and related to activation of a second martensitic transformation taking place below 273K. Using Eq.5.5 and the data reported in Table 5.1, best fits were obtained for dilatometry curves and the results are shown in Figs.5-1(b) and 5-2(b) (red curves) for the slow and fast cooling rates, respectively. Based on the above analysis, it can be said that the proposed model predicts relatively well the dilatation behavior until 325K; however, below this temperature, deviation occurs between experimental results and the predicted ones which may be due to secondary martensitic transformation or abnormal contraction between 325K and173K. The influence of undercooling on the volume fraction of martensite is shown in part c of Figs.5-1 and 5-2. The above data was obtained by finding the values of M_s and b from Eq.5.5 and using K-M

equation. It can be said that the regular behavior ends once 78 percent of austenite is transformed to martensite for the cooling rate of $10K.s^{-1}$ (Fig.5-1(c)) while for the cooling rate of $50K.s^{-1}$ it finishes when 85 percent of austenite is transformed to martensite (Fig. 5-2(c)). Thus, the remaining austenite (22% and 15% respectively) will undergo atypical behavior until the end of the process. The proposed model predicts the presence of 1.5% and 3% retained austenite, in the final microstructure, for fast cooled and slow cooled samples, respectively. The high resolution dilatometer made also possible to screen small variations in expansion or contraction during soaking at austenitizing temperature. For example, Fig.5-1(d) (red dashed lines) shows a value of 0.09% for compressive strain in the case of $10K.s^{-1}$ cooling rate while this value was 0.02% in the case of $50K.s^{-1}$ cooling rate (Fig.5-2(d), red dashed lines,). The occurrence of non-uniform strain during austenitization, as illustrated in Figures 5-1(d) and 5-2(d), was observed repeatedly for many other test conditions carried out by the authors. The detailed quantification of this effect and its impact on the kinetics of martensitic transformation is presently carried out by the authors and will be the subject of a separate communication. In the context of the present paper, it can be said that chemical heterogeneity in the microstructure or stabilization of retained austenite could be possible causes of such effect. Indeed, carbides in AISI D2 tool steel have smaller coefficient of thermal expansion than the parent phase, thereby affecting the normal dilatation of the matrix and generating anisotropic strains [34]. During austenitization, due to the holding at high temperature, the austenite is relaxed from these strains; in contrast because of the partial dissolution of carbides, the strength of austenite is increased [34]. It is relevant to mention that slower cooling rates could also contribute to retained austenite stabilization and therefore to the occurrence of the atypical behavior. This is illustrated in Figs.5-1(c) and 5-2(c), where it can be seen that martensite fraction in slow cooled sample is smaller than in the fast cooled one. Finally, it is important to note that the results obtained in the present investigation reveal a dependency of the value of the ‘constant’ b on the cooling rate employed during testing.

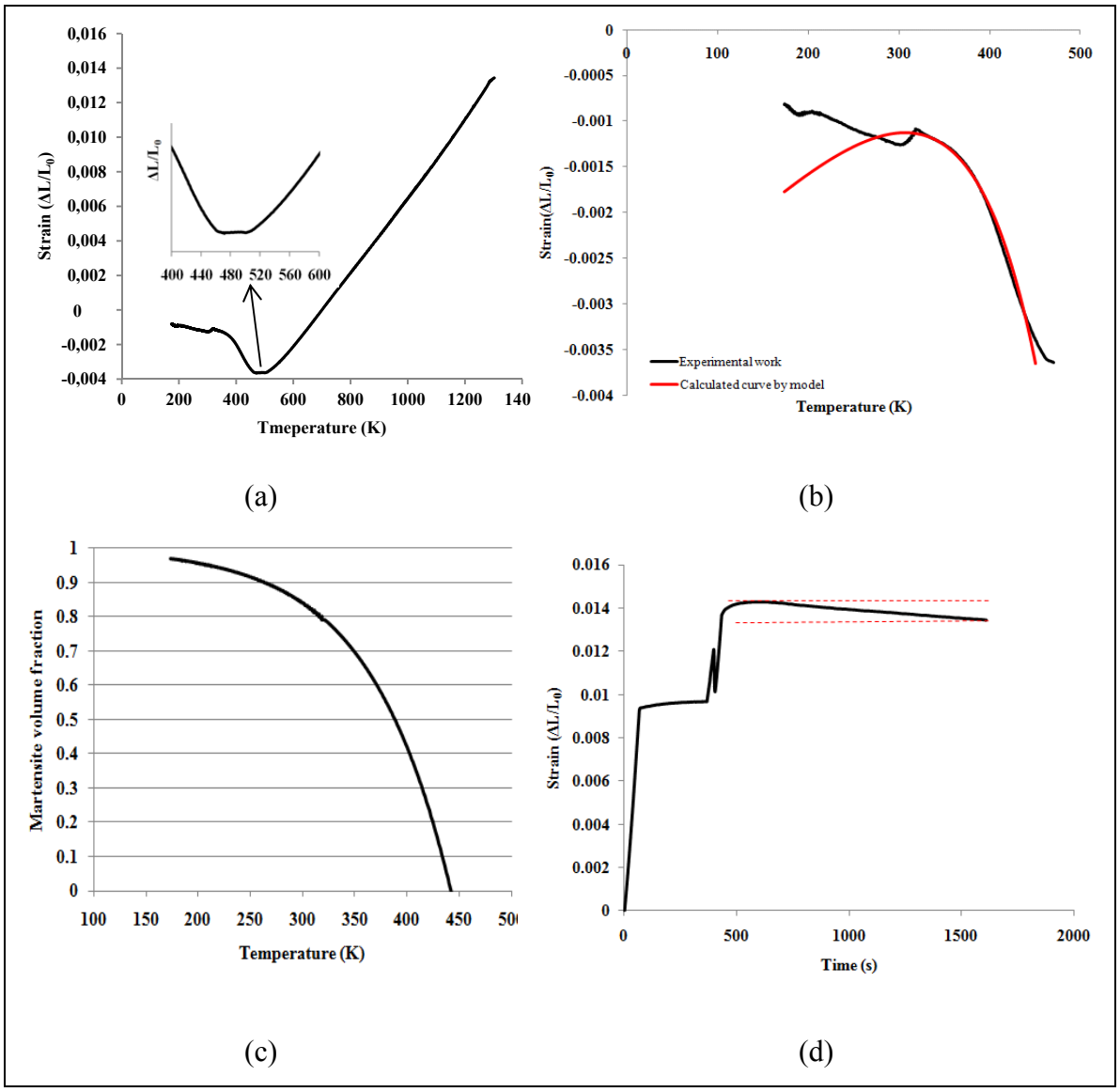

Figure 5-1(a) Dilatation diagram during cooling at the rate of 10K.s^{-1} depicting the start of martensitic transformation(M_s), (b) curve fitting results based on Eq.5.5 in comparison with experimental results in the region where transformation occurs in part a, (c) change in volume fraction of martensite versus under cooling calculated by Eq.5.5, (d) evolution of compressive strain during holding time at austenitization temperature. The maximum compression strain was obtained by subtracting the highest expansion value from the value right before the start of cooling (range is shown by red dashed lines).

While the dependency of b on steel composition has been previously reported [28, 35], to the knowledge of the authors, this is the first time that its variation with cooling rate is demonstrated.

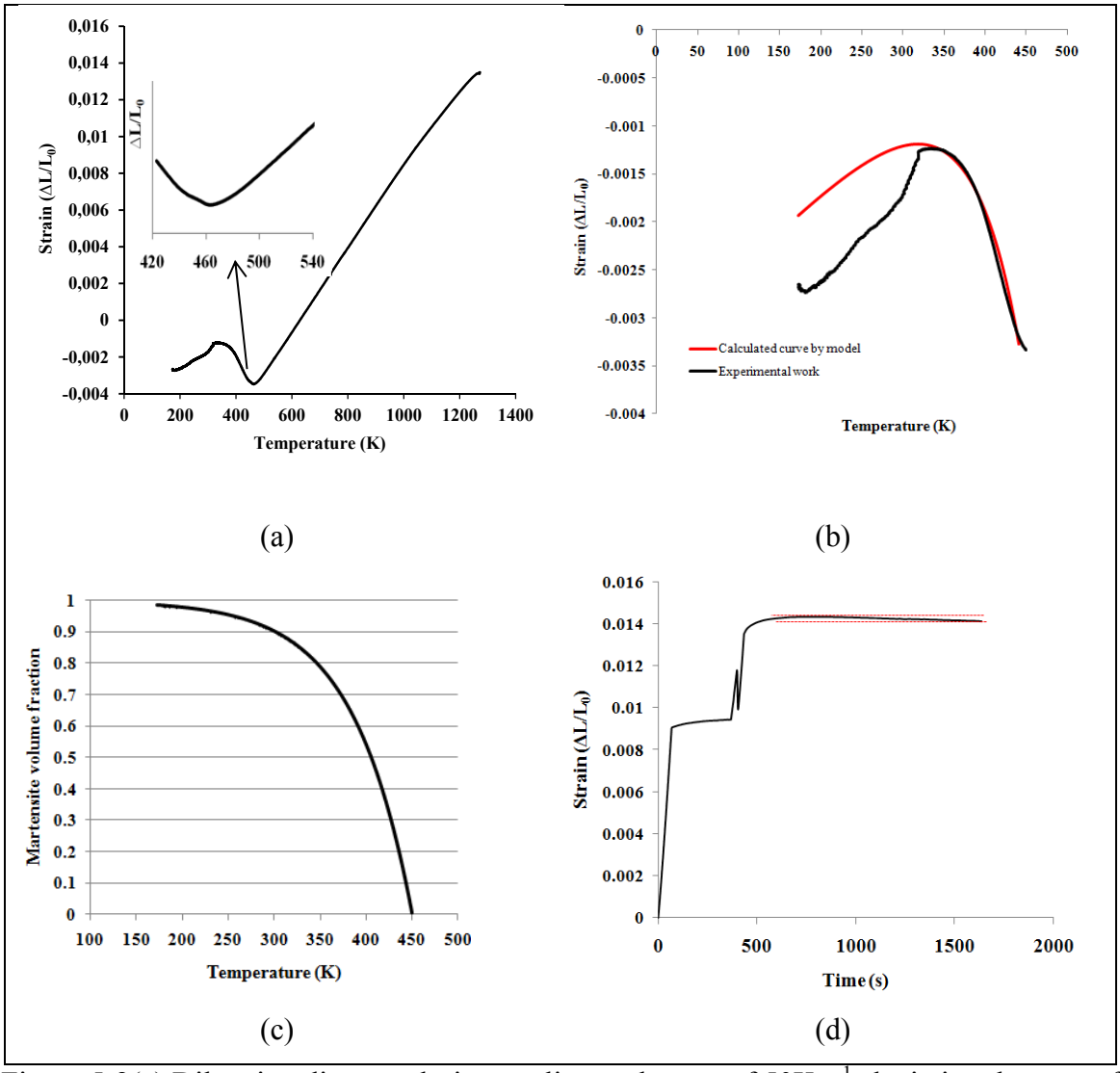

Figure 5-2(a) Dilatation diagram during cooling at the rate of 50K.s^{-1} depicting the start of martensitic transformation(M_s), (b) curve fitting results based on Eq.5.5 in comparison with experimental results in the region where transformation occurs in part a, (c) change in volume fraction of martensite versus under cooling calculated by Eq.5.5, (d) evolution of compressive strain during holding time at austenitization temperature. The maximum compression strain was obtained by subtracting the highest expansion value from the value right before the start of cooling (range is shown by red dashed lines).

5.4.2 Microstructural analysis

Figure 5-3 shows the SEM micrographs of the microstructure obtained after cooling at the rate of 10K.s^{-1}(a) and 50K.s^{-1}(b). They both show similar features such as plate-like

martensite, large primary carbides, and fine secondary carbides (details brought in Introduction); no trace of grain boundaries is observed which confirms similar chemical composition between the product (martensite) and the parent phase (austenite). X-ray diffraction analysis did not show austenite peaks for both heat treatment conditions. In order to investigate possible carbide precipitation before the start of transformation for the lower cooling rate (10K.s^{-1}), back scattered electron (BSE) detector was used.

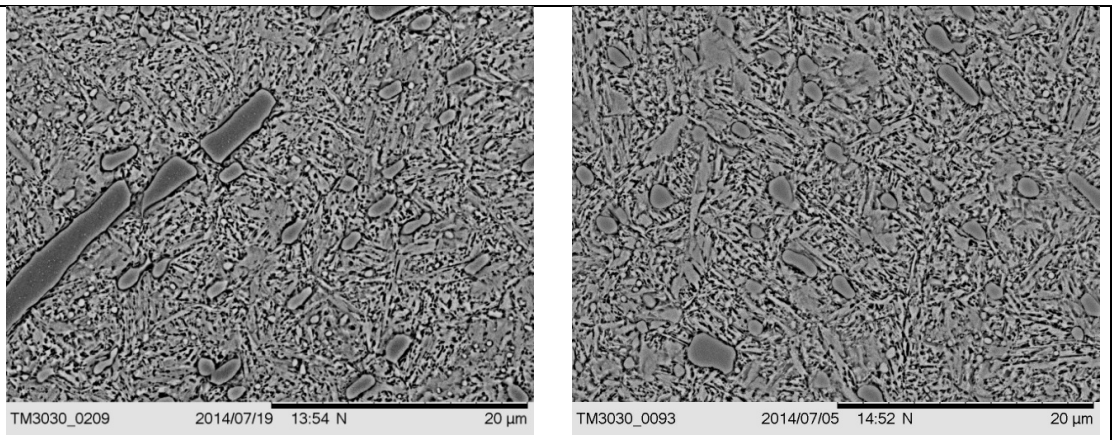

Figure 5-3(a) SEM micrograph of the alloy cooled at the rate of 10K.s^{-1}, (b) SEM micrograph of the alloy cooled at the rate of 50K.s^{-1} (microstructure features: primary large carbides and secondary carbides; no trace of grain boundaries).

The influence of cooling rate on the presence of very fine carbides (below 1µm) is shown in Fig.5-4(a-c). A higher population of carbides with average diameter below 1µm is observed in the samples cooled at 10K.s^{-1} (Fig.5-4(c)). XRD diagrams for both conditions are shown in Fig.5-4(d). The M_7C_3 main XRD peak is located at 2-theta ≈ 44° with M being mostly Cr and Fe. The M_7C_3 peak intensity is higher for slow cooled sample corresponding to higher volume fraction of these carbides. In the figure, the (110) martensite peak located at 44.5° is also shown to distinguish it from the M_7C_3 peak. It is worth mentioning that, as reported by several authors [2, 6, 7] submicron size secondary carbides precipitate in AISI D2 steel during hot forming and will be retained after quenching. However, they can't be detected readily by X-ray diffraction due to their small sizes and TEM is needed to reveal them [6].

The above findings confirm that the splitting phenomenon observed in the dilatometry curve of the slow cooled sample (Fig.5-1(a)) corresponds to carbide precipitation (carbon-depleted austenite) while the splitting observed in the dilatometry curve of the fast cooled sample (Fig.5-2(a)) is related to the occurrence of transformation in carbon-rich austenite. The obtained results are in agreement with those reported by other authors [30, 31].

In order to study the detailed morphology of martensite, TEM observation was carried out on the sample cooled at $50K.s^{-1}$. As shown in Fig.5-5(a-b), the microstructure is mainly composed of plate martensite (Fig.5-5(a)); however, a noticeable amount of lath type morphology is also observed (Fig.5-5(b)). Using the Thermo-Calc software's TCFE7 database and methodology provided in reference [36], the carbon content of austenite at 1303K was estimated to be about 0.52wt%. Considering that low M_s temperature promotes the formation of plate martensite in expense of lath type [37], it is reasonable to observe a mixed morphology of lath and plate martensite. More detailed discussion on the factors controlling martensite morphology will be provided in the discussion section. In addition to the observed plate and lath martensite, nano sized twins were also observed in several areas of the examined samples, as shown in the bright-field TEM images in Fig.5-6 (a-d). A series of highly dense internal transformation nano-twins with a thickness of 10nm are accommodated in the areas expanding over 600nm (Fig.5-6(a-c)). Selected area diffraction (SAD) pattern, taken from area shown by yellow circle in Fig.5-6(c), is presented in Fig.5-6(d) indicating that the nano-twins are located in 112 planes and the relationship between the matrix and the twins. The obtained results are in agreement with those reported by other authors [37-39] on Fe-Cr-C steel where the same type of orientation was observed between the matrix and the nano-twins. It has been reported that internal martensite twins can be considered as transformation twins if they meet the symmetry requirements otherwise they are just demonstrations of adjustment effects [40]. In the present investigation, it was found that (Fig.5-6(d)) the twin plane is always a plane of mirror symmetry with respect to the austenite indicating that the observed nano-twins in the microstructure are internal transformation twins produced as a result of the cryogenic cooling.

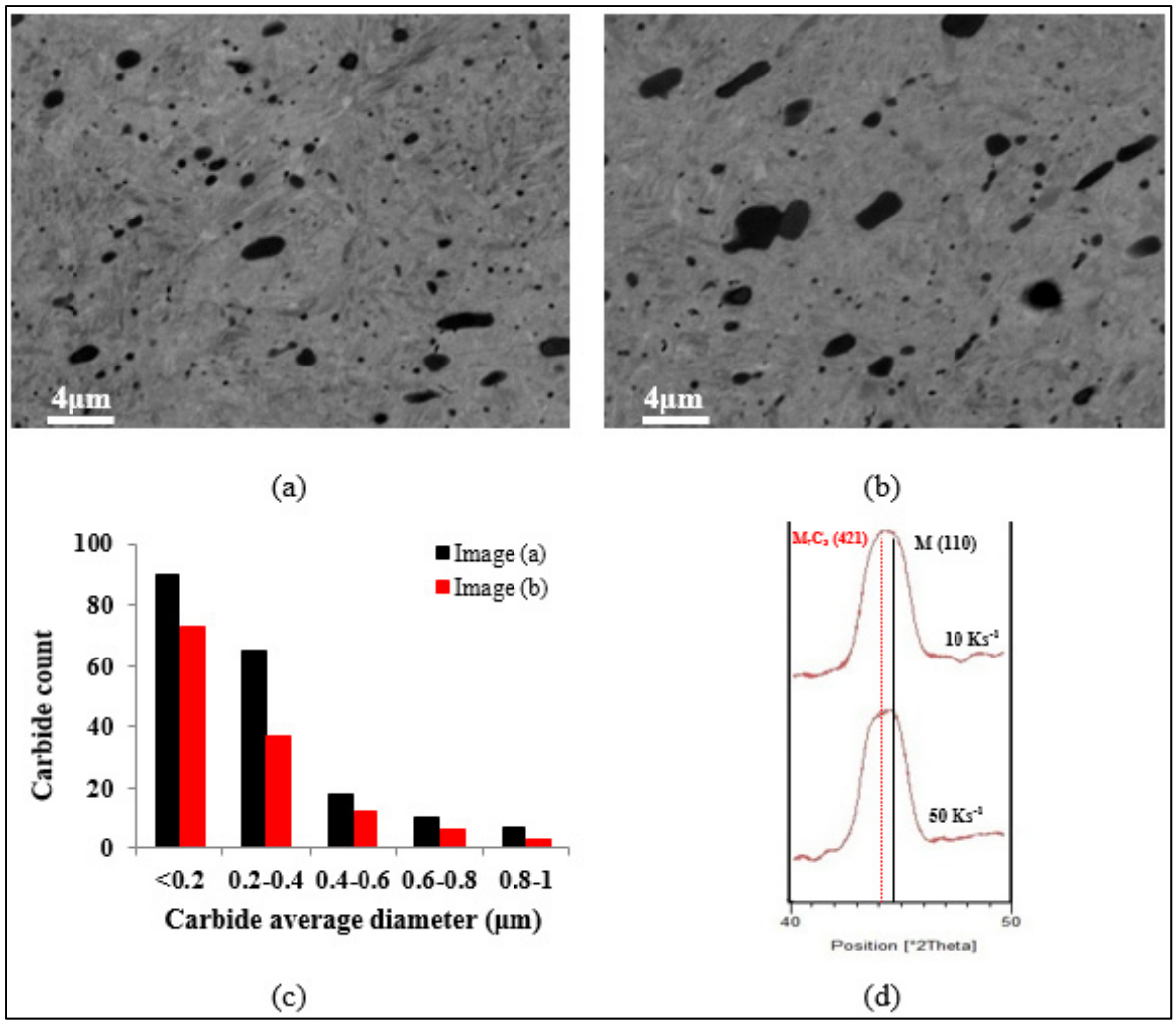

Figure 5-4 The effect of higher cooling rate on the suppression of carbide precipitation during cooling (a) BSE-SEM micrograph from microstructure of the alloyed cooled at the rate of 10K.s^{-1}(b) BSE-SEM micrograph from microstructure of the alloyed cooled at the rate of 50K.s^{-1}, (c) diagram showing the number of carbides with size less than 1µm for conditions in parts (a) and (b), (d) XRD diagrams showing (421) peak of M_7C_3 carbide and (111) of martensite (overlap is due to very close diffraction angles).

5.5 Discussion

5.5.1 Kinetics of martensite formation

The Koistinen and Marburger equation (Eq.5.3) [27] is often used to describe the extent of transformation as function of temperature. In this equation, b is a rate parameter which is

often considered as dependent on the steel composition and can be extracted from empirical equations [35]. In some cases, this parameter has also been considered as K-M original constant value which has been suggested to be about $0.011K^{-1}$ for plain carbon steel [27]. However, using empirical equation described in ref. [35], it was not possible to predict a suitable value for b to be able to obtain the best fit for the obtained results because the empirical equation has been developed for a certain compositional range and as such has limited applicability.

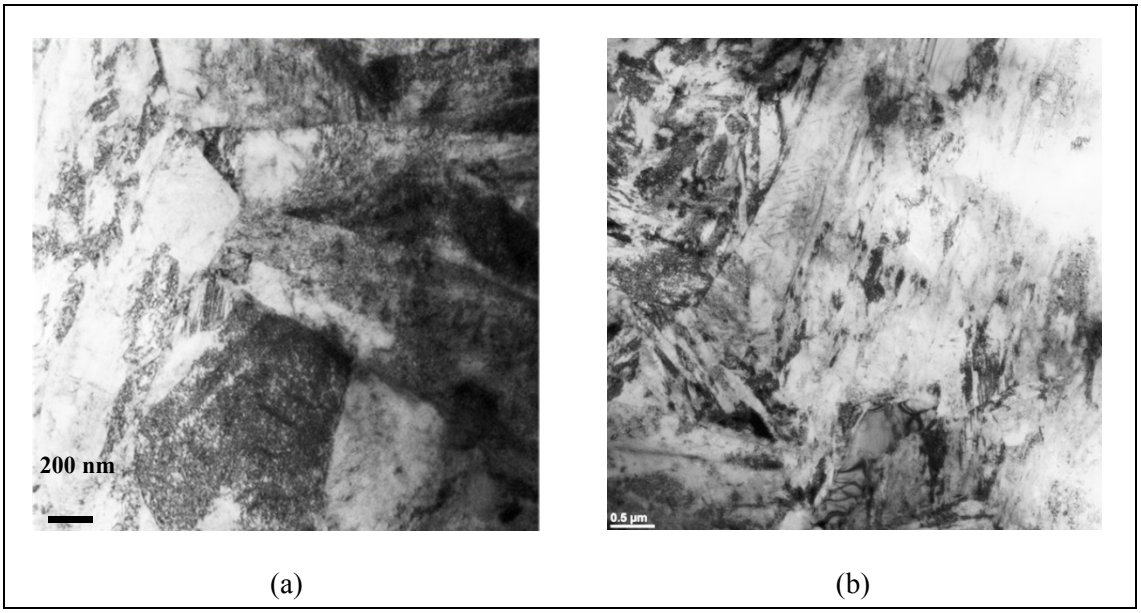

Figure 5-5 Morphology of martensite as result of cooling at the rate of $50K.s^{-1}$ (a) bright-field TEM image of partly plate type martensite (b) bright-field TEM image of lath type martensite.

On the other hand, using a constant value for b as provided in reference [27] it was not possible to obtain an acceptable fit for the experimental results. In the present investigation it was found that the equation proposed by Qui et al. [28] allows for a more accurate prediction of the fraction transformed and the influence of chemical composition and cooling rate are considered in the estimation of the rate parameter b. Fig.5-7 depicts the effect of higher cooling rate on the value of b obtained from Eq.5.5.

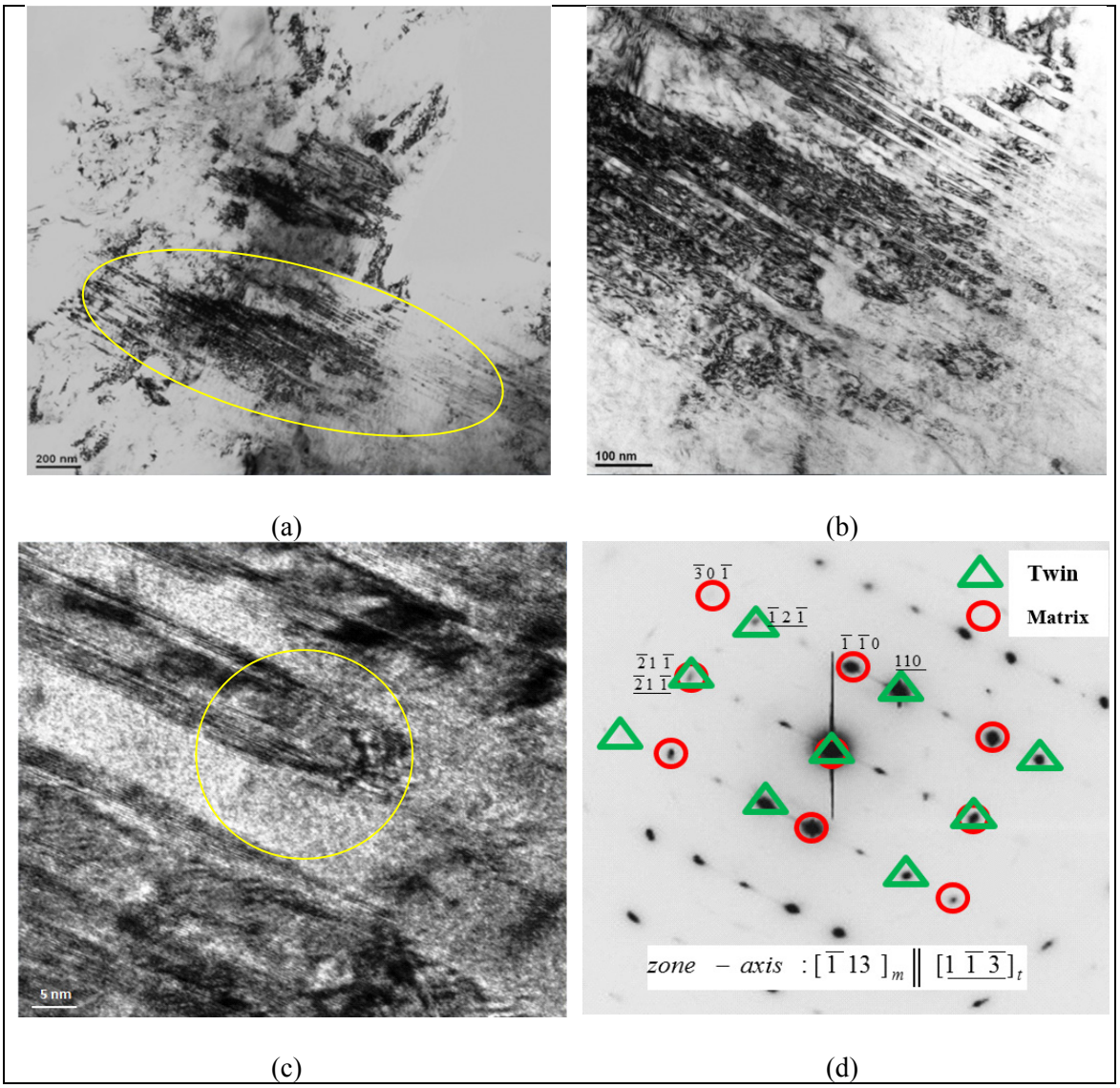

Figure 5-6(a) Nano-twins (circled area) in the substructure of the alloy cooled at the rate of 50K.s^{-1} (b) higher magnification of the same area showing high density of dislocation in smaller bands (≈ 10nm thick) (c) very high magnification showing one nano-twin (yellow circle shows the area over which SAD pattern was taken, (d) corresponding analysis of SAD pattern.

Additionally, parameter b can be defined approximately in terms of the linear relation between chemical driving force of transformation with the number of new martensite plates formed per unit volume as shown below [41, 42].

$$b = -\bar{\vartheta}\phi\left(d(\Delta G)/dT\right) \tag{5.6}$$

where $\bar{\vartheta}$ is the average volume of the newly formed martensite plates caused by temperature variation dT, φ is a proportionality constant, ΔG is the volume free energy change accompanying transformation and T is the temperature. In this research, two different values for b have been found as a result of change in cooling rate (see Table 5.1).

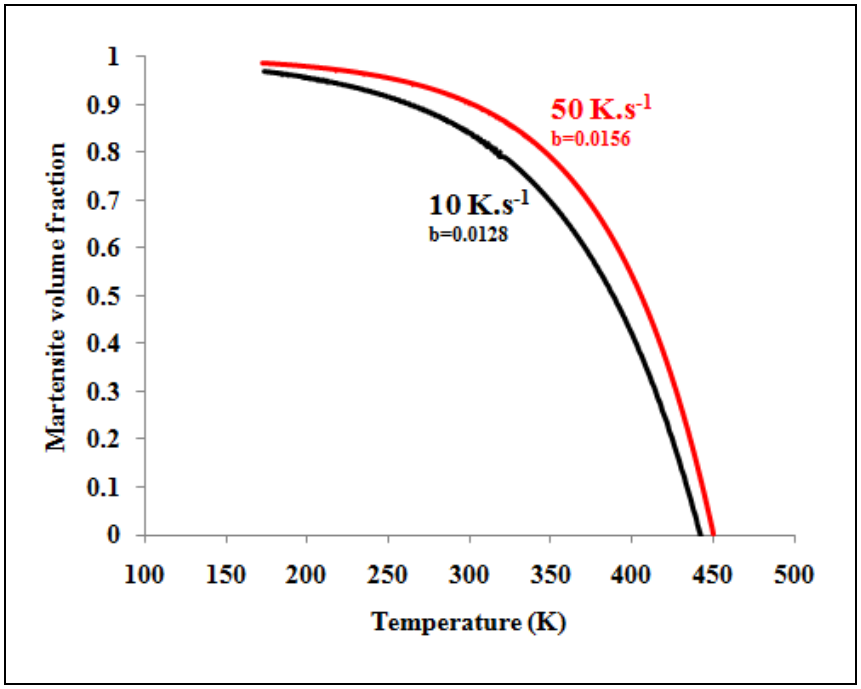

Figure 5-7 Effect of cooling rate on the resulted b factor from Eq.5.5.

The chemical driving force ($\Delta G^{\gamma\to\alpha}$) of austenite to martensite (ferrite) transformation for AISI D2 tool steel can be extracted from Thermo-Calc database TCFE7 (Fig.5-8). If the values of chemical driving force between M_s temperature and 325K, where regular behavior ends (by model), are divided by undercooling (with considering same value for φ); the average volume of martensite phase can be estimated as indicated below.

$$b_{10Ks^{-1}} = 0.0128 = -\bar{\vartheta}\varphi\left(\frac{\Delta G_{325K} - \Delta G_{M_s=444K}}{325-444}\right) = -\bar{\vartheta}\varphi\left(\frac{-3470+2570}{-119}\right) \Rightarrow \bar{\vartheta} = 0.00169\varphi$$

$$b_{50Ks^{-1}} = 0.0156 = -\bar{\vartheta}\varphi\left(\frac{\Delta G_{325K} - \Delta G_{M_s=450K}}{325-450}\right) = -\bar{\vartheta}\varphi\left(\frac{-3470+2547}{-125}\right) \Rightarrow \bar{\vartheta} = 0.00211\varphi$$

Table 5.1 Data used for curve fitting for both 10K.s^{-1} and 50K.s^{-1} cooling rates

	Cooling rate	
Variable	**10K s^{-1}**	**50K s^{-1}**
E_0	-0.00326	-0.00334
α_m $(\times 10^{-6}/K)$	9.36	8.48
b	0.0128	0.0156
M_s First derivative method (K)	470	450
M_s Calculated by model (K)	444	450

The above results indicate that higher average volume fraction of martensite is obtained for higher b value which is in agreement with the results obtained in Fig.5-7 using Eq.5.5 with a variable b value.

5.5.2 Factors controlling martensite morphology

In Fe-C-Cr steels, lath martensite forms at higher M_s temperature compared to plate martensite [37]. The M_s temperature calculated from Eq.5.5 for the first part of the dilatation diagram did not show considerable changes (between 444K and 450K) by increasing the cooling rate from 10 to 50 (K.s^{-1}) indicating that the M_s temperature of AISI D2 steel is not affected by cooling rates in this range. However, significant changes in M_s temperature causing morphology changes from lath to plate type have been reported where very high cooling rates, above 6000K.s^{-1}, were used in ferrous alloys [43]. The strength of austenite and martensite can also affect the morphology of martensite [44]. The active habit plane of martensite can be determined as a function of the resistance of austenite and martensite to dislocations motion [44]. The results obtained in this study revealed the presence of both lath and plate morphologies in the microstructure (Fig.5-5 (a-b)). Also, as indicated in Figs.5-1(d) and 5-2(d), a contractive strain is observed during soaking at austenitizing temperature. The source of this strain can be attributed to chemical inhomogeneity caused by the dissolution of carbides or the stabilization of retained austenite because of the slow cooling [23, 34].

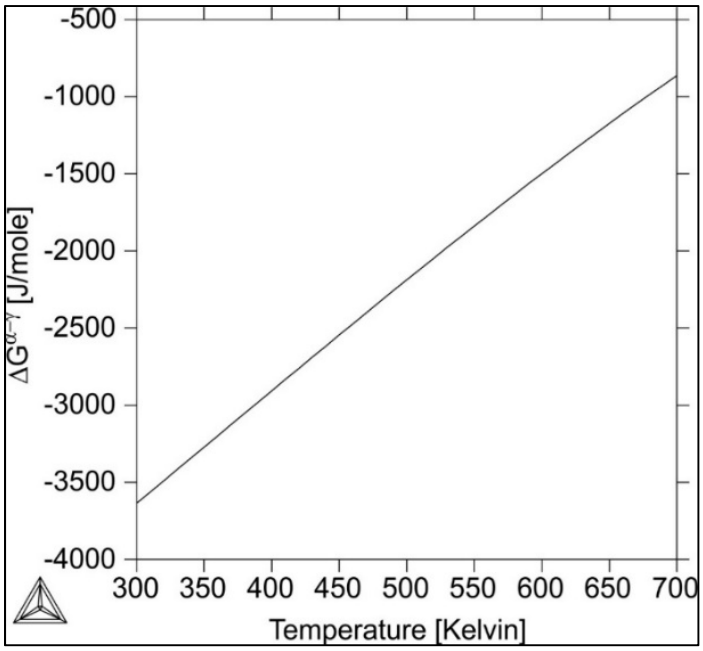

Figure 5-8 Chemical Gibbs free energy changes during diffusionless transformation from austenite to martensite (ferrite) extracted from Thermo-Calc database TCFE7, given for the composition of austenite at 1303K.

The presence of the contraction observed in this study indicates that part of the austenite phase has a higher strength level. Such difference in strength level determines the type of habit plane that will be activated and as a result the martensite morphology which will be formed. In the present investigation plate shaped martensite with $\{225\}_\gamma$ habit plane and highly dislocated platelets or lath martensite with $\{111\}_\gamma$ habit plane was identified. The above results are in agreement with those reported by other authors on the preferred habit planes for these types of martensite [37, 44].

It has been reported that {225} martensite does not have clearly defined midrib while it could be internally twinned [43]. The results obtained in the present investigation are in agreement with the above reports as no trace of midrib was observed in TEM micrographs (Fig.5-5(a-b)) and internal nano-twins were present in the microstructure (Fig.5-6(a-d)). It is well known that low M_s temperatures promote the formation of twins [45]. For the investigated alloy, it was calculated that in the range 325K - 173K, 15% to 22% of austenite transforms to

martensite, respectively (Figs.5-1(c) and 5-2(c)). It is therefore reasonable to assume that the formation of internal nano-twins in this temperature range is due to austenite transformation.

Martensitic transformation is always accompanied with plastic deformation and the dominant deformation mode in austenite could be modified by changes in critical resolved shear stress [34, 45]. The presence of a significant amount of nano-twins observed on the martensite produced during cooling indicates that, under these conditions, the critical resolved shear stress for twinning is lower than the one for slip and therefore austenite to martensite transformation is promoted in expense of slip.

5.6 Conclusions

In this research, martensitic transformation of AISI D2 tool steel via continuous cooling to 173K was investigated. The following main conclusion can be drawn from this investigation:

1. Two distinct regions were identified in the dilatometry diagrams: a) regular behavior where expansion in the curve starts at M_s and reaches the maximum around 325K; and b) an atypical behavior below 325K where the dilatation does not follow normal contraction or another expansion occurs.
2. Kinetics study showed 15% to 22% of martensite formation, depending on the cooling rate, occurs between room temperature and the cryogenic temperature with only 1.5% to 3% of non-transformed austenite in the final microstructure.
3. Microstructural analysis showed the concomitant presence of lath and plate morphologies as well as nano-twins.
4. The occurrence of nano-twins was related to the changes in the deformation mode of austenite when austenite undergoes martensitic transformation between room temperature and cryogenic temperature.
5. M_s temperature, microstructural heterogeneity, and strength of austenite were found as effective factors influencing the morphology of martensite.

Acknowledgements

The authors would like to thank the National Sciences and Engineering Research Council of Canada (NSERC) for their support and financial contribution through the ENGAGE and ENGAGE plus programs. The authors also appreciate the collaboration of DK SPEC Inc. for providing experimental materials, support from CanmetMATERIALS in the framework of RIEM program for dilatometry experiments, Hitachi Canada for privileged access to advanced microscopy facilities.

References

[1] T. Arai et al. ASM Handbook, Heat Treating, ASM International, USA (199).

[2] D. Bombac, M. Fazarinc, A. Saha Podder, G. Kugler, Study of carbide evolution during thermo-mechanical processing of AISI D2 tool steel, Journal of Materials Engineering and Performance 22-3 (2013) 742-747.

[3] G. R. Speich, W. C. Leslie, Tempering of steel, Metallurgical Transactions 3-5 (1972) 1043-1054.

[4] P. F. da Silva Farina, C. A. Barbosa, H. Goldenstein, Microstructural characterization of an AISI D2 tool steel submitted to cryogenic treatment, ASTM special technical publication 1532 (2012) 57-70.

[5] D. Das, A. K. Dutta, K. K. Ray, Influence of varied cryotreatment on the wear behavior of AISI D2 steel, Wear 266 (2009) 297-309.

[6] A.I. Tyshchenko, W. Theisen, A. Oppenkowski, S. Siebert, O.N. Razumov, A.P. Skoblik, V.A. Sirosh, Yu. N. Petrov, V.G. Gavriljuk, Low-temperature martensitic transformation and deep cryogenic treatment of a tool steel, Materials Science and Engineering A 527 (2010) 7027-7039.

[7] V. G. Gavriljuk, V. A. Sirosh, Y. N. Petrov, A. I. Tyshchenko, W. Theisen, A. Kortmann Carbide precipitation during tempering of a tool steel subjected to deep cryogenic treatment. Metallurgical and Materials Transactions A 45-3 (2014) 2453-2465.

[8] H. Ghasemi Nanesa, M. Jahazi, Alternative phase transformation path in cryogenically treated AISI D2 tool steel, Materials Science and Engineering A 634 (2014) 32-36.

[9] V. G. Gavriljuk, W. Theisen , V. V. Sirosh, E. V. Polshin, A. Kortmann, G. S. Mogilny, Y. N. Petrov, Y. V. Tarusin , Low-temperature martensitic transformation in tool steels in relation to their deep cryogenic treatment , Acta Materialia 61 (2013) 1705-1715.

[10] M. Preciado, M. Pellizzari, Influence of deep cryogenic treatment on the thermal decomposition of Fe-C martensite, Journal of Materials Science 49-23 (2014) 8183-8191.

[11] S. G. Singh, J. Singh, R. Singh, H. Singh, Metallurgical principles of cryogenically treated tool steels - A review on the current state of science, International Journal of Advanced Manufacturing Technology 54 (2011) 59-82.

[12] A. Oila, C. Lung, S. Bull S Elastic properties of eta carbide (η-Fe_2C) from ab initio calculations: application to cryogenically treated gear steel, Journal of Materials Science 49 (2014) 2383-2390.

[13] Y. M. Rhyim, S. H. Han, Y. S. Na, J. H. Lee, Effect of deep cryogenic treatment on carbide precipitation and mechanical properties of tool steel. Solid State Phenomena 118 (2006) 9-14.

[14] D. N. Collins, J. Dormer, Deep cryogenic treatment of a D2 cold-work tool steel, Heat Treatment of Metals 24-3 (1997) 71-74.

[15] A. P. Gulyaev, Improved methods of heat treating high speed steels to improve the cutting properties, Metallurgy 12 (1937) 65-70.

[16] D. Das, A. K. Dutta, K. K. Ray, Influence of temperature of sub-zero treatments on the wear behaviour of die steel, Wear 267 (2009) 1371-1380.

[17] D. Das, A. K. Dutta, K. K. Ray, Sub-zero treatments of AISI D2 steel: Part I. Microstructure and hardness. Materials Science and Engineering A527 (2010) 2182-2193.

[18] E. A. Huallpa, J. C. Sánchez, L. R. Padovese, H. Goldenstein, Determining M_s temperature on a AISI D2 cold work tool steel using magnetic Barkhausen noise, Journal of Alloys and Compounds 577 (2013) S726-S730.

[19] D. Das, K. K. Ray, Structure–property correlation of sub-zero treated AISI D2 steel. Materials Science and Engineering A 541 (2012) 45-60.

[20] D. Das, A. K. Dutta, K. K. Ray, On the refinement of carbide precipitates by cryotreatment in AISI D2 steel. Philosophical Magazine 89-1 (2009) 55-76.

[21] D. Das, A. K. Dutta, K. K. Ray Structure-property correlation of cryotreated AISI D2 steel, Advanced Materials Research 117 (2010) 49-54.

[22] C. García de Andrés, F. G. Caballero, C. Capdevila, L. F. Alvarez, Application of dilatometric analysis to the study of solid-solid phase transformations in steels, Materials Characterization 48 (2002) 101-111.

[23] H. Y. Yu, A new model for the volume fraction of martensitic transformations, Metallurgical and Materials Transactions A 28 (1997) 2499-2506.

[24] P. Motyca, M. Kövér, Evaluation Methods of Dilatometer Curves of Phase Transformations, COMAT 2012, conference proceedings, Parkhotel Plzen, Czech Republic, EU Czech Republic (2012).

[25] H. S. Yang, H. K. D. H. Bhadeshia, Uncertainties in dilatometric determination of martensite start temperature, Materials Science and Technology 23-5 (2007) 556-560.

[26] J. Yamamoto, S. Meguro, Y. Muramatsu, N. Hayakawa, K. Hiraoka, Analysis of martensite transformation behavior in welded joints of low transformation-temperature materials, Quarterly Journal Japan Welding Society 25 (2007) 560-568.

[27] D. P Koistinen, R. E. Marburger, A general equation prescribing the extent of the austenite-martensite transformation in pure iron-carbon alloys and plain carbon steels, Acta Metallurgica 7 (1959) 59-60.

[28] H. Qiu, J. Qi, F. Yin, K. Hiraoka, Determining of parameters for fitting the dilatation curve of austenite-martensite transformation in Cr-Ni steels, ISIJ International 49-1 (2009) 146-148.

[29] M. Gouné, O. Bouaziz, S. Allain, K. Zhu, M. Takahashi, Kinetics of bainite transformation in heterogeneous microstructures, Materials Letters 67-1 (2012) 187-189.

[30] Nahamin Pardazan Asia, 〈http://en.metsofts.ir/〉, Iran (2014).

[31] C. García de Andrés, J. A. Jiménez, L. F. Álvarez, Splitting phenomena occurring in the martensitic transformation of Cr13 and CrMoV14 stainless steels in the absence of carbide precipitation, Metallurgical and Materials Transactions A 27-7 (1996) 1799-1805.

[32] F. G. Caballero, L. F. Alvarez, C. Capdevila, C. García de Andrés, The origin of splitting phenomena in the martensitic transformation of stainless steels, Scripta Materialia 49-4 (2003) 315-320.

[33] I. A. Wierszyllowski, Martensitic transformation of austenite below 273 K. dilatometric and magnetic studies, Journal de Physics IV France 07 (1997) C5-417 -422.
[34] J. Wei, O. Kessler, M. Hunkel, F. Hoffmann, P. Mayr, Anisotropic phase transformation strain in forged D2 tool steel, Materials Science and Technology 20 (2004) 909-914.
[35] S. M. C. van Bohemen, Bainite and martensite start temperature calculated with exponential carbon dependence, Materials Science Technology 28 (2012) 487-495.
[36] M. Yaso, S. Morito, T. Ohba, K. Kubota, Microstructure of martensite in Fe–C–Cr steel, Materials Science and Engineering A 481-482 (2008) 770-773.
[37] M. Umemoto, E. Yoshitake, I. Tamura, The morphology of martensite in Fe-C, Fe-Ni-C and Fe-Cr-C alloys, Journal of Materials Science 18 (1983) 2893-2904.
[38] H. Y. Lee, H. W. Yen, H. T. Chang, J. R. Yang, Substructures of martensite in Fe-1C-17Cr stainless steel, Scripta Materialia 62-9 (2010) 670-673.
[39] D. Das, K. K. Ray, On the mechanism of wear resistance enhancement of tool steels by deep cryogenic treatment, Philosophical Magazine Letters 92-6 (2012) 295-303.
[40] H. K. D. H. Bhadeshia, D. V. Edmonds, A direct analysis of twinning in a low alloy martensite, Phase Transformations, York Conference, the Institution of Metallurgists 2-11 (1979) IV-4-8.
[41] H. K. D. H. Bhadeshia, An aspect of the nucleation of "burst" martensite in steels, Journal of Materials Science 17 (1982) 383-386.
[42] C. L. Magee, The nucleation of martensite: in: H. I. Aaronson, V. F. Zackay (Eds.), Phase transformations: ASM International, Materials Park, Ohio, USA (1970) 115-156.
[43] S. J. Donachie, G. S. Ansell, The effect of quench rate on the properties and morphology of ferrous martensite, Metallurgical Transactions A 6 (1975) 1863-1875.
[44] R. G. Davies, C. L. Magee, Influence of austenite and martensite strength on martensite morphology, Metallurgical Transactions 2 (1971) 1939-1947.
[45] O. Johari, G. Thomas, Factors determining twinning in martensite, Acta Metallurgica 13(1965) 1211-1212.

CHAPTER 6

ARTICLE5: CARBON ORDERING AND FORMATION OF TRANSITION CARBIDES DURING MARTENSITIC TRANSFORMATION AT CRYOGENIC TEMPERATURES

Hadi Ghasemi Nanesa[a], Mohammad Jahazi[a], Reza Naraghi[b]

[a] Department of Mechanical Engineering, École de Technologie Supérieure, 1100 rue Notre-Dame Ouest, Montréal (QC) H3C 1K3 Canada.

[b] Department of Materials Science and Engineering, KTH Royal Institute of Technology, Brinellvägen 23, SE-10044 Stockholm, Sweden

An article adopted from this chapter has been submitted to Journal of Philosophical Magazine.

Abstract

In this study, a methodology is proposed to calculate the chemical driving force of martensitic transformation at cryogenic temperatures taking into account the contribution from Zener-ordering. It is shown that the energy barrier for transformation is the sum of the strain energy required for the activation of martensitic transformation and the cooling rate-dependent strain energy stored in austenite which was determined in the present study. Changing the cooling rate from $10K.s^{-1}$ to $50K.s^{-1}$ led to 16% reduction in the associated strain energy. For the sample cooled at $50K.s^{-1}$, the spontaneous formation of η-carbides was observed. A combination of thermodynamic calculations and microstructural observations was used to rationalize the presence of carbon rich regions formed from ordered BCT martensite as nucleation sites for these carbides.

6.1 Introduction

AISI D2 steel is a high carbon high chromium steel known for its superior high strength and high wear resistance [1, 2]. It contains 1.54wt%C and 12wt%Cr and other alloying elements

such as Mo, V, Si, Mn. The initial microstructure is composed of soft ferrite and hard carbides. Conventional hardening treatment of this alloy, consisting of solutionizing in the austenitic region [2] and air or gas cooling to room temperature results in a microstructure composed of fresh martensite, a mixture of M_7C_3, M_2C, and $M_{23}C_6$ carbides, and some retained austenite [3-7]. The presence of the retained austenite is related to the effect of alloying element on pushing down the martensite finish temperature to sub-zero temperature [3-7]. The retained austenite decomposes into ferrite and cementite or bainite during subsequent tempering between 573K and 773K deteriorating the mechanical properties of the alloy [3]. Therefore, with the objective to achieve full martensitic transformation and improve mechanical properties, cooling to cryogenic temperatures (200K-77K) has been added to the above cycle [8-15]. The transformation of retained austenite to martensite and the formation of transition carbides, called η-carbides have been suggested as possible root causes for the cryogenic effect [9, 10, 13-16]. The transformation of retained austenite to martensite at cryogenic temperatures has been the subject of many publications [8-16]; however, there is still no general agreement on the operating mechanisms for this transformation. Specifically, Tyshchenko et al. [6] and Gavriljuk et al. [7, 8] have reported that the transformation of retained austenite to martensite occurs under isothermal conditions. Recently, the present authors reported that cooling rates above $10K.s^{-1}$ along with cryogenic temperatures close to 173K must be applied in order to athermally transform the retained austenite to martensite [17].

A comprehensive study of martensitic transformation should consider both thermodynamic and kinetic aspects. In the case of AISI D2 steel, while the formation of martensite have been studied by a large number of authors [8, 13-15, 17], little or no data is available on the thermodynamics of martensitic transformation during cooling to cryogenic temperatures. Most of the available reviews on thermodynamics of austenite to martensite transformation are based on assumptions from room temperature and above (≥ 300K) and accordingly the calculation of chemical driving force and energy barriers may not be fully applicable to cryogenic conditions [18-20]. Also, as originally proposed by Zener [21], the tetragonality of Fe-C martensite is the combined effect of a diffusionless transformation and a

thermodynamically stable ordered distribution of carbon atoms. Therefore, there exists a critical temperature (depending on the carbon content) below which the ordered body centered tetragonal (BCT) structure is thermodynamically favored to disordered body centered cubic (BCC) one. For a rigorous evaluation of the Gibbs free energy of martensitic transformation at cryogenic temperatures, in addition to the chemical driving force and energy barriers, the contribution from carbon ordering must be also considered [22,23].

In the present study, a methodology is proposed to calculate the chemical deriving force for martensitic transformation at cryogenic temperatures which also includes the influence of carbon ordering (i.e. FCC → Ordered BCT). The proposed approach is based on a recent thermodynamic description of Fe-C system by Naraghi et al. [23]. The applicability of the thermodynamic description is assessed for temperatures down to 0 K and the possibility of a secondary ordering (α''-ordering) versus Zener-ordering is investigated for the temperature range where carbon atoms can be mobile i.e. > 223K [6]. Also, the influence of cooling rate on the total energy barrier for martensitic transformation is studied and this contribution is quantified for two different cooling rates. Transmission Electron Microscopy (TEM) and Energy Dispersive Spectroscopy (EDS) are used to study the influence of cooling rate to cryogenic temperature on possible precipitation of transition carbides.

6.2 Materials and methods

The as-received AISI D2 material was a 15mm thick normalized sheet with the nominal chemical composition of Fe-1.54wt%C-0.33wt%Si-0.32wt%Mn-11.88wt%Cr-0.76wt%Mo-0.75wt%V-0.008 wt%P-0.008wt%S. In the present study, high resolution BÄHR DIL 805 A/D dilatometer with cryogenic temperature testing capabilities was used to study martensitic transformation. The equipment has a resolution of 50nm and has been successfully used by Yang and Bhadeshia [24] to reveal very low martensite volume fraction in the order of 0.0011. Samples were cut into 10mm height and 4mm diameter cylinders. They were then heated to 1303K and maintained for 1200 seconds followed by continuous cooling to 173K at $10K.s^{-1}$ or $50K.s^{-1}$. Detailed analysis of the dilatometry curves was

reported in a recent study by the present authors [17] and the following relations were established:

$$E = E_0 - 3.83\times10^{-6} + \alpha_m T - 4.235\times10^{-3}\exp(-b(M_s - T)) \quad (6.1)$$

$$E_{10(K.s^{-1})} = -0.00326 - 3.83\times10^{-6} + 9.36\times10^{-6}T - 4.235\times10^{-3}\exp(-0.0128(444 - T)) \quad (6.2)$$

$$E_{50(K.s^{-1})} = -0.00334 - 3.83\times10^{-6} + 8.48\times10^{-6}T - 4.235\times10^{-3}\exp(-0.0156(450 - T)) \quad (6.3)$$

The transformation rate parameter b can be extracted from Eq.6.1 [17] where E is the total dilatation, E_0 is the dilatation at M_s temperature, αm is the expansion coefficient of martensite, and T is temperature (K). It is important to note that, the above equations were used to estimate the volume fraction of martensite and the obtained results were validated with the equation proposed by Harris and Cohen [25, 17]. For microstructural studies, thin films from the samples were prepared by Precision Ion Polishing System (PIPS) and were then examined using an FEI Tecnai G2 F20 200kV Cryo-STEM scanning transmission electron microscope operated at 200kV in TEM mode equipped with energy dispersive spectroscopy analysis.

6.3 Identification of transformation variables

In this section, the transformation variables such as chemical driving force of martensitic transformation and transformation strain energy are introduced to investigate the possible formation of Zener-ordered BCT and α”-ordered martensite by cryogenic cooling.

6.3.1 Chemical driving force for FCC-austenite to BCC-martensite transformation

The chemical driving force for martensitic transformation without ordering, ΔG (BCC-FCC), is defined as the difference between the Gibbs free energies of the starting FCC austenite structure and the BCC martensite structure [26]. Martensitic transformation initiates at a specific temperature, M_s, corresponding to the point where the chemical driving force can overcome the strain energy required for the formation of martensite. An accurate analysis of

the martensitic transformation would require knowing the evaluation of thermodynamic variables (e.g. heat capacity) as a function of temperature in the range 0 to 300K. However, as discussed in the introduction, the existing models [18-20, 26, 27] have been developed on assumptions that make them valid only from room temperature (300K) and above. Since martensitic transformation in AISI D2 steel continues until cryogenic temperatures, the temperature dependence of heat capacity in the temperature range 0 - 300K must be considered for accurate estimation of the chemical driving force. To this end, a thermodynamic reassessment of Fe-C system by Naraghi et al. [23] is used to estimate the variation of heat capacity with temperature for a Fe-0.52wt%C. The choice of this 'simple' alloy is based on the fact that, to the knowledge of the authors, no thermodynamic data is available on the contribution of substitutional elements to the chemical driving force needed for Zener-ordering as well as on their partitioning to carbides in D2 steel in the 0 - 300K temperature range.

The chemical composition of austenite at 1303K was determined using TCFE7 database of Thermo-Calc software and the results are shown in Table 6.1. It can be seen that although the nominal carbon content of the investigated D2 steel is 1.54wt% (6.7at%), only 0.52wt% (2.3at%) is soluble in austenite at 1303K and the rest is present in the form of carbides. The M_s temperature for Fe-0.52wt%C alloy is estimated about 600K [26]. The calculated chemical driving force at this temperature, without considering the contribution from Zener ordering, for the Fe-0.52wt%C alloy is about 1630J.mol^{-1} (Fig.6-1(a)). In contrast, the M_s value for D2 tool steel obtained from dilatometry tests is 450K [17]. This difference, which is due to the effect of solute elements present in D2 steel, may result in underestimation of the chemical driving force at cryogenic temperatures. In order to address this issue, the chemical driving force of martensitic transformation at 450K was investigated for D2 tool steel using ThermoCalc software and TCFE7 database. The result, as shown in Fig.6-1(b), indicated that the chemical driving force at M_s =450K predicts a value of 2550J.mol^{-1} which is almost the same value predicted for Fe-0.52%wt C simple alloy. Therefore, a total value of 2550J.mol^{-1} for the chemical driving force needed for the activation of martensitic transformation of D2 steel at 450K was considered. For the final cooling temperature of 173K, the chemical

driving force without contribution from Zener ordering is determined to be 3840J.mol^{-1} from Fig.6-1(b).

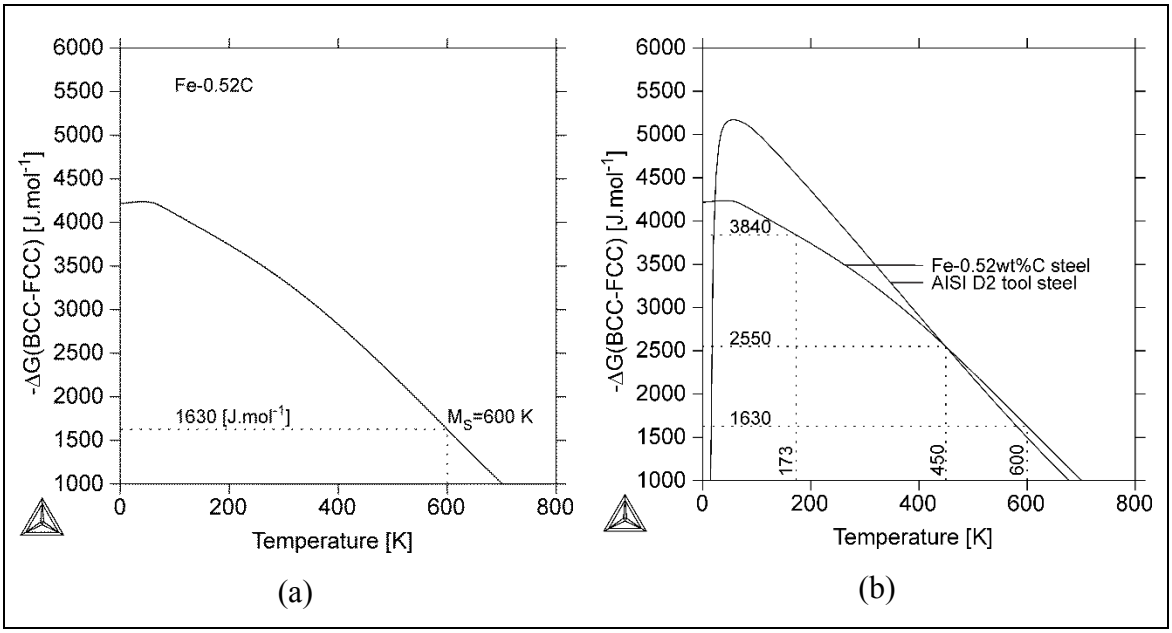

Figure 6-1 Chemical driving force for FCC to BCC transformation of (a) a Fe-0.52wt%C steel as a function of temperature obtained by the thermodynamic description in [23] (b) AISI D2 tool steel by ThermoCalc software and TCFE7 database.

Table 6.1 Chemical composition of austenite at 1303 K calculated by Thermo-Calc software-TCFE7 database (atomic fraction)

Element	Fe	C	Cr	Si	Mn	Mo	V
Atomic fraction	balance	0.0233	0.0678	0.0074	0.0032	0.0031	0.0017

6.3.2 Zener-ordering contribution to chemical driving force for martensitic transformation

Zener has proposed that martensite tetragonality is not due solely to non-diffusional transformation and other effects, such as carbon ordering may also contribute and therefore must be considered in the evaluation of the chemical driving force [21]. In the present work, the ordering contribution to Gibbs free energy changes of martensitic transformation is calculated based on the approach proposed by Zener. In the calculations, the carbon content

of the investigated D2 steel at austenitization temperature (0.52wt%C, 1303K) was considered. It must be also noted that, the ordered martensite is not stable and will finally undergo a spinodal decomposition producing carbon-rich and carbon-depleted regions during heating up and aging at room temperature [23]. Fig.6-2(a-b) shows the contribution to the chemical driving force from the Zener-ordering and α"-ordering for a Fe-0.52C composition as function of temperature from 300K down to 0K. This figure, as will be discussed later, will help identifying the operational mechanisms as a function of temperature. It should be noticed that carbon atoms are almost immobile at temperatures below 223K [6, 8] therefore, both diagrams in Fig. 6-2(a-b) are physically valid from 223K and above. In addition, the critical temperature (T_c) at which the Zener-ordered-BCT martensite becomes thermodynamically more stable than the disordered BCC martensite was determined from Fig.6-2(b) to be 360K. T_c corresponds to the point where the red curve starts deviating from the black one. By adding the contribution from Zener ordering to the chemical driving force, the sum of chemical driving force of FCC-austenite to Zener ordered BCT martensite transformation at cryogenic temperature of 173K is determined to be 4170J.mol^{-1}.

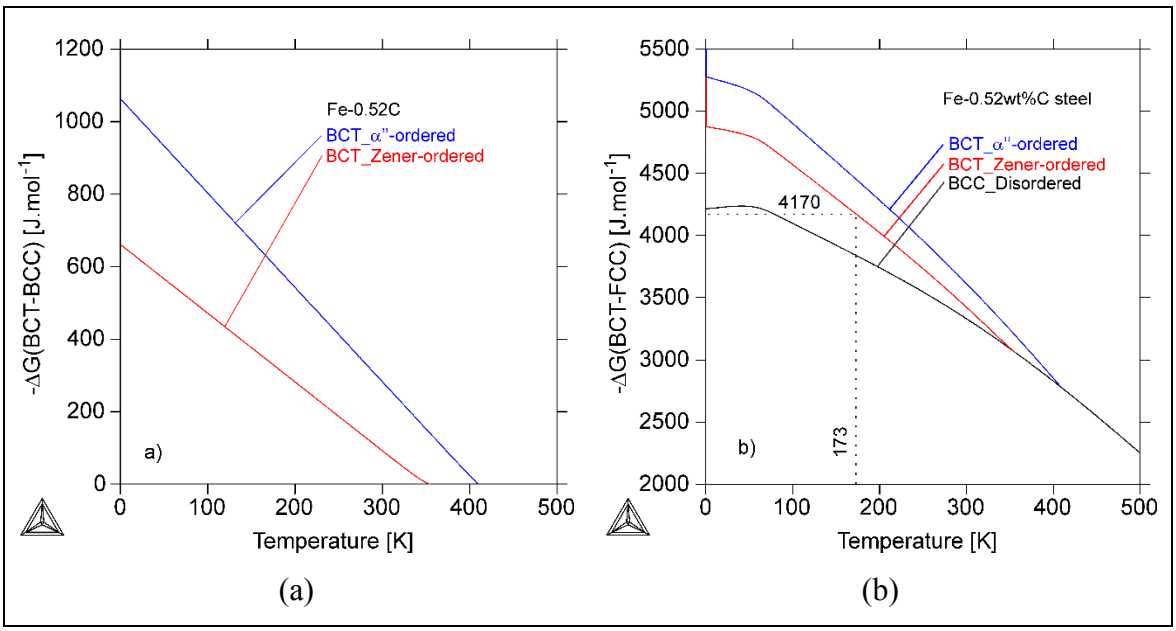

Figure 6-2 (a) Contribution from Zener-ordering and α"-ordering to Gibbs free energy of BCC for a Fe-0.52wt%C steel, (b) Gibbs free energy changes of FCC to BCT transformation including Zener-ordering and α"-ordering contributions for a Fe-0.52wt%C steel.

6.3.3 Estimation of the energy barriers of martensitic transformation

Hsu [20] proposed the following equations to estimate the strain energy for carbon accommodation in BCT crystal structure:

$$E(BCT\text{-}FCC) = 2.1\sigma + Cte(J.mol^{-1}) \quad (6.4)$$

$$\sigma_y = 130 + 2800(x_c) + 0.2(800 - T) \quad (6.5)$$

σ_y is the yield strength of austenite (σ) and a function of carbon content (x_c) and cooling temperature (T). In Hsu's study, the constant value (Cte) was calculated to be 900J.mol^{-1}. This value includes stored energies in dislocated martensite, deformed austenite, twinned martensite (if present), as well as dilatational and interfacial energies [20]. In the present study, the above equations were used to estimate the strain energy required to activate the transformation of FCC austenite to BCC martensite (E (BCC-FCC)) at M_s.

6.3.4 Cooling rate-dependent strain energy (χ)

In addition to the transformation strain energy, as indicated in Eq.6.5, cooling rate also generates strain energy (χ). This strain energy relates the transformation rate parameter (b) to the first derivative of the volumetric free energy changes accompanying transformation (as shown in Eq.6.6 below) [28].

$$\chi = \frac{1}{b} d(-\Delta G(BCT\text{-}FCC)) / dT \quad (6.6)$$

Examination of equation 6 indicates that, higher cooling rates (i.e. larger b values) lower the associated strain energy. This has been related to less capture of carbon atoms by dislocations associated with the martensitic transformation when higher cooling rates are employed [28]:
From Eqs.6.2 and 6.3, b was calculated to be 0.0128 and 0.0156 for the samples cooled at10K.s^{-1} and 50K.s^{-1}, respectively. In Fig.6-2(b), it can be assumed that the -ΔG (BCT-FCC) from M_s to 100K is almost linear. The linear dependence of the chemical driving force for martensitic transformation versus temperature has also been reported in a recent study by

Chatterjee and Bhadeshia [29]. The value of χ obtained from Eq.6.6 should be added to the strain energy obtained from Eq.6.4.

In summary, it can be said that the Zener-ordered BCT martensite and subsequently α"-ordered martensite may form after cryogenic treatment and subsequent heating up to room temperature and aging, respectively if the following conditions are met:

1) The carbon content of the alloy should be more than the critical value required for the activation of order/disorder transition [23], and
2) The total driving force should be at least equal to the strain energy at any temperature below M_s.

6.4 Results and discussion

6.4.1 Interactions between thermodynamic variables

The evolution of the chemical driving force with temperature for the formation of BCC disordered, Zener-ordered BCT, and α"-ordered martensite is shown in Fig.6-2(b). From this figure, it can be seen that at a certain threshold temperature (77K), the variation of ΔG for BCC disordered martensite with temperature becomes very small indicating that by cooling below this temperature, the chemical driving force contributes little to the progress of martensitic transformation. Below 223K, carbon atoms are essentially immobile [6, 8] then the contribution of Zener ordering to chemical driving force has only thermodynamic sense and not a physical impact. The chemical driving force at 173K and the strain energy, using Eqs. 6.4 and 6.5, were calculated to be 4170J.mol^{-1} and 1570J.mol^{-1}, respectively. Also χ was determined by using Eq.6.6, the first derivation of the BCT-Zener-ordered curve (red curve in Fig.6-2(b)), and the rate parameter b (Eqs.6.2 and 6.3). The obtained values for χ were 460J.mol^{-1} and 380J.mol^{-1} for the samples cooled at 10K.s^{-1} and 50K.s^{-1} rates, respectively.

Van Bohemen and Sietsma [28] have reported the same trend for the additional strain energy required for the continuation of martensitic transformation when different rate parameters are used. However, in their report, the variation in parameter b is related to the chemical

composition and not to the cooling rate. Donachie and Ansell [30] reported that the lower strain energy associated with higher cooling rate is due to higher amount of carbon present in interstitial sites. Faster cooling rates will reduce the mobility of carbon atoms and therefore more carbons will be trapped in the interstitial sites of the martensite crystal structure.

On the basis of the above analysis, it can be said that the total strain energy for the low and high cooling rate conditions will be 2030(1570+460)J.mol^{-1}, 1950(1570+380)J.mol^{-1}, respectively. Therefore by cooling to 173K, the total driving force even without the ordering contribution i.e. 3840J.mol^{-1} will be higher than the strain energies. Although because the martensite at that temperature is ordered, the driving force i.e. 4170J.mol^{-1} will be even higher than the disordered martensite.

6.4.2 Spontaneous formation of η-carbides after cryogenic cooling and reheating to 300 K

Figures 6-3(a-b) and 6-4(a-d) show TEM micrographs from microstructures of samples cooled at 10K.s^{-1} and 50K.s^{-1} to 173K and reheated back to room temperature. For both conditions, the martensitic microstructure was found to be a mixture of plates and laths with some nano-twinned martensite [17]. For the sample cooled at 50K.s^{-1}, additional feature called lens-shaped particles, as shown in Fig.6-4(a), were observed inside the martensite plate. It is important to note that such particles were not present in the sample cooled at 10K.s^{-1}.

Dark field TEM micrograph from the same plate of martensite (Fig.6-4(c)) complemented by selected area diffraction (SAD) pattern of these particles shown in Fig.6-4(d) indicates that these carbides are η-carbides. The formation of η-carbide was firstly reported by Hirotsu and Nagakura [31] in tempered high carbon martensite. The formation of this carbide has been also reported in the early stage of decomposition in iron-carbon martensite [32]. The SAD pattern shown in Fig.6-4(d), is also very similar to the one reported by Meng et al. [16] who associate it to η-carbides formed after cryogenic treatment at 93K followed by tempering temperature at 453K. In contrast, V. G. Gavriljuk et al. [8] reported the formation of ε-

carbides in samples cooled at rates about 100 times slower the ones used in the present investigation. It is also worth noting that, the distinction between these two carbides is rather difficult since they both have orthorhombic crystal structures and with minor changes in the local composition of the alloy or processing conditions one could be favored for the other.

Accurate quantitative chemical analysis of these nano-size carbides by EDS analysis is very difficult; however, the difference between the concentration of alloying elements can be an indirect method for differentiating the eutectic carbides (M_7C_3) of AISI D2 from η-carbides [2]. In the present investigation, the same approach was used and EDS analysis coupled with STEM was carried out and the results are presented in Fig.6-4(e) and (f). The carbon was excluded from measurements because the focused electron beam burns the surface of the sample and generates error in the measurements of carbon content. The carbides are named as point 1 for eutectic carbides and point 2 for the η-carbides. The analysis revealed major differences in the chemical composition of the η-carbides and the eutectic ones. In eutectic carbides, Cr is the dominant element in composition as reported by Večko Pirtovšek et al. [33] while in the η-carbides; the main element is Fe [16]. To the best of authors' knowledge, no report exists on the spontaneous formation of η-carbides at room temperature. Therefore, the presence of η-carbides in the microstructure of the sample quenched at $50K.s^{-1}$ indicates that cooling rate influences the mechanism of martensitic transformation at cryogenic temperature. Further investigation on the kinetic aspects of the formation of η-carbides without tempering is required. However, the continuation of martensitic transformation during reheating from cryogenic temperature overlaps with the formation of carbon rich regions [34] thereby affecting the dilatometry diagrams and the calculation of activation energy for each phenomenon. New experiments need to be conducted to study this aspect in future.

6.4.3 Rationalization of η-carbide formation by Zener-ordered BCT martensite approach

The formation of transition η-carbides after cryogenic treatment and low temperature tempering (close to 473K) has been reported as one of the main root causes for the observed

improved mechanical properties in tool steels [9]. However, the regions where these carbides can form have not been studied yet. In some reports, it has been mentioned that the interactions between carbon atoms and mobile dislocations generated during martensitic transformation at cryogenic temperature provide carbon clusters which act as nucleation sites for transition carbides during subsequent tempering at 473K [8, 9, 13, 16, 17]. The occurrence of spinodal decomposition in Fe-C solid solution was first introduced by Kurdyumov and Lysak [35] and supported by TEM observations of Izotov and Utyevsky [36]. The above findings were later confirmed by Taylor et al. [37] in Fe-Ni-C alloy and by Genin et al [38] in Fe-C alloys. Recent work by Naraghi et al. [23], based on thermodynamic calculations in the Fe-C system, indicated that ordering of carbon atoms followed by spinodal decomposition takes place in the martensite. The above sequence of events is considered as the most probable cause for the formation of carbon rich regions at room temperature which become nucleation sites for temper carbides in Fe-C steels [23].

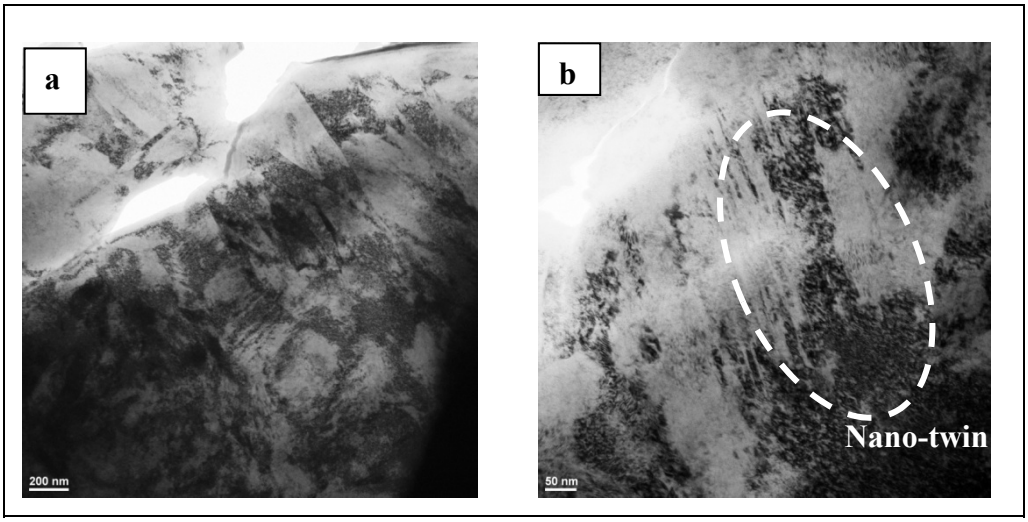

Figure 6-3 Martensite morphology obtained after cooling at the rate of $10K.s^{-1}$ (a) bright-field TEM image of mixed plate and lath morphology (b) nano-twins (circled area) in the substructure of the alloy cooled at the rate of $10K.s^{-1}$.

In the present investigation, the above concept was expanded to cryogenic temperatures above which carbon atoms are mobile i.e. $T \geq 223K$. For instance Gavriljuk et al. [6, 8, 39] reported that 250K is the start temperature of carbon clustering.

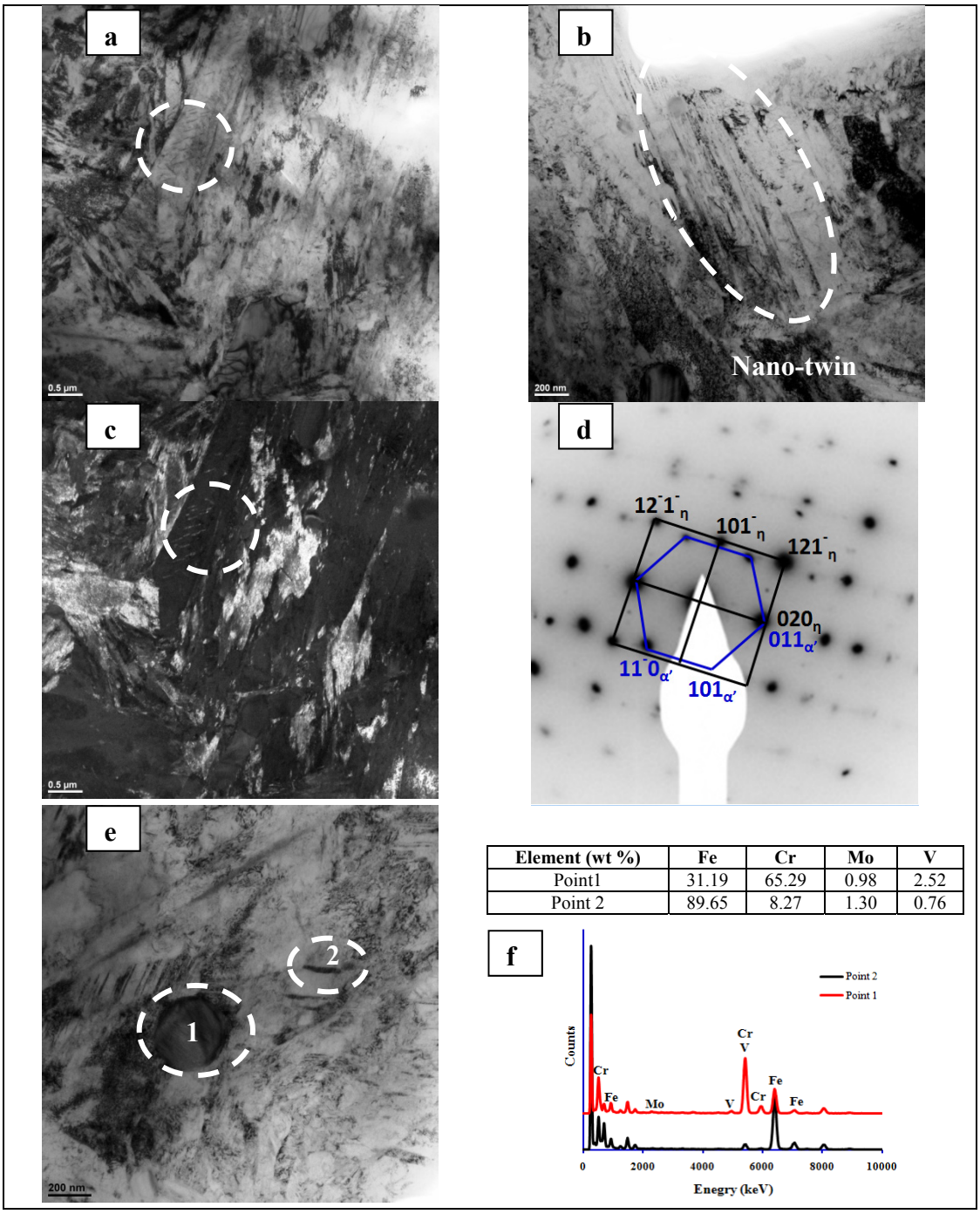

Element (wt %)	Fe	Cr	Mo	V
Point1	31.19	65.29	0.98	2.52
Point 2	89.65	8.27	1.30	0.76

Figure 6-4 (a) Lens-shaped particles circled inside the plate of martensite (b) nano-twins (circled area) in the substructure of the alloy cooled at the rate of 50K.s^{-1} (c) dark filed TEM micrograph from the same plate of martensite illustrated part a (d) selected area diffraction (SAD) pattern of these particles showing the η-carbides (e) chemical analysis taken over areas numbered 1 and 2, (f) the chemical composition and EDS diagrams showing two types of carbides.

This temperature was selected for investigating the state of ordering and spinodal decomposition and the obtained results are shown in Fig.6-5. In this figure, the carbon-rich inflection points for Zener-ordered martensite are positioned out of the scale of the graph and near to a Fe-C50at% (17.7wt%) alloy [23]. It means that for the Zener-ordered martensite at 223 K and above (i.e. BCT_Zener-ordered graph in Fig.6-5), the carbon rich regions will have a composition near 50at% C (17.7wt%). This value is not consistent with experimental data reported by Zhu et al. [40] who obtained a composition close to 11at% (2.59wt%) using advanced 3D atom probe. Under these conditions, spinodal decomposition of α"-ordered martensite is therefore a possible mechanism which could provide carbon rich regions with a composition close to the ones reported in practice [40]. The latter could become favorable nucleation sites for η-carbides which would form during heating from cryogenic temperature and holding at room temperature.

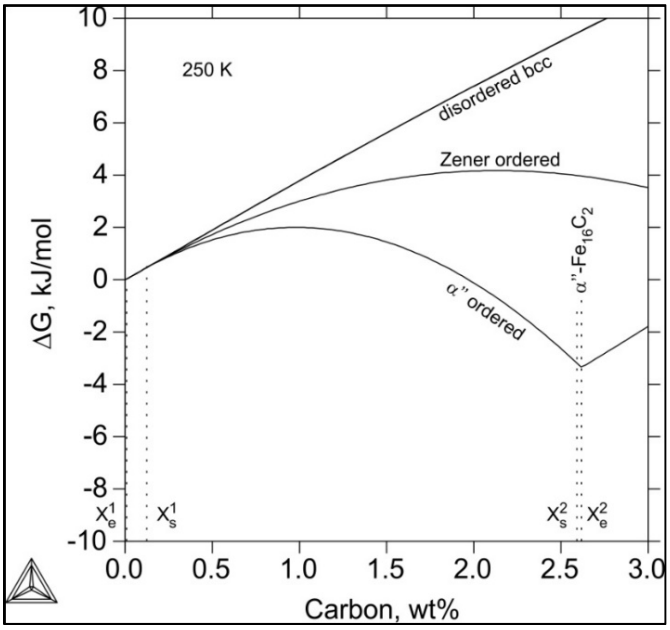

Figure 6-5 Gibbs free energy diagrams of disordered, Zener-ordered, and α″-ordered in simplified Fe-C alloy at 250K obtained by the thermodynamic description in [23]. X^1_s and X^2_s symbols denote the limits of spinodal decomposition and X^1_e and X^2_e representing the boundaries for the miscibility gap obtained by the common tangent-construction.

It is also worth mentioning here that the present authors have recently observed and reported the occurrence of splitting phenomena in dilatometry diagrams that corresponds to carbide precipitation (carbon-depleted austenite) for the slow cooled sample ($10K.s^{-1}$) and the formation of partially carbon-rich austenite, without carbide precipitation, before the activation of martensitic transformation for the fast-cooled sample ($50K.s^{-1}$) [17]. There may exist a relationship between the formation of such partially carbon-rich regions and the nucleation sites for the formation of η-carbides. Future investigations on this matter may further extend our understanding about the mechanism responsible for the spontaneous formation of η-carbides.

6.5 Conclusions

In this study, the transformation variables involved in the transformation of FCC-austenite to Zener-ordered and α"-ordered martensite were determined. Both cooling rates of $10K.s^{-1}$ and $50K.s^{-1}$ showed the potential in achieving α"-ordered martensite. For the sample cooled at $50K.s^{-1}$, spontaneous formation of η-carbides was observed after reheating to room temperature and holding at room temperature. The carbon-rich regions, formed during heating from temperatures above 223K where carbon atoms are mobile, were suggested as possible nucleation site for the spontaneous formation of η-carbides. The introduced thermodynamic approach was successfully used to rationalize the formation of η-carbides from carbon rich regions.

Acknowledgements

The authors would like to thank the National Sciences and Engineering Research Council of Canada (NSERC) and MITACS Canada for their financial supports. The authors also appreciate the collaboration of DK SPEC Inc. for providing experimental materials, support from CanmetMATERIALS in the framework of RIEM program for dilatometry experiments.

References

[1] G. Roberts, G. Krauss, R. Kennedy, Tool Steels: 5th Edition, ASM International®, USA (1998).

[2] D. Bombac, M. Fazarinc, A. Saha Podder, G. Kugler, Study of carbide evolution during thermo-mechanical processing of AISI D2 tool steel Journal of Materials Engineering and Performance 22 (2013) 742-747.

[3] G. R. Speich, W. C. Leslie, Tempering of steel, Metallurgical Transactions 3-5 (1972) 1043-1054.

[4] P. F. da Silva Farina, C. A. Barbosa, H. Goldenstein, Microstructural characterization of an AISI D2 tool steel submitted to cryogenic treatment, Journal of ASTM International 8-5 (2011) 1-8.

[5] D. Das, A. K. Dutta, K. K. Ray, Influence of varied cryotreatment on the wear behavior of AISI D2 steel, Wear 266 (2009) 297-309.

[6] A. I. Tyshchenko, W. Theisen, A. Oppenkowski, S. Siebert, O. N. Razumov, A. P. Skoblik, V. A. Sirosh, Y. N. Petrov, V. G. Gavriljuk, Low-temperature martensitic transformation and deep cryogenic treatment of a tool steel, Materials Science and Engineering A 527 (2010) 7027-7039.

[7] V. G. Gavriljuk, V. A. Sirosh, Y. N. Petrov, A. I. Tyshchenko, W. Theisen, A. Kortmann, Carbide precipitation during tempering of a tool steel subjected to deep cryogenic treatment, Metallurgical and Materials Transactions A 45-3 (2014) 2453-2465.

[8] V. G. Gavriljuk, W. Theisen, V. V. Sirosh, E. V. Polshin, A. Kortmann, G. S. Mogilny, N. Petrov, Y. V. Tarusin, Low-temperature martensitic transformation in tool steels in relation to their deep cryogenic treatment, Acta Materialia 61 (2013) 1705-1715.

[9] S. G. Singh, J. Singh, R. Singh, H. Singh, Metallurgical principles of cryogenically treated tool Steels-a review on the current state of science, International Journal of Advanced Manufacturing Technology 54 (2012) 59-82.

[10] Y. M. Rhyim, S. H. Han, Y. S. Na, J. H. Lee, Effect of deep cryogenic treatment on carbide precipitation and mechanical properties of tool steel, Steel Solid State Phenomena 118 (2006) 9-14.

[11] D. N. Collins, J. Dormer, Deep cryogenic treatment of a D2 cold-worked tool steel, J Heat Treating Metals 3 (1997) 71-74.

[12] E.A. Huallpa, J.C. Sánchez, L.R. Padovese, H. Goldenstein, Determining Ms temperature on a AISI D2 cold work tool steel using magnetic Barkhausen noise, Journal of Alloys and Compounds 577 (2013) S726-S730.

[13] S. Li, L. Deng, X. Wu, The mechanism investigation of deep cryogenic treatment on high alloy martensitic steel by low frequency internal friction, Cryogenics 50-8 (2010) 433-438.

[14] D. Das, A. Dutta, K. K. Ray, Sub-zero treatments of AISI D2 steel: Part I. Microstructure and hardness, Materials Science and Engineering A 527 (2010) 2182-2193.

[15] D. Das, A. Dutta, K. K. Ray, On the refinement of carbide precipitates by cryotreatment in AISI D2 steel, Philosophical Magazine 89-1 (2009) 55-76.

[16] F. Meng, K. Tagashira, R. Azuma, H. Sohma, Role of Eta-Carbide Precipitations in the Wear Resistance Improvements of Fe-12Cr-MoV-1.4C Tool Steel by Cryogenic Treatment, ISIJ International 34-20 (1994) 205-210.

[17] H. Ghasemi Nanesa, M. Jahazi, R. Naraghi, Martensitic transformation in AISI D2 tool steel during continuous cooling to 173 K, Journal of Materials Science 50-17 (2015) 5758-5768.

[18] G. Ghosh, G. B. Olson, Kinetics of FCC – BCC heterogeneous martensitic nucleation- I. The critical driving force for athermal nucleation, Acta Metallurgica Materialia 42-10 (1994) 3361-3370.

[19] G. Ghosh, G. B. Olson, Computational thermodynamics and the kinetics of martensitic transformation, Journal of Phase Equilibria 22 (2001) 199-207.

[20] T. Y. Hsu, An approximate approach for the calculation of M_s in iron-base alloys, Journal of Materials Science 20 (1985) 23-31.

[21] C. Zener, Kinetics of the decomposition of austenite, Trans. AIME 167 (1946) 550-595.

[22] R. Naraghi, M. Selleby, Stability of Fe-C martensite- effect of Zener ordering, 1st World Congress on Integrated Computational Materials Engineering, TMS (The Minerals, Metals & Materials Society) (2011) 235-240.

[23] R. Naraghi, M. Selleby, J. Ågren, Thermodynamics of stable and metastable structures in Fe–C system, CALPHAD 46 (2014) 148-158.

[24] H.-S. Yang, H. K. D. H. Bhadeshia, Uncertainties in dilatometric determination of martensite start temperature, Materials Science and Technology 23-5 (2007) 556-560.

[25] H. Ghasemi Nanesa, M. Jahazi, T. Levasseur, on the martensitic transformation of AISID2 tool steel through cryogenic cooling, Proceedings of the International Conference on Solid-Solid Phase Transformations in Inorganic Materials (2015) 641-642.

[26] A. Stormwinter, A. Borgenstam, J. Ågren, Thermodynamically Based Prediction of the Martensite Start Temperature for Commercial Steels, Metallurgical and Materials Transactions A 43 (2012) 3870-3879.

[27] H. K. Yeddu, A. Borgenstam, P. Hedström, J. Ågren, A phase-field study of the physical concepts of martensitic transformations in steels, Materials Science and Engineering A 538 (2012) 173-181.

[28] S.M.C. Van Bohemen, J. Sietsma, Martensite Formation in Partially and Fully Austenitic Plain Carbon Steels, Metallurgical and Materials Transactions A 40 (2009) 1059-1068.

[29] S. Chatterjee, H. K. D. H. Bhadeshia, Transformation induced plasticity assisted steels: stress or strain affected martensitic transformation?, Materials Science Technology 23-9 (2007) 1101-1104.

[30] S. J. Donachie, G. S. Ansell, The effect of quench rate on the properties and morphology of ferrous martensite, Metallurgical Transactions A 616-6 (1975) 1863-1875.

[31] Y. Hirotsu, S. Nagakura, Crystal structure and morphology of the carbide precipitated from martensitic high carbon steel during the first stage of tempering, Acta Metallurgica 20 (1972) 645-655.

[32] G. Krauss, Martensite in steel: strength and structure, Materials Science and Engineering A 273-275 (1999) 40-57.

[33] T. Večko Pirtovšek, G. Kugler, M. Terčelj, The behaviour of the carbides of ledeburitic AISI D2 tool steel during multiple hot deformation cycles, Materials Characterization 83 (2013) 97-108.

[34] H. Ghasemi Nanesa, H. Touazine, M. Jahazi, Influence of cryogenic process parameters on microstructure and hardness evolution of AISI D2 tool steel, Journal of Advanced Manufacturing Technology (2015) (Online version) 1-10.

[35] G.V. Kurdyumov, L.I. Lysak, Use of single crystals to study the structure of temper martensite, Journal of Technical Physics 16 (1946) 1307.

[36] V.M. Izotov, L.M. Utyevsky, On the Structure of Martensite crystals in High Carbon Steel, Physics of Metals and Metallography 25-1 (1968) 98-110.

[37] K.A. Taylor, L. Chang, G.B. Olson, G.D.V. Smith, M. Cohen, J.B. Vander Sande, Spinodal decomposition during aging of Fe-Ni-C martensites, Metallurgical Transactions A 20-12 (1989) 2717-2737.

[38] O.N.C. Uwakweh, J.-M.R Genin, J.-F. Silvain, Electron microscopy study of the aging and first stage of tempering of high-carbon martensite, Metallurgical Transactions A 22-4 (199) 797-806.

[39] K. Ullakko, V. G. Gavriljuk, Effects of coherent interfaces in the freshly formed iron-nickel-carbon martensites, Acta Metallurgica and Materialia 40-10 (1992) 2471-2482.

[40] C. Zhu, A. Cerezo, G. D. W. Smith, Carbide characterization in low-temperature tempered steels, Ultramicroscopy 109 (2009) 545-552.

CONCLUSIONS

From analysis and discussions provided in each article, the main contributions of this thesis in the field of cryogenic treatment of AISI D2 tool steel are:

1) It was demonstrated that conventional cryogenic treatments of AISI D2 tool steels fails in achieving only martensitic microstructure which could result in inconsistent results after cryogenic treatment. The existence of an alternative microstructure was approved by dilatometry analysis and microstructural observation using SEM and TEM. It was shown that cooling rates above conventional rates are required to obtain a fully martensitic microstructure.
2) Using design of experiments and statistical analysis of the results, it was shown that tempering temperature is the most significant individual factor. While, other factors are not significant individually, but in combination, they produce synergetic effect and can significantly affect microstructure and hardness.
3) The numerical analysis of dilatation data showed that the cooling until room temperature does not give complete martensitic transformation in this steel and in order to achieve full transformation the cooling should be extended to cryogenic temperatures around 173K.
4) Transformation variables during cryogenic cooling were determined to be chemical driving force, Zener ordering contribution to Gibbs free energy, strain energy required for the activation of transformation, cooling rate-dependent strain energy. Using an extended thermodynamic model to cryogenic temperatures, it was shown that carbon ordering by Zener effect occurs at cryogenic temperatures and it is more stable than dis-ordered martensite. Also, it was found that the Zener-ordered martensite finally undergoes a secondary ordering phenomenon which is known as spinodal decomposition. The spinodal decomposition generates carbon rich regions which eventually act as nucleation sites for the precipitation of η-carbides.

RECOMMENDATIONS

The main purpose of this study was to better understand physical metallurgy of cryogenic treatment and investigate the effect of cryogenic process parameters on hardness and microstructure evolution. To complete the study, following extended investigations are suggested:

1) Martensitic transformation can be progressed by either athermal nature or isothermal nature which is not fully understood during cryogenic cooling. Previous attempts have suggested isothermal nature for martensitic transformation during holding time at cryogenic temperatures which may be different from athermal nature. It is suggested to investigate both modes and find the relationship between the nature of transformation and the formation of η-carbides during aging at room temperature.
2) It was attempted to investigate spontaneous formation of η-carbides after cryogenic cooling and aging at room temperature by thermodynamic analysis and experimental observations. However, the formation of η-carbides is a diffusion-based phenomenon and it is essential to investigate its kinetics at room temperature. It was suggested that splitting phenomenon could be a root cause for the formation of η-carbides. Therefore, this parameter should be taken into account during kinetic analysis.

LIST OF BIBLIOGRAPHICAL REFERENCES

Arai, T., et al., ASM Handbook Vol. 4: Heat treating, ASM International (1991).

Babu, P. S., Rajendran, P., Rao, K. N., Cryogenic treatment of M1, EN19, and H13 tool steels to improve wear resistance. J Inst Engineering India MM 86 (2005) 64-66.

Barron, R. F., Cryogenic treatment of metals to improve wear resistance, Cryogenics 22 (1982) 409-413.

Bhadeshia, H. K. D. H., Design of ferritic creep-resistant steel, ISIJ International 4-6 (2001) 626-640.

Bhadeshia, H. K. D. H., Martensite in steels, http://www.msm.cam.ac.uk/phase-trans/2002/martensite.html

Bhadeshia, H. K. D. H., Multiple, Simultaneous, Martensitic Transformations: Implications on Transformation Texture Intensities, Materials Science Forum 762 (2013) 9-13.

Blankinship, S., Ultra-cold could help freeze plant repairs, Power Engineering 105 (2001) 13-16.

Cohen, P., Kamody, D., Cryogenics goes deeper. Cutting Tool Engineering l50-7 (1998) 46-50.

Collins, D. N., Cryogenic treatment of tools steels, Advanced Materials Processing 154-6 (1998) H23.

Collins, D. N., Deep cryogenic treatment of tool steels: A review, Heat Treatment of Metals 23-2 (1996) 40-42.

Collins, D. N., Dormer, J., Deep cryogenic treatment of a D2 cold-work tool steel, Heat Treatment of Metals 24(3) (1997) 71-74.

Da Silva, F. J., Franco, S. D., Machado, A. R., Ezugwu, E. O., Souza, Jr. A. M., Performance of cryogenically treated HSS tools. Wear 261 (2006) 674-685.

Dhokey, N. B., Nirbhavne, S., Dry sliding wear of cryotreated multiple tempered D-3 tool steel, Journal of Materials Processing Technology 209-3 (2009) 1484-1490.

Dobbins, D. B. , Cryogenic treatment can boost life, Metalforming, May (1995) 29-32.

Dymchenko, V. V., Safronova, V. N., Refrigeration treatment of quenched roll steel. Tyazhel Mashinostr 9 (1993) 29-32.

Gavriljuk, V. G., Theisen, W., Sirosh, V. V., Polshin, E. V., Kortmann, A., Mogilny, G. S., Petrov, Y. N., Tarusin, Y. V., Low-temperature martensitic transformation in tool steels in relation to their deep cryogenic treatment , Acta Materialia 61 (2013) 1705-1715.

Ghasemi-Nanesa, H., Jahazi, M., Simultaneous enhancement of strength and ductility in cryogenically treated AISI D2 tool steel, Materials Science and Engineering A 598 (2014) 413-419.

Kamody, D. J., US Patent 5,259,200, 1993.

Kamody, D., Cryogenics process update. Advanced Materials Processing 155-6 (1999) H67-H69.

Kamody, D., Process for the cryogenic treatment of metal containing materials. US Patent No.5875636, 1999.

Kelkar, R., Nash, P., Zhu, Y., Understanding the effects of cryogenic treatment on M2 tool steel properties, Heat Treating Progress 7 (2007) 57-60.

Krauss, G., Martensite in steel: Strength and structure, Materials Science and Engineering A 273-275 (1999) 40-57.

Lal, D. M., Renganarayanan, S., Kalanidhi, A., Cryogenic treatment to argument wear resistance of tool and die steels, Cryogenics 41 (2001) 149-155.

Lal, D. M., Renganarayanan, S., Kalanidhi, A., Effect of cryotreatment on T1 type high speed steel tool material, Indian Journal of Cryogenics 21 (1996) 41-44.

Marder, A.R., Krauss, G., The morphology of martensite in iron-carbon alloys, Trans. ASM, 60 (1967) 651-660.

Meng, F., Tagashira, K., Azuma, R., Sohma, H., Role of eta-carbide precipitations in the wear resistance improvements of Fe-12Cr-Mo-V-1.4C tool steel by cryogenic treatment, ISIJ International 34 (1994) 205-210.

Miller, P. C., Cryogenic: Deep cold solves heat treat problems, Tooling & Production (1980) 82-86.

Molinari, A. , Pellizzari, M., Gialanella, S., Straffelini, G., Stiasny, K. H., Effect of deep cryogenic treatment on the mechanical properties of tool steels, Journal of Materials Processing Technology 118 (2001) 350-355.

Moore, K. E., Collins, D. N., Cryogenic treatment of three heat-treated tool steels. Key Engineering Materials 86-87 (1993) 47-54.

Nishiyama, Z., Martensitic Transformation, ACADEMIC PRESS, New York, USA, (1978).
Paulin, P., Frozen gears. Gear Technology 10 (1993) 26-29.

Preciado, M., Bravo, P. M., Alegre, J. M., Effect of low temperature tempering prior cryogenic treatment on carburized steels, Journal of Materials Processing Technology 176-1-3 (2006) 41-44.

Reed-Hill, R. E. , Abbaschian, R., Physical metallurgy principles; 3rd ed., PWS Publishing Company, Boston (1992).

Reitz, W., Pendray, J., Cryoprocessing of materials: a review of current status, Materials Manufacturing Processes 16-6 (2001) 829-840.

Roberts, G., Krauss, G., Kennedy, R., Tool Steels: 5th Edition, ASM International®, USA (1998).

Singh, S. G., Singh, J., Singh, R., Singh, H., Metallurgical principles of cryogenically treated tool steels - A review on the current state of science, International Journal of Advanced Manufacturing Technology 54 (2011) 59-82.

Speich, G. R., Leslie, W. C., Tempering of steel, Metallurgical Transactions 3-5 (1972) 1043-1054.

Stratton, P. F., Optimising nano-carbide precipitation in tool steels, Materials Science and Engineering A 449-451 (2007) 809-812.

Tarkany, N., Tips for choosing tool steels, heat treatment, and surface treatments (2000). http://www.daytonprogress.com/tech/dayton_tech-balancing.pdf

Teymuri, S. C., Najafabadi, M. A., Ebrahimian, S. A., Fracture toughness determination of heat treated AISI D2 tool steel using AE technique, ISIJ International 51-2 (2011) 305-312.

Tyshchenko, A. I., Theisen, W., Oppenkowski, A., Siebert, S., Razumov, O. N., Skoblik, A. P. V., Sirosh, A., Petrov, Y. N., Gavriljuk, V. G., Low-temperature martensitic transformation and deep cryogenic treatment of a tool steel, Materials Science and Engineering A 527 (2010) 7027-7039.

Wang, C. C., Wear resistance study on cryogenic treated AISI D2 steel. MSc thesis, Tatung University (2006).

Weast, R. C., Handbook of chemistry and physics, 62nd ed. CRC C (1981-1982) D161-D162.

Wilson, E.A., γ→α transformation in low carbon irons, ISIJ International 34 (1994) 615-630.

Yugandhar, T., Krishnan, P. K., Bhaskar Rao, C. V., Kalidas, R., Cryogenic treatment and its effects on tool steel. Proceedings of 6th International Tooling Conference, Karlstad University, Sweden, September (2002) 671-684.

Yun, D., Xiaoping, L., Hongshen, X., Deep cryogenic treatment of high-speed steel and its mechanism, Heat Treating Metals 3 (1998) 55-59.

Yang, H. S., Wang, J., Shen, B. L., Liu, H. H., Gao, S. J., Huang, S. J., Effect of cryogenic treatment on the matrix structure and abrasion resistance of white cast iron subjected to destabilization treatment. Wear 26 (2006) 1150-1154.

Zener, C., Kinetics of the decomposition of austenite, Transactions AIME 167 (1946) 550-595.

Zhirafar, S., Rezaeian, A., Pugh, M., Effect of cryogenic treatment on the mechanical properties of 4340 steel, Journal of Materials Processing Technology 186-1-3 (2007) 298-303.

Zurecki, Z., Cryogenic quenching of steel revisited. Air Products & Chemicals, Inc. (2005) 106-113.